UNITED NATIONS UNIVERSITY

UNU-GTP

ORKUSTOFNUN

Meyjarauga hot spring, Hveravellir, Kjölur, Central Iceland

Melissa Anne De Freitas

NUMERICAL MODELLING OF SUBSIDENCE IN GEOTHERMAL RESERVOIRS: CASE STUDY OF THE SVARTSENGI GEOTHERMAL SYSTEM, SW-ICELAND

Report 5
November 2018

UNITED NATIONS UNIVERSITY
UNU-GTP
Geothermal Training Programme

Orkustofnun, Grensasvegur 9,
IS-108 Reykjavik, Iceland

Reports 2018
Number 5

NUMERICAL MODELLING OF SUBSIDENCE IN GEOTHERMAL RESERVOIRS: CASE STUDY OF THE SVARTSENGI GEOTHERMAL SYSTEM, SW-ICELAND

MSc thesis
School of Engineering and Natural Sciences
Faculty of Earth Sciences
University of Iceland

by

Melissa Anne De Freitas
Energy Unit
Ministry of National Security, Air & Sea Port Development
Kingstown
ST. VINCENT AND THE GRENADINES
melissa.defreitas@gov.vc; m.defreitas89@gmail.com

United Nations University
Geothermal Training Programme
Reykjavík, Iceland
Published in November 2018

ISBN 978-9979-68-485-5 (PRINT)
ISBN 978-9979-68-486-2 (PDF)
ISSN 1670-7427

This MSc thesis has also been published in October 2018 by the
School of Engineering and Natural Sciences, Faculty of Earth Sciences
University of Iceland

INTRODUCTION

The Geothermal Training Programme of the United Nations University (UNU) has operated in Iceland since 1979 with six-month annual courses for professionals from developing countries. The aim is to assist developing countries with significant geothermal potential to build up groups of specialists that cover most aspects of geothermal exploration and development. During 1979-2018, 694 scientists and engineers from 61 developing countries have completed the six month courses, or similar. They have come from Africa (39%), Asia (35%), Latin America (14%), Europe (11%), and Oceania (1%). There is a steady flow of requests from all over the world for the six-month training and we can only meet a portion of the requests. Most of the trainees are awarded UNU Fellowships financed by the Government of Iceland.

Candidates for the six-month specialized training must have at least a BSc degree and a minimum of one-year practical experience in geothermal work in their home countries prior to the training. Many of our trainees have already completed their MSc or PhD degrees when they come to Iceland, but many excellent students with only BSc degrees have made requests to come again to Iceland for a higher academic degree. From 1999, UNU Fellows have also been given the chance to continue their studies and study for MSc degrees in geothermal science or engineering in co-operation with the University of Iceland. An agreement to this effect was signed with the University of Iceland. A similar agreement was also signed with Reykjavik University in 2013. The six-month studies at the UNU Geothermal Training Programme form a part of the graduate programme.

It is a pleasure to introduce the 61st UNU Fellow to complete the MSc studies under a UNU-GTP Fellowship. Melissa Anne de Freitas, a Reservoir Engineer from the Energy Unit at the Ministry of National Security in St. Vincent and the Grenadines, completed the six-month specialized training in *Reservoir Engineering* at UNU Geothermal Training Programme in October 2014. Her research report was entitled: *Geothermal resource assessment of the Wotten Waven geothermal field – Dominica, West Indies.* After two years of geothermal work for St. Vincent, she came back to Iceland for MSc studies at the School of Engineering and Natural Sciences, Faculty of Earth Sciences, University of Iceland in August 2016. In September 2018, she defended her *MSc thesis* in *Geophysics* presented here, entitled: *Numerical modelling of subsidence in geothermal reservoirs: case study of the Svartsengi geothermal system, SW-Iceland.* Her studies in Iceland were financed by the Government of Iceland through a UNU-GTP Fellowship from the UNU Geothermal Training Programme. We congratulate Melissa on the achievements and wish her all the best for the future. We thank the School of Engineering and Natural Sciences, Faculty of Earth Sciences, University of Iceland for the co-operation, and her supervisors for the dedication.

Finally, I would like to mention that Melissa's MSc thesis with the figures in colour is available for downloading on our website *www.unugtp.is*, under publications.

With warmest greetings from Iceland,

Lúdvík S. Georgsson, Director
United Nations University
Geothermal Training Programme

ACKNOWLEDGEMENTS

I am extremely grateful to the United Nations University Geothermal Training Programme (UNU-GTP), and by extension the Government of Iceland, for granting me the opportunity to pursue my studies at the University of Iceland. I would like to acknowledge and extend my heartfelt gratitude to the director, Lúdvík S. Georgsson, and his deputy, Ingimar G. Haraldsson. I am thankful to the staff of the UNU-GTP, Málfrídur Ómarsdóttir, Markús Wilde and Thórhildur Ísberg for their support during this time.

I would like to express my deepest gratitude to my supervisors Gudni Axelsson and Páll Einarsson for their excellent guidance and constant supervision. Special thanks to my external examiner Lárus Thorvaldsson, for his feedback.

To Stefan Finsterle, thank you for not only allowing me to test your subsidence module, but also for personally taking the time to assist me along the way.

I would like to acknowledge Mike O´Sullivan, John O´Sullivan, Adrian Croucher, Benedikt Steingrímsson, Grímur Björnsson, Valdís Gudmundsdóttir and Gunnar Thorgilsson, for their invaluable assistance during the preparation of this project. I would also like to express special thanks to Clare Baxter, and Seequent Limited, for granting me an academic license for Leapfrog Geothermal free of cost for the duration of this project.

Special thanks to HS Orka, for allowing access to and granting permission to utilise and publish the Svartsengi data.

I would like to thank the Prime Minister of St. Vincent and the Grenadines – Dr. Hon. Ralph E. Gonsalves for his usual support and granting me permission to pursue my studies at the University of Iceland.

I take this opportunity to thank my parents and friends back home for their unwavering support, encouragement, motivation and prayers.

Heartfelt thanks to my colleagues at the UNU-GTP and my roommates for all the good times shared during the past two years. May God richly bless you all.

Finally, thanks to God Almighty, through whom nothing is impossible.

DEDICATION

To my parents, for their continued support and encouragement.

ABSTRACT

The Svartsengi-Eldvörp geothermal system is a high-temperature system situated within the Reykjanes Peninsula oblique rift in south-west Iceland, a part of the boundary between the North America and Eurasia plates. Extensive regional ground subsidence ranging from 7 to 14 mm/year has been observed from 1975 to 2015, with the maximum changes in elevation detected in the production field at Svartsengi. Numerous studies done throughout the years have sought to identify and isolate the various signals that contribute to the observed subsidence. Recently, the combined analysis of a variety of geodetic studies have proposed a natural subsidence velocity of 6 mm/year along the central volcanic rift within the Reykjanes Peninsula. This project however, seeks to contribute to the existing deformation studies at Svartsengi by setting up a TOUGH2 numerical model of the Svartsengi geothermal system, calibrated against the average annual mass extraction and reinjection rates from 1975 to 2015. One-dimensional subsidence modelling was performed with the model, using a newly developed subsidence module in iTOUGH2. The model reveals that high permeabilities, pressure drawdown and changes in the rates of production and reinjection have been major factors that have influenced the contribution of geothermal production to the total observed vertical deformation at Svartsengi. Modelled results indicate an average subsidence velocity of 3-4 mm/year as a result of mass extraction due to geothermal activity. Coupled with the natural subsidence value previously determined, this value is capable of accurately representing the total subsidence observed at Svartsengi. This numerical model is therefore a valuable tool for predicting subsidence rates due to future production at Svartsengi and Eldvörp.

TABLE OF CONTENTS

LIST OF FIGURES

Page

LIST OF TABLES

1. INTRODUCTION

The Svartsengi geothermal system is a high-temperature system located on the Reykjanes Peninsula in South-West Iceland. It is characterised by high permeabilities, uniform pressure conditions and isothermal reservoir temperatures of 240°C below 900 m depth within the main production zone (Björnsson and Steingrímsson, 1991). Temperatures have been observed to increase towards the southwest, with higher temperatures of 268°C observed at Eldvörp 6 km southwest of Svartsengi.

Large scale geothermal exploitation at Svartsengi commenced in October 1976. The Svartsengi geothermal plant is a combined heat and power (CHP) plant and is the first geothermal power plant in the world to combine generation of electricity with the production of hot water for district heating (Verkís 2016). Today it has a total installed capacity of 150 MW_{th} of thermal power and 75 MW_e of electrical power, with an electrical generation capacity of over 150 GWh/year.

Svartsengi, being located on the Reykjanes Peninsula, is prone to many complex crustal deformation processes. Active tectonism, volcanism and seismicity have long since been identified as major contributors to ground deformation occurring in Svartsengi, with observed subsidence velocities fluctuating in the range of 7-14 mm/year during 1975 to 2015 (Eysteinsson, 2000; Magnússon, 2009; 2013; 2015). The onset of geothermal production at Svartsengi saw the formation of a large subsidence bowl around Svartsengi and Eldvörp, with over 0.36 m of subsidence observed between 1975 and 2014 (Magnússon, 2015). A direct correlation between the pressure drawdown and subsidence led Eysteinsson (2000) to infer that geothermal production at Svartsengi was one of the major contributors to the vertical deformation observed during this period.

Numerical modelling plays a vital role in comprehending the nature of geothermal systems. It is employed in estimating the properties and production potential of geothermal systems, as well as utilised as a resource management device. It is the most powerful tool of geothermal reservoir engineering, used globally to simulate the response of geothermal reservoirs to a variety of scenarios (Axelsson, 2013). Though used extensively for geothermal resource assessment, recently, geothermal reservoir models have begun to include subsidence resulting from geothermal production as an additional calibration factor. A radially symmetric model, combining geomechanical modelling with mass and heat flow modelling using TOUGH2 was developed for the Wairakei geothermal field in New Zealand (Koros et al., 2016). It accurately replicated the subsidence that has occurred at Wairakei due to 50 years of production. The authors therefore concluded that it is a valuable tool in predicting the future rates of subsidence as a result of production at the Wairakei geothermal field.

Subsidence in the Reykjanes Peninsula has been extensively monitored, with numerous studies done to isolate the various signals that contribute to ground deformation. A combined analysis of a variety of geodetic studies and lithological logs (Vadon and Sigmundsson, 1997; Fridleifsson and Richter, 2010) have proposed a background subsidence rate of approximately 6 mm/year along the central rift zone of the Reykjanes Peninsula, however, to date, the contribution of geothermal production to subsidence hasn't been directly measured. Numerous numerical production models have been developed for Svartsengi throughout the last 40 years of production (e.g. Bödvarsson, 1988; Björnsson, 1999; Ketilsson, 2007), but these have neglected to directly include the response of the reservoir to subsidence.

This thesis is aimed at isolating the geothermal signal of the total subsidence observed in Svartsengi through the creation of a TOUGH2 numerical reservoir model, calibrated against the production response based on 40 years of geothermal exploitation from 1975 to 2015. Further objectives of this thesis include:

(1) To review available information regarding the conceptual model of the Svartsengi geothermal system.
(2) To review available studies in crustal deformation, more specifically the subsidence observed in Svartsengi, and by extension the Reykjanes Peninsula.
(3) To develop a numerical model of the entire Svartsengi geothermal system, simulating the natural state and production response.

(4) To calculate the subsidence in Svartsengi due to geothermal production by numerical modelling, incorporating the newly developed one-dimensional subsidence module in iTOUGH2 and comparing with observed data.
(5) To propose further steps in subsidence modelling with TOUGH2.

The first part of this thesis consists of a general introduction, including Chapters 1 to 3, which gives an overall background of the Svartsengi geothermal system. Chapter 2 contains a general summary of the geological setting of the Reykjanes Peninsula, as well as previous geological, geophysical and reservoir models of the Svartsengi system. Chapter 3 contains the details of 40 years of geothermal exploitation at Svartsengi, and summarises the observed subsidence and pressure changes observed from 1975 to 2015. The fourth chapter, 'Methodology', describes the approach taken to create a TOUGH2 numerical model for the Svartsengi high-temperature geothermal system. Chapter 5 presents and discusses the results obtained as a result of model calibration. The final chapter 'Conclusions and Recommendations' summarises the implications of the results by presenting an insight into the Svartsengi reservoir and discusses further work.

2. GEOLOGY AND PREVIOUS STUDIES OF THE SVARTSENGI GEOTHERMAL SYSTEM

2.1 Geological setting

Iceland is located astride the Mid-Atlantic Ridge, on top of a hotspot fed by a deep mantle plume (Figure 1A) situated under the Vatnajökull glacier (Wolfe et al. 1997). The Mid-Atlantic Ridge is spreading at a rate of approximately 17-19 mm/year in Iceland according to geological and geodetic observations (DeMets et al., 1994). Its boundary consists of rifting and transform segments separating the North-American and Eurasian tectonic plates; and is defined by a narrow zone of deformation revealed by the epicentres of earthquakes. In the south-west, the Reykjanes Ridge segment of the Mid-Atlantic Ridge comes onshore at the Reykjanes Peninsula, extending from there with an azimuth trend of 70° along the entire peninsula (Einarsson, 2008). The westward motion of the ridge with respect to the proximity of the deep mantle plume has resulted in an offset from the plate boundary. This oblique plate motion appears to be accommodated by left-lateral shear along a N76°E striking zone, at a rate of approximately -0.2 μstrain/year (Hreinsdóttir et al., 2001).

The Reykjanes Peninsula is almost completely covered by postglacial basaltic lavas, as well as with interglacial lavas and hyaloclastites (Clifton and Kattenhorn, 2006). It is characterised by four major volcanic systems- Reykjanes, Krísuvík, Brennisteinsfjöll and Hengill (Figure 1B) arranged en echelon along the plate boundary- each with its own individual magma supply. The main characteristic tectonic features on the peninsula are a vast number of NE-SW trending volcanic fissures, normal and oblique faults cross cut by a series of N-S oriented right lateral strike-slip faults. These fissures and normal faults are grouped into swarms and are named after the geothermal areas that occur in their central path- Reykjanes, Svartsengi, Krísuvík, Brennisteinsfjöll and Hengill (Einarsson, 2008).

At the Hengill triple junction, the Reykjanes Peninsula branches into the South Iceland Seismic Zone (SISZ) and the Western Volcanic Zone. The SISZ, characterised by an E-W plate motion is 10-15 km wide. It is a transform zone with faults delineating an E-W trending belt. Individual faults however, have a N-S trend, in a manner described as 'book-shelf' faulting (Einarsson et al., 1981). At the eastern end of the SISZ lies the Eastern Volcanic Zone (EVZ), characterised by long linear structures, normal faults, and eruptive fissures defining a strong NE trend (Einarsson, 2008).

2.1.1 The magnetic structure of the Reykjanes Peninsula

Magnetic field mapping is extremely valuable in determining dominant geological trends and discovering anomalous structures in the sub-terrain. A magnetic field map of the Reykjanes Peninsula is presented in Figure 2. A positive WSW-ENE trending magnetic anomaly is present along the southern and central part of the peninsula corresponding to the locations of the fissure swarms, with magnetic lows observed over the high-temperature geothermal fields.

2.1.2 Crustal deformation

Iceland's geographical location has made it a very tectonically and volcanically active area with a vast geothermal potential, subject to a range of crustal deformation processes. A variety of geodetic studies have been conducted since the 1930's to test Wegener's hypothesis of continental drift, as well as other subsequent theories of plate tectonics (Einarsson et al., 2006).

A large number of GPS surveys were performed in recent decades to estimate surface deformation resulting from plate spreading, earthquakes and magma movements (Sturkell et al., 1994; Hreinsdóttir et al., 2001; Árnadóttir et al., 2004; 2006; Keiding et al., 2008). A range of deformation signals detected by continuous GPS (CGPS) networks include; plate motion, co- and post-seismic activity, volcanism, geothermal utilisation, seasonal signals associated with the loading and unloading of snow, and glacial isostatic adjustment (Geirsson et al., 2011). Ground deformation due to geothermal exploitation will be further discussed in Chapter 3.

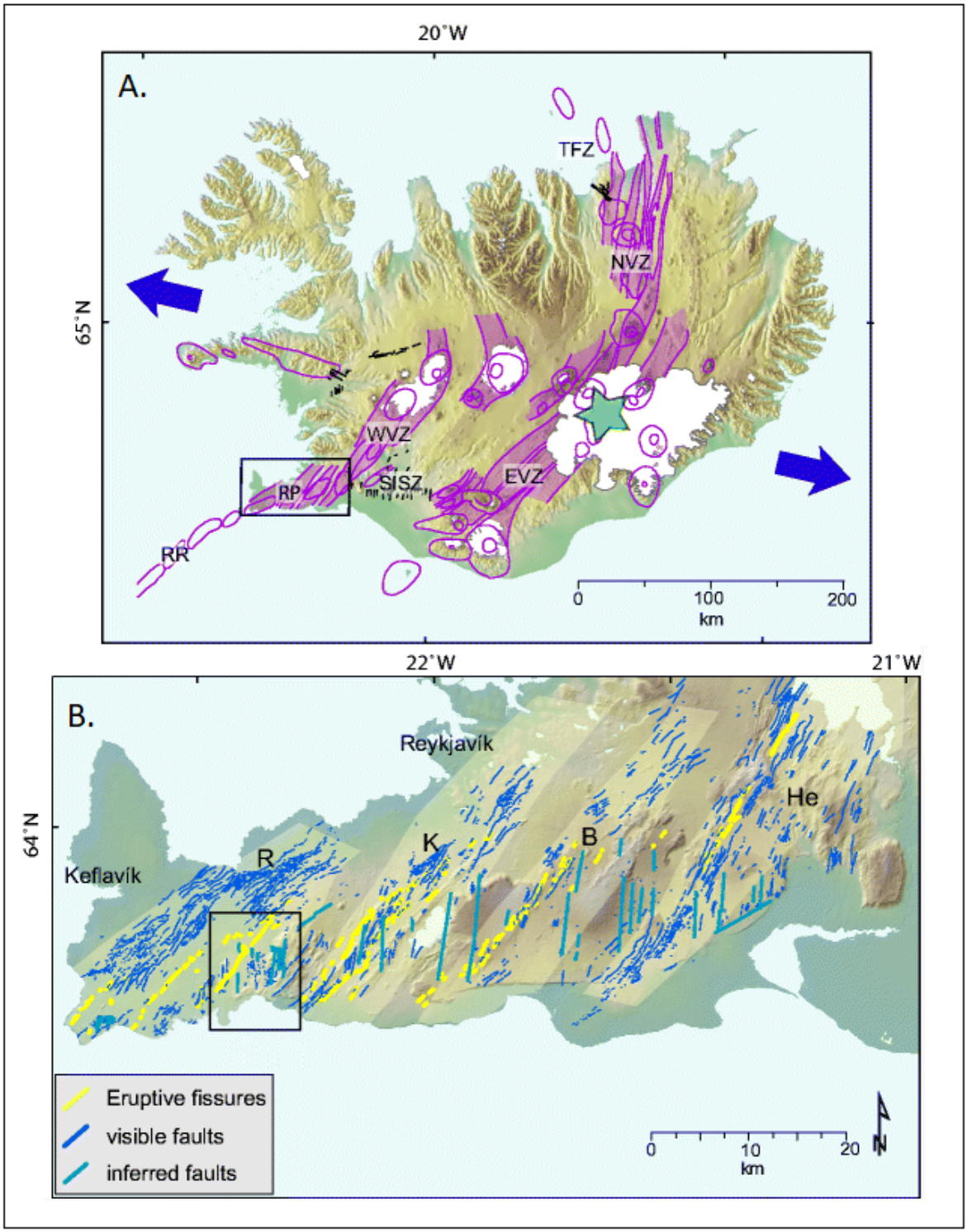

FIGURE 1: (A) Tectonic map of Iceland (Einarsson and Saemundsson, 1987) modified by Clifton and Kattenhorn (2006) showing ridge segments. The centre of the mantle plume is indicated by green star. The shaded purple areas denote volcanic systems, while the white areas represents the glaciers. Dark blue arrows indicate the direction of plate motion. (B). Map of Reykjanes Peninsula showing main tectonic features and fissure swarms (Clifton and Kattenhorn, 2006)

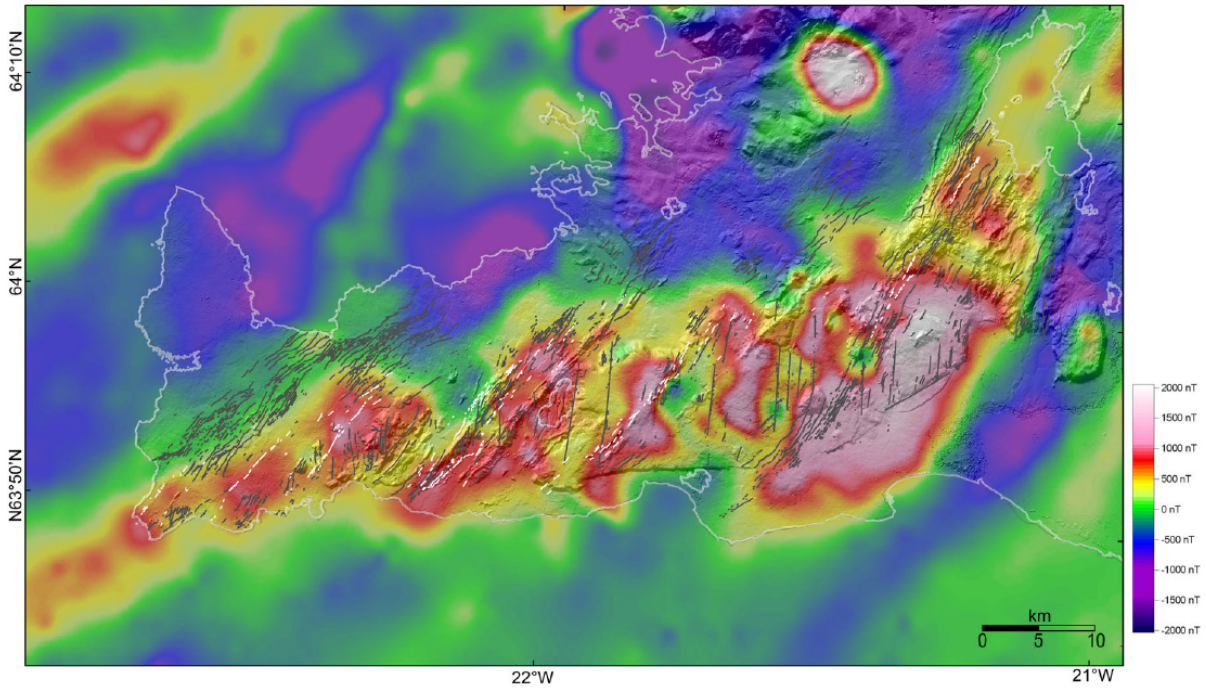

FIGURE 2: Magnetic anomaly map of the Reykjanes Peninsula (Kristjánsson and Jónsson, 2018)

2.2 Sub-surface geology

The Svartsengi-Eldvörp high-temperature system lies within the active volcanic zone of the outer Reykjanes Peninsula shown in Figure 1(B). The Svartsengi field lies within a basaltic lava field at low elevations between 20-30 m a.s.l. surrounded by low hyaloclastite mountains. Eldvörp is located approximately six kilometres WSW from the Svartsengi field. Though previously treated as separate systems, numerous studies have since proven a clear connection between Svartsengi and Eldvörp.

There are currently 25 wells drilled in the main Svartsengi field, and one in Eldvörp, attaining depths from a few hundred metres to just over 2000 m b.s.l.. The first three wells were drilled into the steam cap of the Svartsengi area in the early 1970s. Following a resistivity survey of the Reykjanes Peninsula (Georgsson, 1981), well 4 was successfully drilled into the deeper liquid-dominated high-temperature system. Lithological logs were subsequently constructed and the main alteration features were identified (Franzson, 1983; 1987). Further XRD and petrographic analysis of cutting samples were completed in an effort to evaluate aquifers and their geological connections.

An ENE-WSW cross-section of the first 12 wells is presented in Figure 3. It summarises the main alteration features, as well as the relationship between the alteration mineralogy found in wells 2-10 and their formation temperatures. The elevation of the mixed-layer clay and chlorite zones observed in the east corresponds to the reservoir's expanding steam zone. Further correlation between the resistivity, temperature and alteration mineralogy is discussed in Chapter 2.3.

Hyaloclastite layers of thickness 100 m are scattered throughout the profile, with an exception of the layer located between 300-600 m b.s.l., which was observed in most of the deeper wells. Although hyaloclastites are among the most porous and permeable rocks, they alter very readily into palagonite and then later, dominantly into clays (Franzson, 2017). This alteration significantly reduces its permeability. Hyaloclastite is therefore an appropriate caprock to the system, since it prevents inflow of the colder, higher pressured groundwater into the reservoir.

Dislocations of hyaloclastite boundaries observed Figure 3 indicate faults dissecting the strata. Intrusives, anticipated to range from dykes to sills (Franzson, 2017) are observed below 800 m depth.

The location of aquifers in Figure 3 were assessed on the basis of circulation losses that occurred during drilling. A notable absence of feed points between 400 and 600 m is attributed to the presence of the system's hydrothermal caprock. Franzson (2017) further concluded that aquifers above 500 m are connected to stratigraphic boundaries, while those in the reservoir (below 800 m) relate generally to intrusive boundaries.

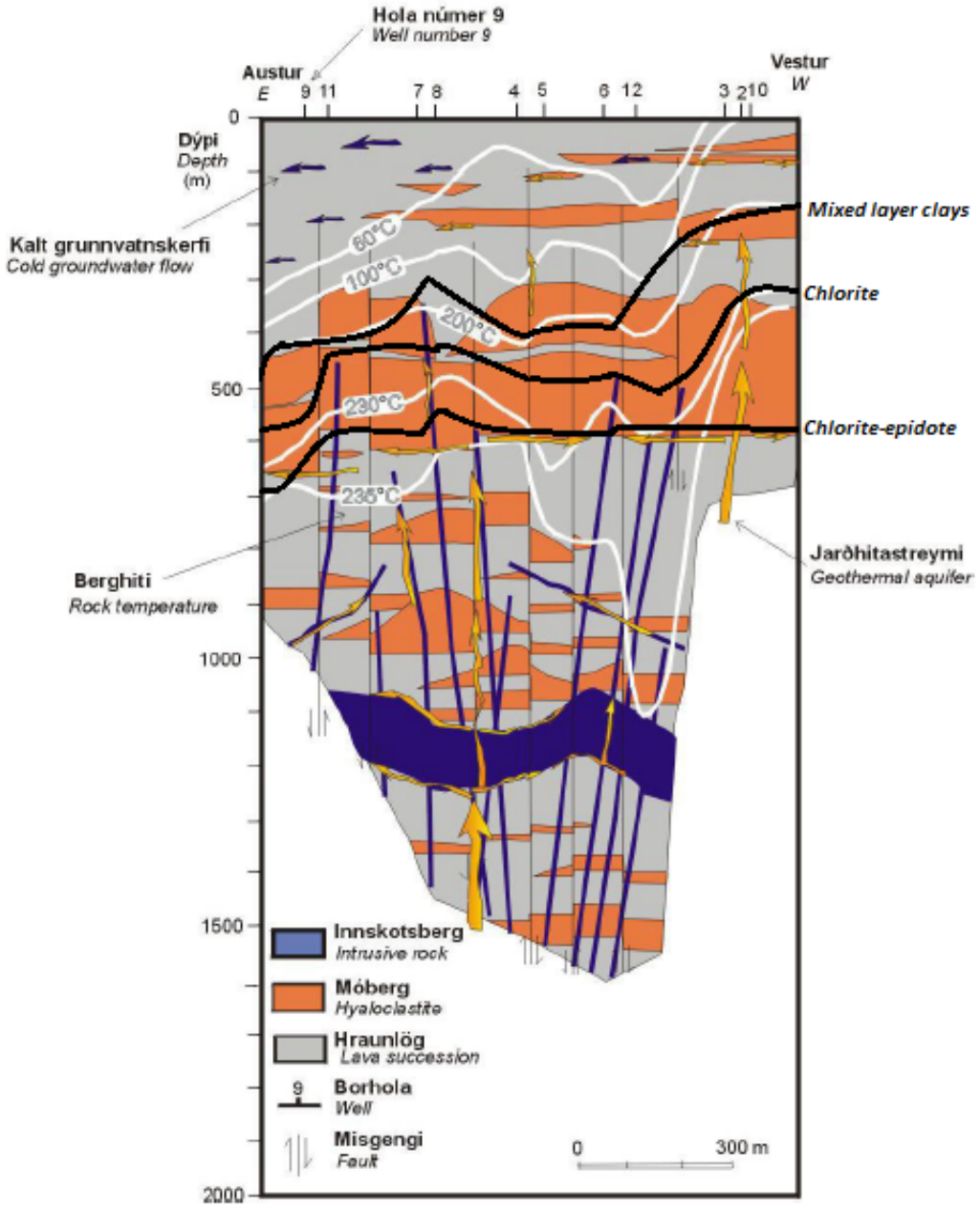

FIGURE 3: Geological cross-section, modified from Franzson (1990)

Geothermal reservoirs are characterised by extensive fracturing and high permeability (Gudmundsson and Thórhallsson, 1986). High permeabilities within the reservoir are thought to result from near vertical intrusives and fractures, resulting in high vertical permeabilities. A hydrological model of the Svartsengi area presented by Kjaran et al. (1979 and 1980) found the average permeability of the reservoir to be in the range of 100-150 mDarcy.

2.3 Resistivity structure

A DC resistivity survey conducted along the western Reykjanes Peninsula revealed a shallow, continuous east-west striking low resistivity zone along the Reykjanes plate boundary (Georgsson, 1981). Figure 4 illustrates the resistivity profile of the surveyed area at a depth of 800 m b.s.l. Highly conductive layer observed over the Svartsengi, Eldvörp and Reykjanes geothermal areas led Georgsson (1981) to infer that exploitable geothermal energy may be harnessed in the uppermost 1-2 km.

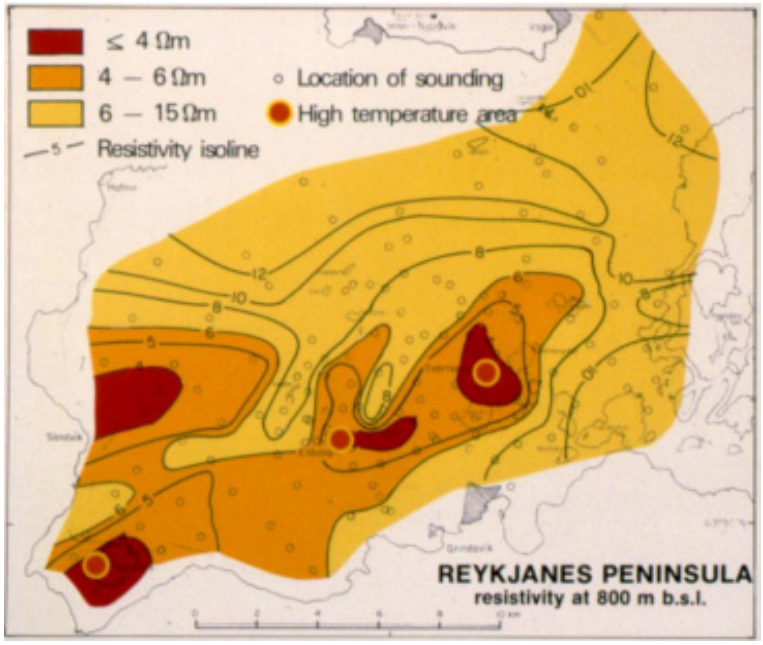

FIGURE 4: DC resistivity distribution of the Reykjanes Peninsula at 800 m b.s.l. (Georgsson, 1981)

A Transient Electromagnetic (TEM) survey aimed at delineating the high-temperature fields at Svartsengi and Eldvörp revealed a common reservoir extending from Eldvörp to the north of Svartsengi, with clearly defined boundaries, spanning an area of 30 km^2 at 1000 m b.s.l. (Karlsdóttir, 1998). The results presented in Figure 5 reveal a resistivity profile synonymous with that of a high-temperature geothermal field. The surface resistivity surveys of the high-temperature geothermal systems in the volcanic zones of Iceland have uncovered similar resistivity structures, correlating to the distribution of alteration mineralogy within the reservoir (Árnason et al., 2000). In these systems, the resistivity is relatively high in cold unaltered rocks outside the reservoir. A low-resistivity cap is observed on the outer, upper margins of the reservoirs, underlain by a highly resistive core.

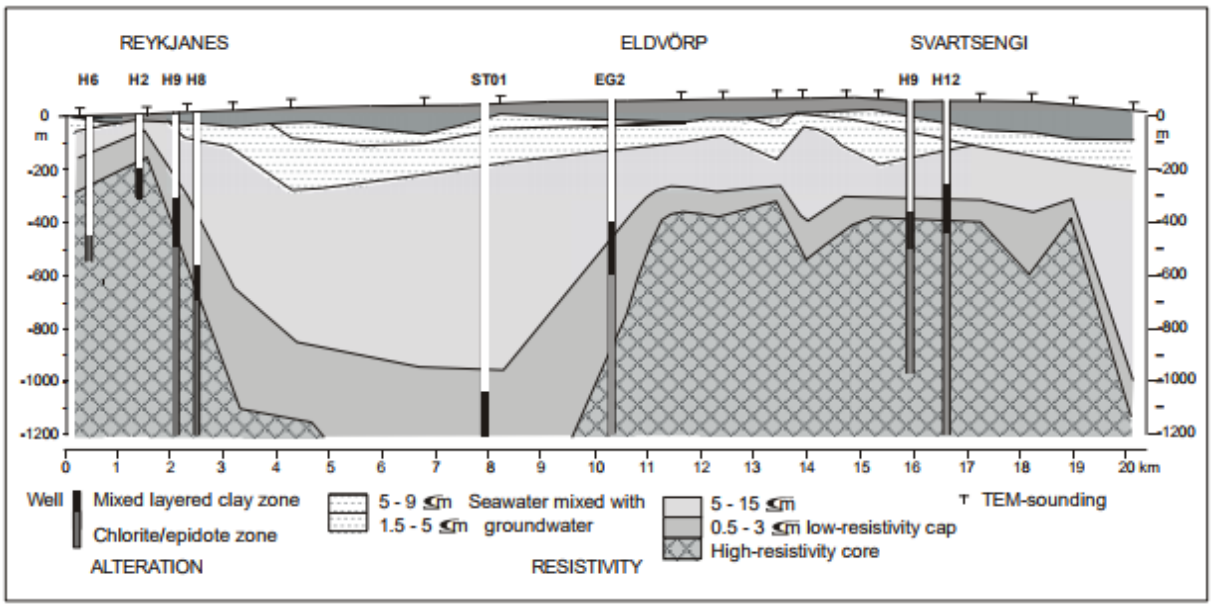

FIGURE 5: ESE-WNW trending TEM cross-section along the outer Reykjanes Peninsula (Karlsdóttir, 1998)

A vast magnetotelluric (MT) network was set up to further study the resistivity profile of the Svartsengi-Eldvörp geothermal field (Karlsdóttir and Vilhjálmsson, 2015). The resistivity structure obtained confirms the earlier TEM model by Karlsdóttir (1998). The high resistivity core is observed prominently in Figure 6A at 850 m b.s.l. clearly extending WSW as a ridge towards Eldvörp. At 3000 m depth, a high-resistivity anomaly of approximately 100 Ωm (denoted by the blue areas in Figure 6B), intersected by a WSW-ENE trending lower resistivity zone extends through Eldvörp and Svartsengi. This zone lies along the narrow seismic zone that marks the axis of the oblique rift along the Reykjanes Peninsula. The resistivity profile may therefore be indicative of the intersection of the seismic zone with the Reykjanes Peninsula and Svartsengi fissure swarms- indicating possible heat sources (Karlsdóttir and Vilhjálmsson, 2015).

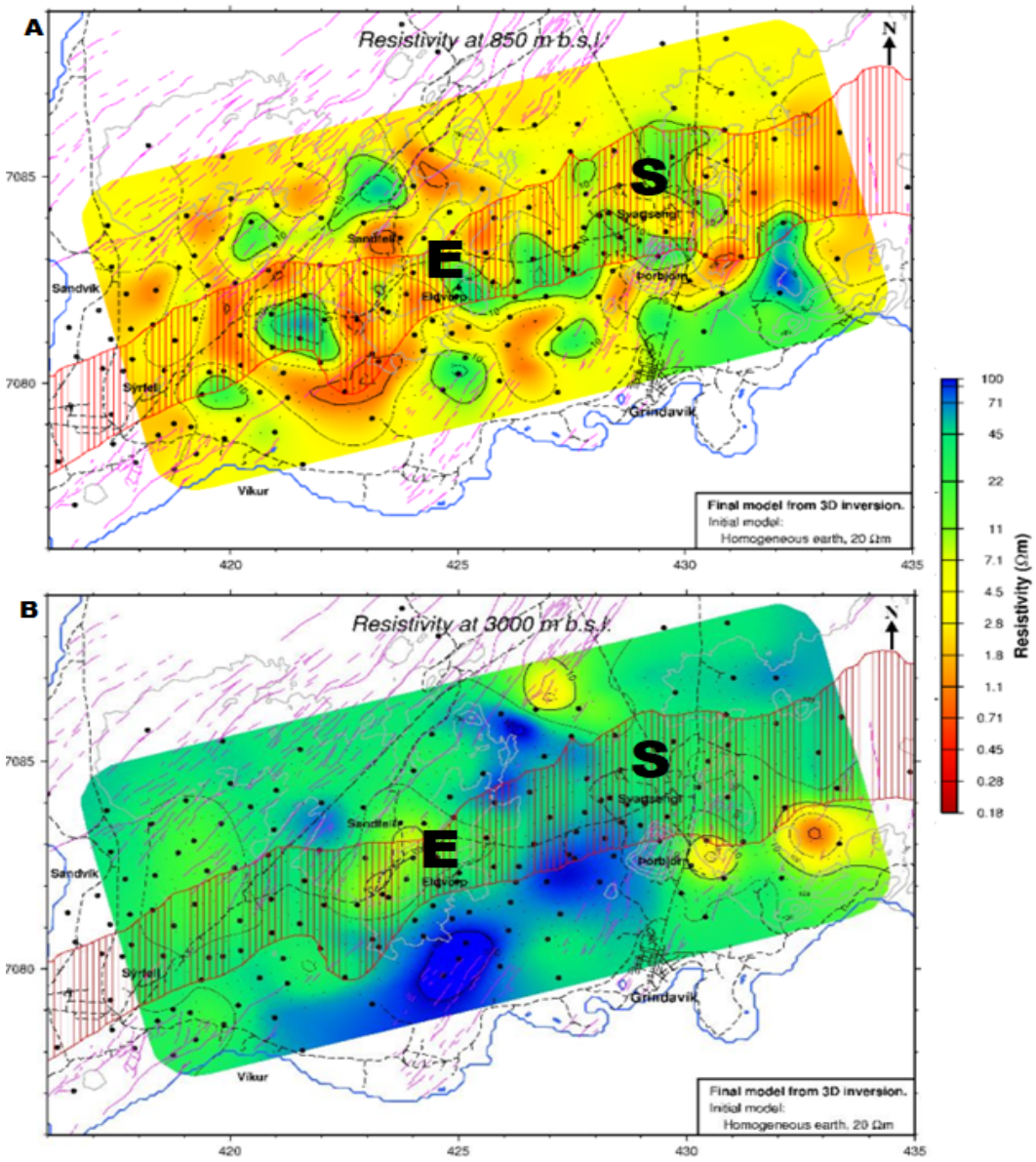

FIGURE 6: Resistivity profile, modified from Karlsdóttir and Vilhjálmsson (2015) of the Svartsengi-Eldvörp field at (A) 850 m b.s.l. and (B) 3000 m b.s.l. showing the locations of Eldvörp (E) and Svartsengi (S)

Resistivity cross-sections (locations shown in Figure 7) traversing W-E through Eldvörp and Svartsengi, extending to depths of 3000 and to 8000 m b.s.l., illustrate the continuous low-resistivity cap that denotes the boundary of the geothermal areas. Svartsengi and Eldvörp appear to be part of the same geothermal system, each however with different upflow zones as illustrated in both Figures 7 and 8.

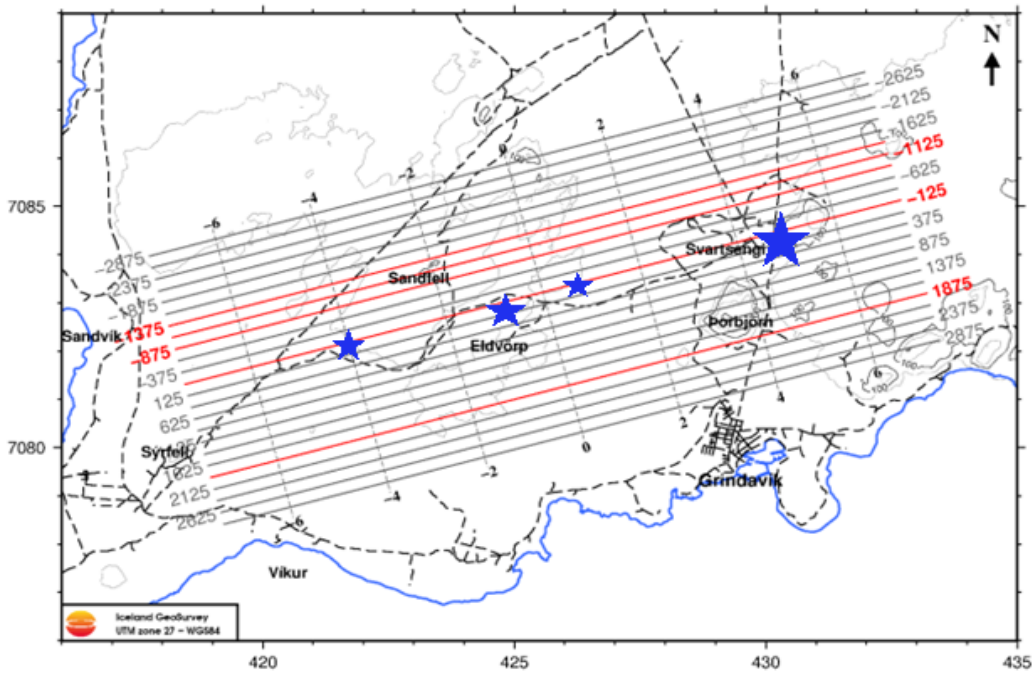

FIGURE 7: Map of the Svartsengi region showing the locations of W-E cross-sections, modified from Karlsdóttir and Vilhjálmsson (2015) with blue stars indicating the location of upflows

Figure 8 reveals the upflow zones, or the up-doming of the high-resistivity core into the overlying low resistivity. With respect to the origin point, instances of up-doming are observed at 4-5 km towards the east under Svartsengi; at 1 km to the east between Svartsengi and Eldvörp; at approximately 1 km to the west under Eldvörp; and another at about 4-5 km towards the west of the surveyed area. A clear reservoir boundary, consistent with Karlsdóttir (1998) is observed west of Eldvörp, where the cap rock dips vertically below depths of 3000 m b.s.l.

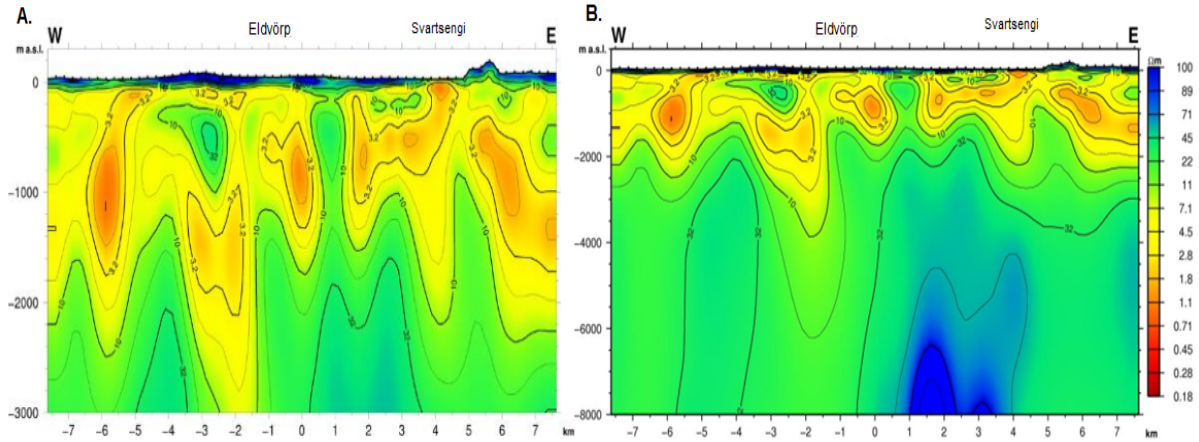

FIGURE 8: Resistivity cross-section through Svartsengi down to (A) 3000 and (B) 8000 m depth b.s.l., modified from Karlsdóttir and Vilhjálmsson (2015), with arrows pointing towards upflow areas

A comparison between the resistivity profile and thermal alteration derived from well data shows that resistivity measurements reflect the alteration in the geothermal field (Karlsdóttir, 1998). The low-resistivity cap coincides with the more conductive smectite-zeolite and mixed layer clay zones, whereas the high resistivity core corresponds to the chlorite-epidote zone. This observation is of utmost importance, since the temperature dependence of the alteration mineralogy makes it possible to interpret the resistivity profile in terms of temperature. The upper boundary of the low resistivity cap layer

corresponds to temperatures within the range of 50 and 100°C, while the transition from the low resistivity cap to the resistive core corresponds to temperatures between 230 and 250°C. Providing that the thermal alteration is in equilibrium with temperature of the geothermal system, the mapping of the resistivity structure may in fact be the mapping of isotherms (Árnason et al., 2000).

2.4 Formation temperature

Figure 9 shows the location of wells within the Svartsengi geothermal system. Formation temperatures were calculated through the analysis of numerous temperature logs, with an accuracy of 2-3°C (Björnsson and Steingrímsson 1991). The determination of the formation temperature is valuable in geothermal resource estimation, as it represents the initial, undisturbed temperature of the system. Formation temperature profiles displayed in Figure 10 reveal uniformed temperatures of 240°C below 900 m depth within the main production zone. Temperatures are, however, observed to increase towards the southwest, with higher temperatures of over 268°C at Eldvörp (Figure 11).

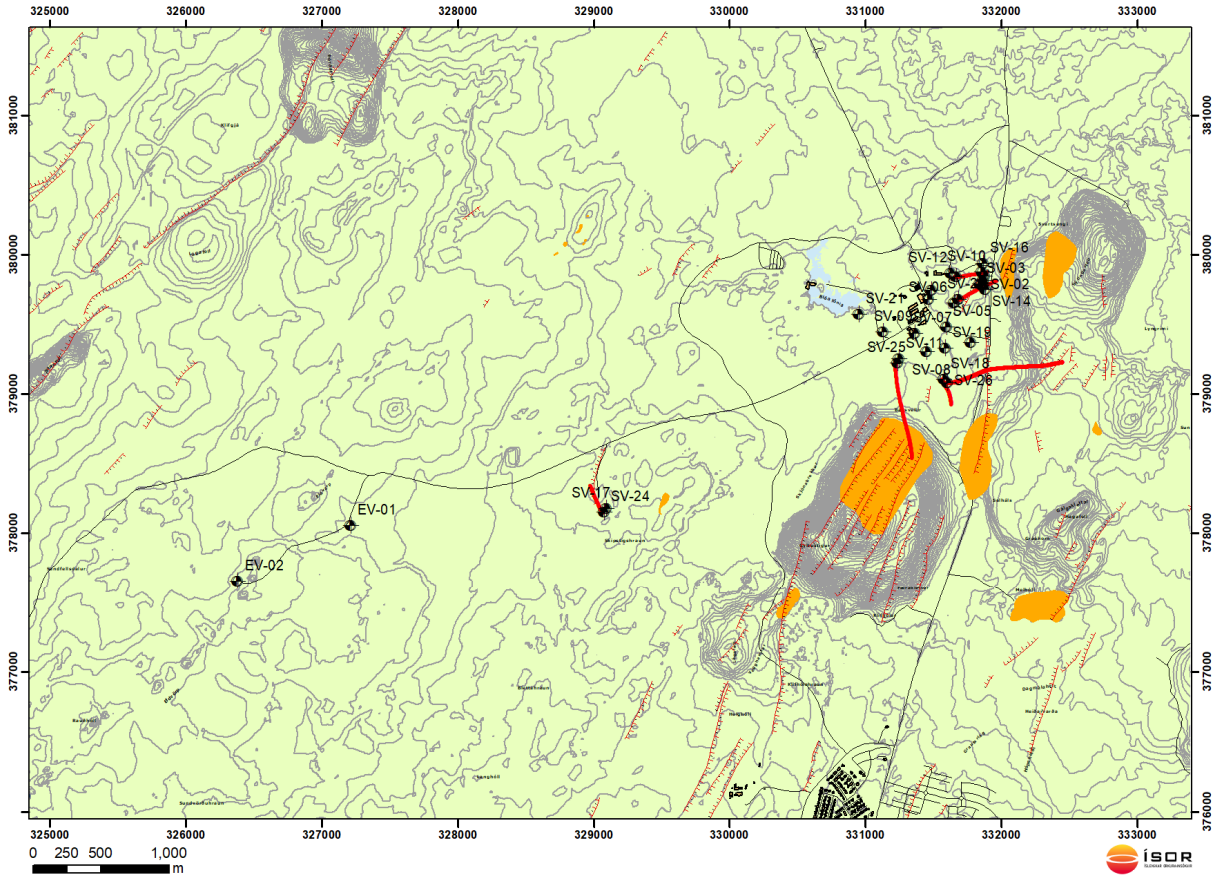

FIGURE 9: Map revealing the location of boreholes within the Svartsengi geothermal system (Gudmundsdóttir, 2016); directionally drilled wells are indicated in red

The formation temperature profiles in Figure 10 and Figure 11 reveal pertinent information on the physical characteristics of the reservoir (Jónsson, 2012). There are two observable zones within the reservoir. Wells SV-02, SV-03 and SV-10 lie on the boiling point curve, and are thus producing from the steam zone. Although they are not included in the analysis for this thesis, wells SV-14, SV-16, SV-20, SV-22 and SV-23 are also producing from the shallow steam zone while the remaining wells are producing from the liquid-dominated reservoir. In these wells, the temperature remains relatively constant with depth, indicating highly permeable reservoir with good convective mixing (Grant and Bixley, 2011).

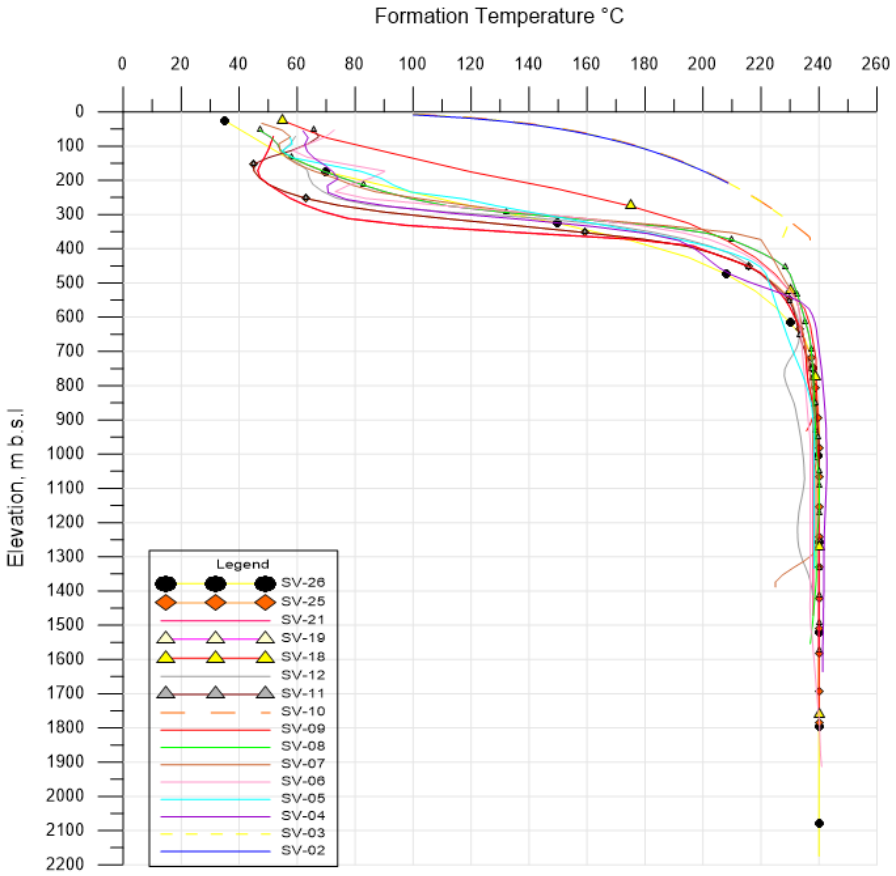

FIGURE 10: Formation temperature profiles of boreholes within the main well field

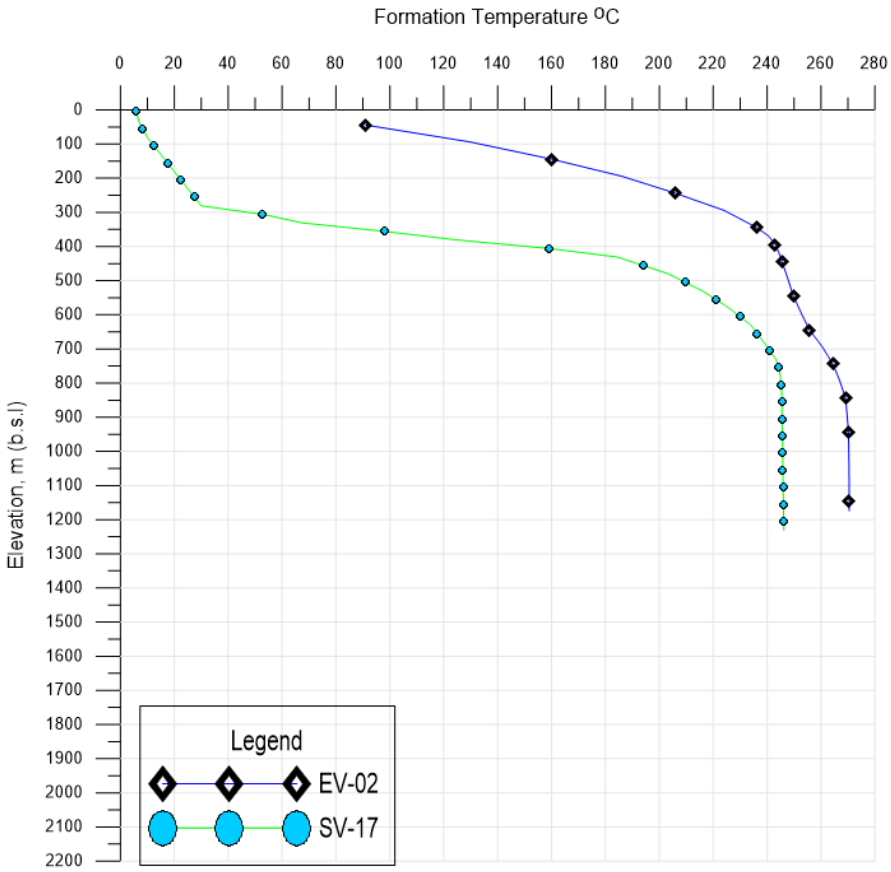

FIGURE 11: Formation temperature profiles for EV-02 (Eldvörp) and SV-17

2.5 Conceptual model

A variety of conceptual models have been developed to reflect the status of the Svartsengi Geothermal area (Björnsson and Steingrímsson, 1991; Franzson, 1983; 1987; 2017; Gudmundsson and Thórhallsson, 1986). Conceptual models are spatial representations of the physical features of a system incorporating essential features of the system, obtained through thorough interpretation of all available exploration (geological, geochemical, and geophysical), drilling and well data (Grant and Bixley, 2011). They compile information not only on the system's geological structure and reservoir boundaries, but also on the temperature, pressure and fluid interactions within the field.

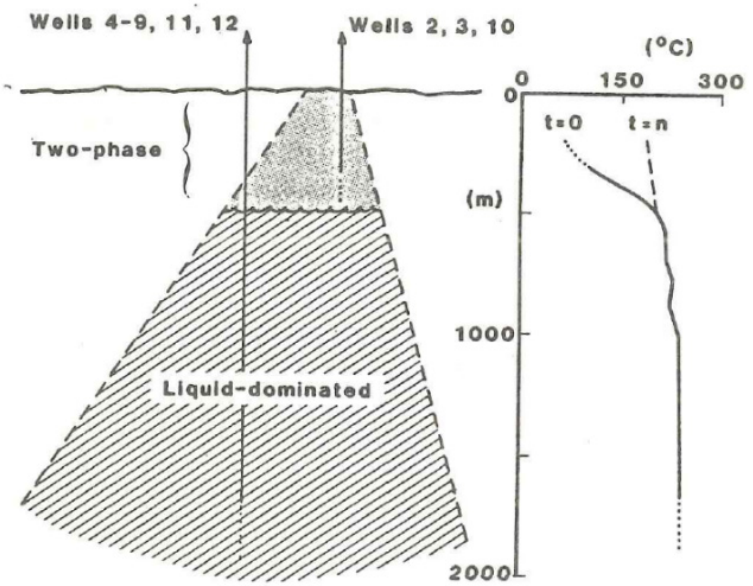

FIGURE 12: Early conceptual model, developed by Gudmundsson and Thórhallsson (1986) showing a two-phase reservoir

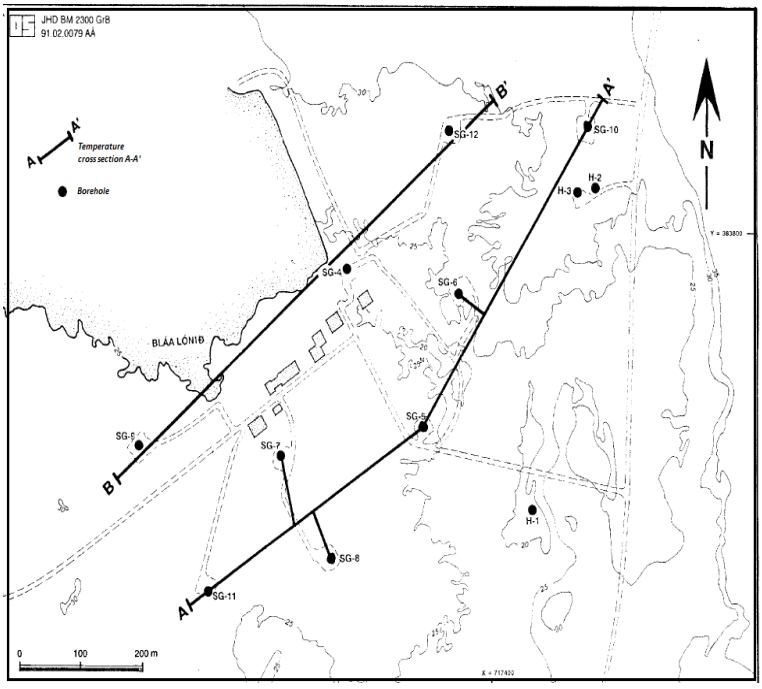

FIGURE 13: Location of temperature cross-sections A-A' and B-B' (Björnsson and Steingrímsson, 1991)

Gudmundsson and Thórhallsson (1986) describe the Svartsengi geothermal area as a large unconfined liquid-dominated reservoir of hot water-filled rock, surrounded by warm and cold aquifers. Steam leaks observed near shallow wells SV-2, SV-03 and SV-10 provided evidence of the development of a steam zone in the north-east portion of the field after a few years of fluid production. This was made evident by borehole data, which revealed temperatures profiles on or near the boiling point curve. A conceptual model consisting of a pyramid-shaped liquid-dominated reservoir, overlain by a two-phase steam zone (Figure 12) was developed. The model assumed a liquid-dominated reservoir with temperatures between 235°C to 240°C extending from below 500 m b.s.l. to at least 2 km depth. It was furthermore assumed to be completely isolated from the warm surface groundwater system between 0 to 300 m depth.

Early formation temperature cross-sections are illustrated in Figure 13 and Figure 14. This confirmed the location of three aquifer systems within the Svartsengi field; warm groundwater system located between depths of 30-300 m flowing laterally to the south-west; the main liquid-dominated reservoir at depths exceeding 600 m; and a two-phase chimney in the north-east part of the field. Further analysis of the temperature profiles revealed a temperature anomaly close to well 4, which Björnsson and Steingrímsson (1991) interpreted as the main upflow zone of the geothermal system, feeding the permeable horizontal intrusive layers as well as the steam chimney of the two-phase system.

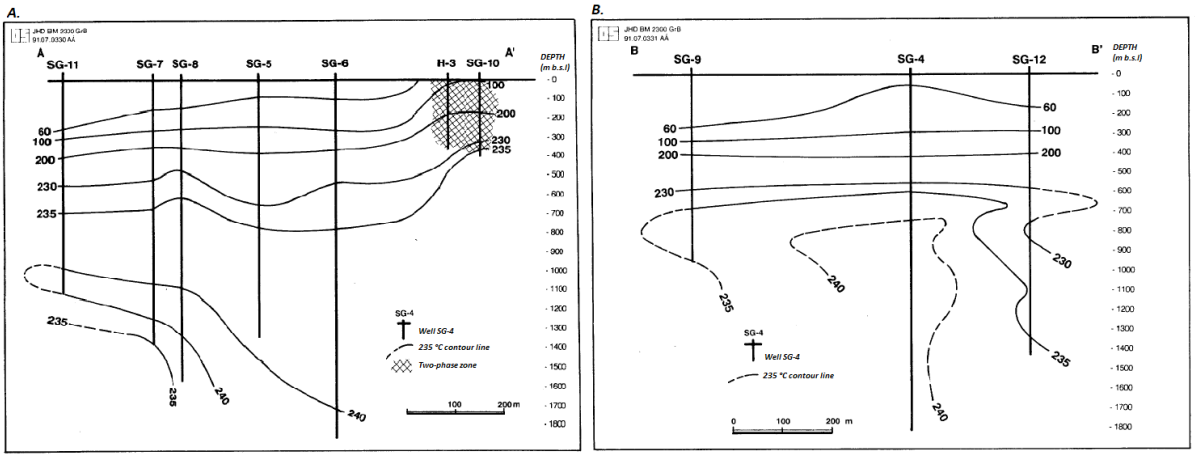

FIGURE 14: Temperature cross-sections (A) A-A' and (B) B-B'
(Björnsson and Steingrímsson, 1991)

An updated conceptual model was then proposed (Björnsson and Steingrímsson, 1991) and is presented in Figure 15, which incorporates these observations. Two upflow zones were illustrated, the other being an upflow along the Eldvörp fissure swarm earlier proposed by Franzson (1987) which also serves as a recharge to the reservoir (Figure 16).

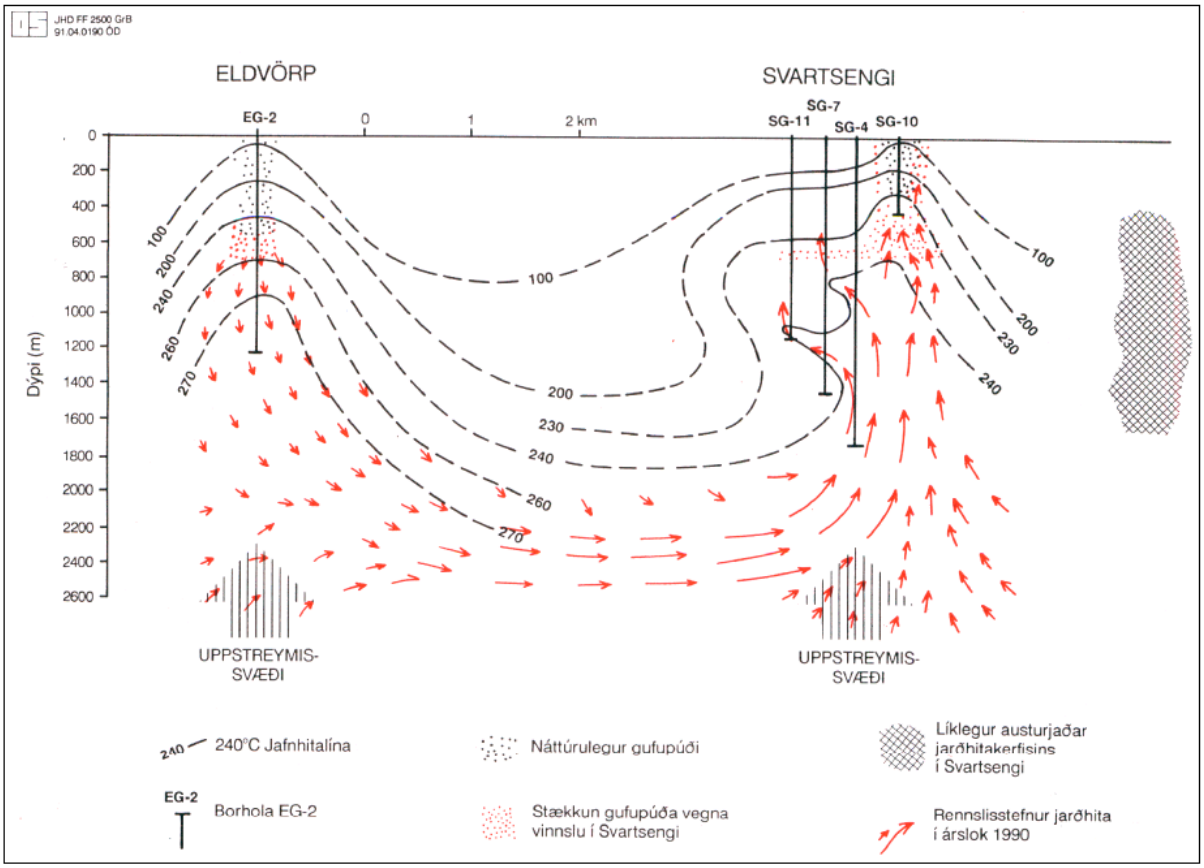

FIGURE 15: Temperature model of the Svartsengi reservoir (Björnsson and Steingrímsson, 1991)

Similarly, Franzson (2017) envisaged two reservoirs, with the upper one extending from 600 m b.s.l. down to depths exceeding 2000 m b.s,l. He proposed that the upper reservoir is heated from either surrounding low temperature aquifers, or by the deep hot upflows from the lower reservoir. The lower reservoir however, may be related to the deep convective flows associated with the upflow along the volcanic fissures.

2.6 Earlier reservoir models

The Svartsengi geothermal field has been under exploitation since 1976, and has a well-documented production and pressure drawdown history. During the first few years of production, a steam zone developed in the north-east part of the field, and many reservoir models have since been constructed to predict the effect of increased production. Bödvarsson (1988) successfully created a simple numerical model to investigate the effects of the two-phase zone on the pressure decline (Figure 17). It assumed a radial two-dimensional model with an average permeability of 85 mDarcy. The model revealed that about 25% of the fluids recharging the wellfield come from the two-phase zone, with a counter-flow of steam and water observed in the steam zone.

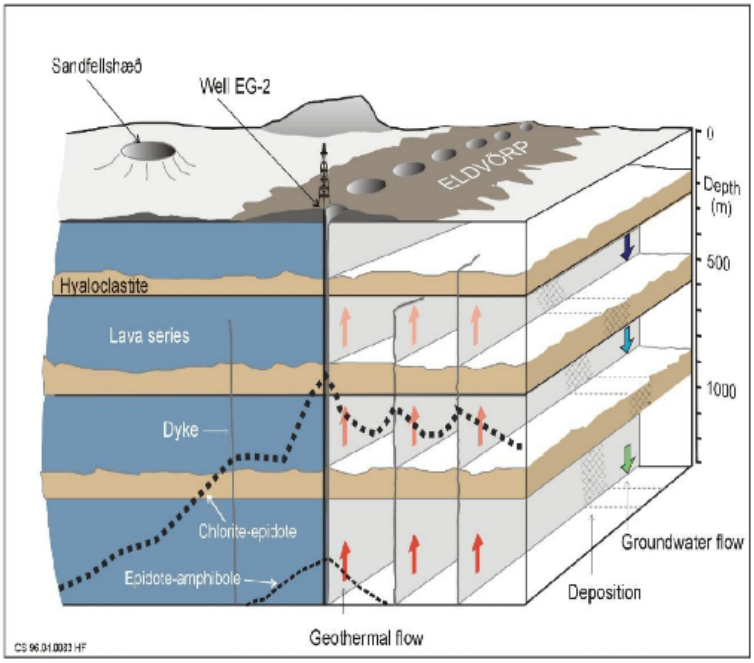

FIGURE 16: Geological conceptual model of Eldvörp, modified from Franzson (1987)

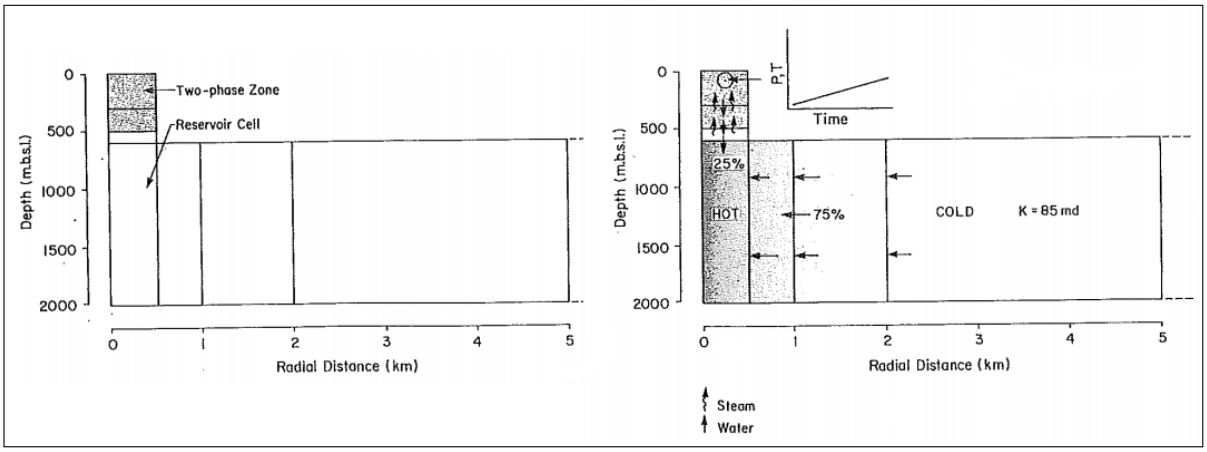

FIGURE 17: Radial reservoir model showing the assumed steam and liquid flow patterns in a simple numerical model of the Svartsengi system, with the location of hot and cold fluid zones specified (Bödvarsson, 1988)

Later, due to a planned expansion of the Svartsengi power plant, a simple radial model, consisting of a vertical steam-zone column and a radial, horizontal base layer was constructed and was able to accurately simulate the conditions in the natural and production state of the reservoir (Björnsson 1999). This model (Figure 18) consists of a multi-layer centre covering an area of 2 km^2, which simulates the steam zone. Underlain is a radial layer extending laterally to 9 km, which at the time was the measured extent of land subsidence. Permeabilities ranged between 20 to 100 mDarcy. Two feed zones are present in the model; the upper feed zone at 400 m depth is used to represent the shallow steam zone, and the lower feed zone at 1000 m depth accounts for all remaining production at Svartsengi. A 'safety valve' in the form of a productivity index was applied for the model to simulate the discharge of fluid to the surface.

More recently, the production model by Ketilsson (2007) in Figure 19 reproduced the conditions of the main production area within the Svartsengi reservoir. This model took into account more physical

conditions and properties that have been observed in the Svartsengi geothermal field, and a rather good fit was found to observed data series for pressure history, temperature and production enthalpy.

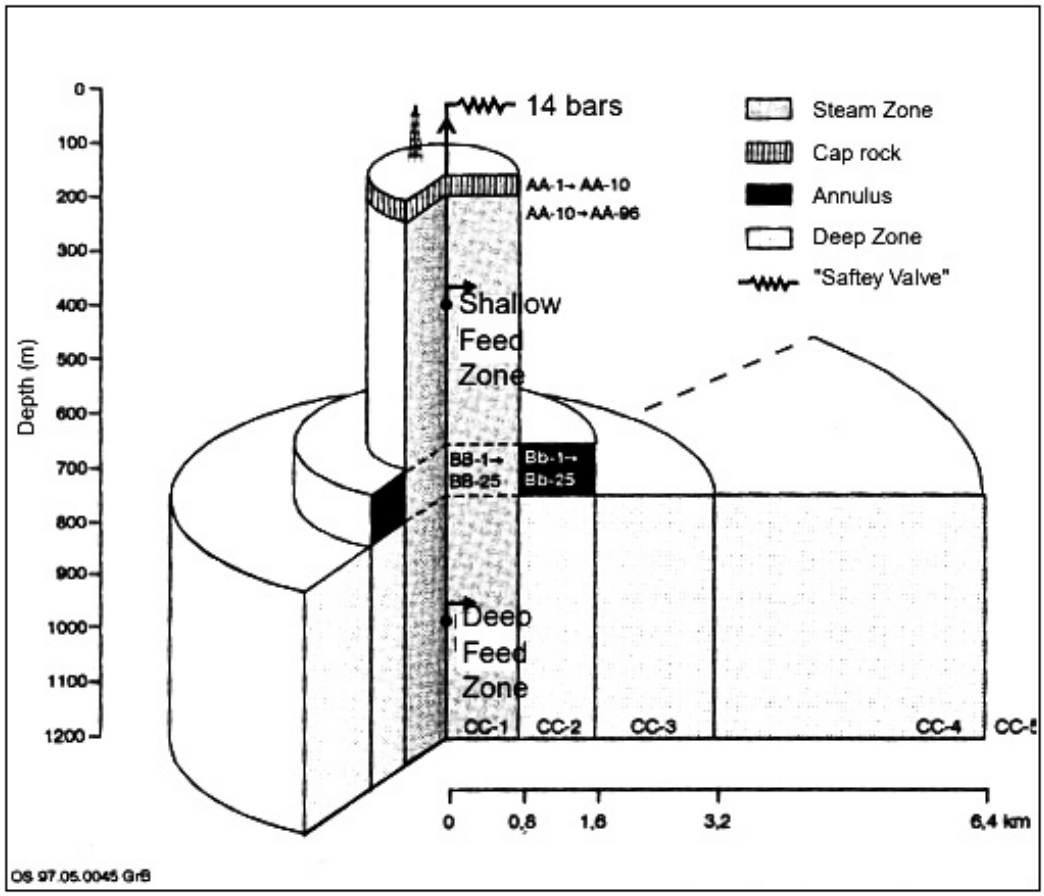

FIGURE 18: Reservoir model by Björnsson (1999) used to predict the performance of the steam zone in the Svartsengi reservoir

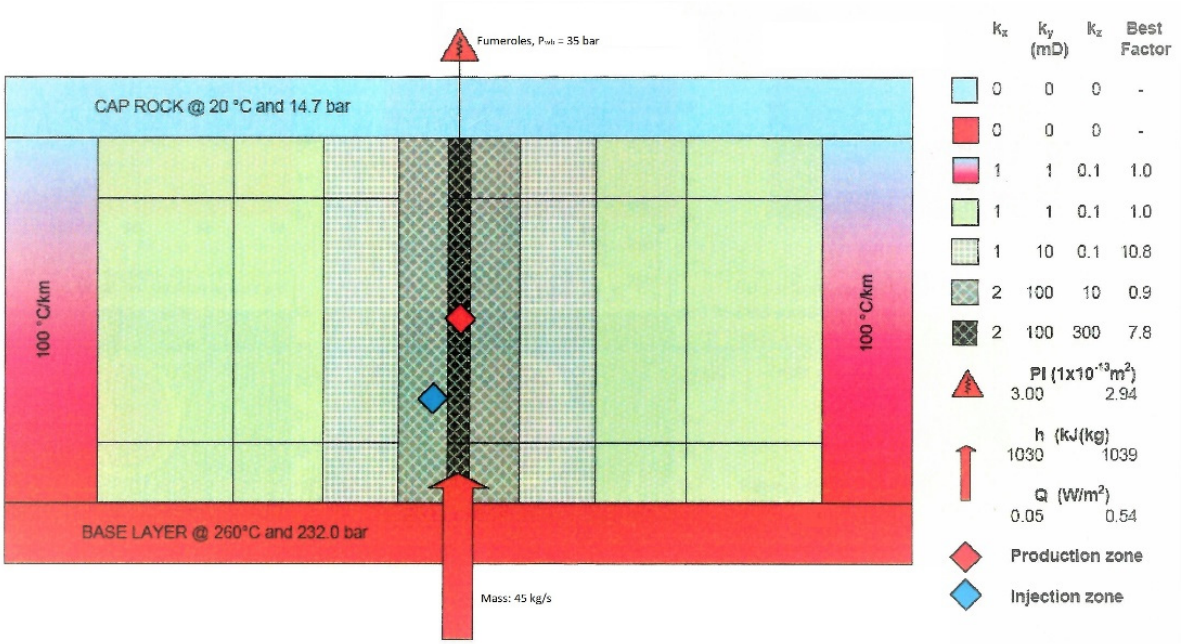

FIGURE 19: Production model showing the permeability distribution of the main well field at Svartsengi (Ketilsson, 2007)

3. MASS EXTRACTION AND RESERVOIR RESPONSE

3.1 Production history

Production at Svartsengi commenced in October 1976. Figure 20 shows the annual average production and reinjection at Svartsengi from 1976 to 2016. There was a step-wise increase in production from 1976 to 1982, from 0.36 to 7.73 million tons per year, equivalent to 11.43 and 245 kg/s average production, respectively. During the following years, from 1983 to 1999, the average annual production fluctuated in the range of 7.21 to 10 million tons, equivalent to 220 and 300 kg/s average production, respectively. From 2000-2006, the average production declined slightly, but has increased since 2006. The total production in 2016 was 14.4 million tons, equivalent to 456 kg/s on average. This represents a 6% decrease from 2014, when production was 15.4 million tons, equivalent to 488 kg/s - the maximum production that has occurred at Svartsengi during the period 1976-2016.

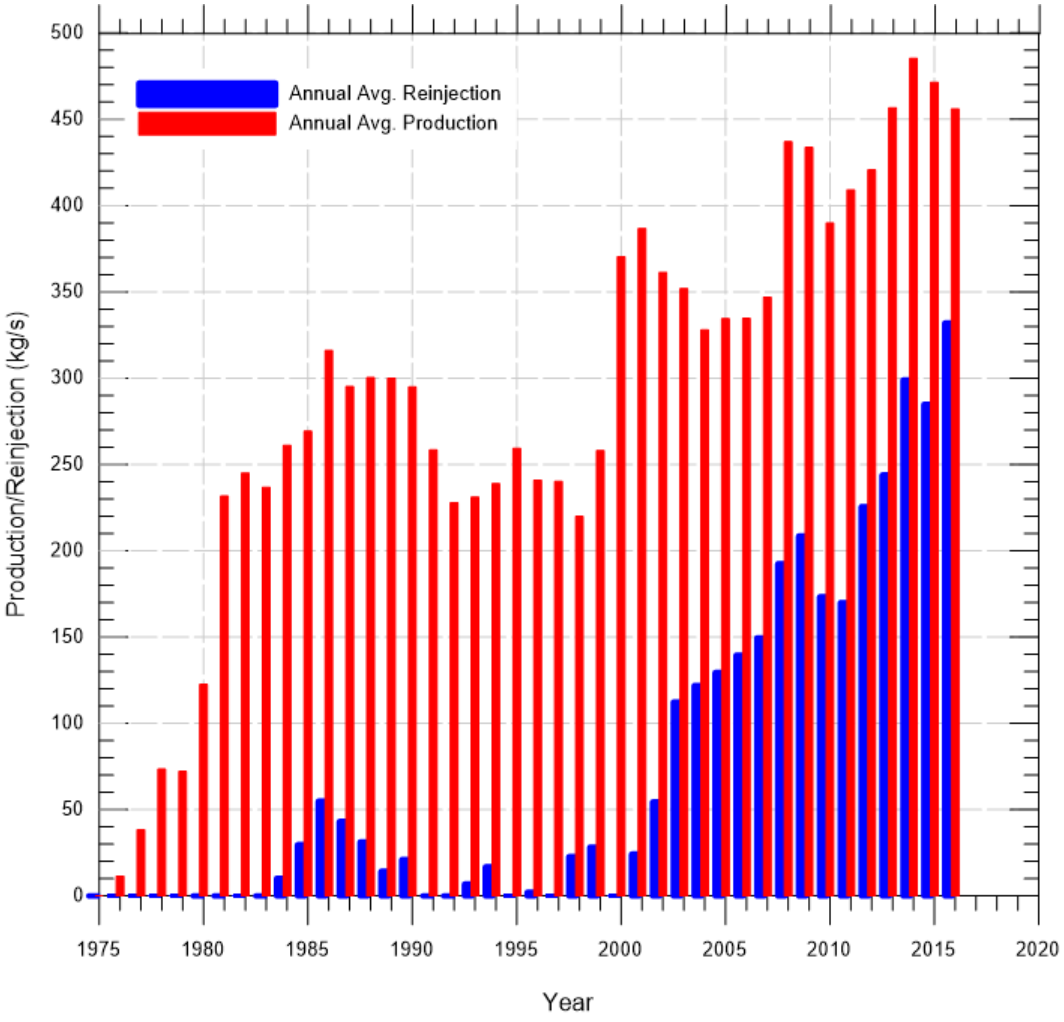

FIGURE 20: Production history at Svartsengi for the period 1975-2016

3.1.1 Reinjection

The first reinjection well, SV-12, was drilled in 1982, to a depth of 1488 m b.s.l.. It was drilled based on two criteria: it was drilled within the confirmed reservoir; and if reinjection into the well was not feasible, the well would then be utilised for production (Gudmundsson, 1983). The average annual rate of reinjection is presented alongside the average annual production in Figure 20.

Well SV-12 was used for reinjection during 1984-1988, however reinjection was discontinued following recommendations provided as a result of a reinjection test performed in 1982 (Gudmundsson, 1983),

which indicated that cooling will occur as a result of long-term reinjection. When reinjection into SV-12 was discontinued, reinjection into SV-05 commenced and continued until 1990. In 1993, intermittent reinjection continued into SV-06 until 2000. These wells are all located in the main production field, and if reinjection would have continued at the same flow rates, though it may offer some pressure support, rapid cooling would have occurred (Thórhallsson et al., 2004).

SV-17 was drilled in 1998 as a reinjection well, about 2.3 km away from the main well field (Figure 9). It was drilled with the intention of providing adequate pressure support for the system, without the risk of cooling. Reinjection here commenced in 2000. A second reinjection well, SV-24, was later drilled into the same platform as SV-17.

In 2016, the average annual reinjection into the Svartsengi reservoir was 10.5 million tons, equivalent to 332 kg/s. This is equal to approximately 72.8% of the production in 2016, representing a net production of 3.9 million tons, equivalent to 124 kg/s during that year.

3.1.2 Pressure drawdown

One of the characteristics of the Svartsengi reservoir is an almost uniform pressure distribution throughout the field due to very high permeabilities. Pressure histories are therefore very similar for all wells. The observed pressure drawdown at an elevation of 900 m b.s.l. for the period 1980-2017 is depicted in Figure 21.

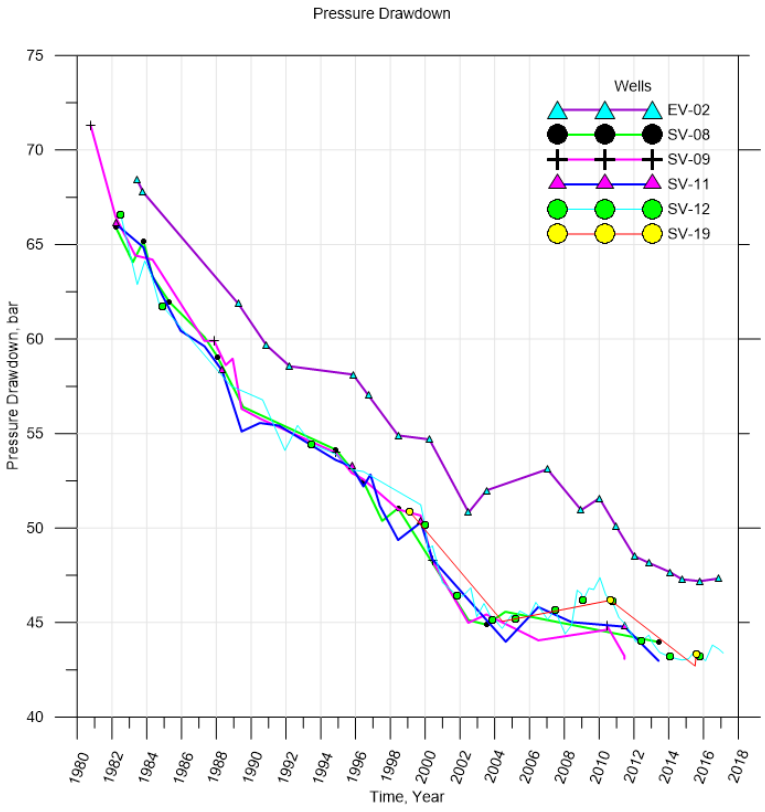

FIGURE 21: Pressure decline (1980-2017) at 900 m b.s.l. in SV-08, SV-09, SV-11, SV-12, SV-19 and at 1100 m b.s.l. in EV-02

The drawdown rate in the liquid-dominated part of the reservoir has been similar in all the wells drilled into the field but the drawdown has been highly variable during the observed period (Figure 21). The total drawdown in Svartsengi since 1975 is approximately 34 bars. The pressure drawdown in Eldvörp at 1100 m depth follows the same trend as the decline in Svartsengi, with pressure in both fields reacting strongly to reinjection in Svartsengi.

Before large-scale reinjection commenced in 2000, there was a rapid pressure decline in Svartsengi and Eldvörp of approximately 22 bars and 15 bars, respectively. As reinjection steadily increased during the following years, there was little pressure decline in Svartsengi during 2004-2008, followed by pressure recovery during 2009-2010, which was attributed to down-flow in a newly drilled reinjection well (Gudmundsdóttir, 2016). EV-02 however, appears to be more affected by reinjection into SV-17, with a greater pressure recovery observed there between 2002 and 2007. The pressure drawdown in Eldvörp is a few bars less than in Svartsengi since there is no production in that part of the field. This observed pressure connection between Svartsengi and Eldvörp corroborates the hydrological connection between the two areas and therefore confirms that Eldvörp is a part of the Svartsengi geothermal field (Gudmundsdóttir, 2016)

3.2 Subsidence and changes in elevation

3.2.1 GPS and geodetic levelling

Ground deformation may result from load variation on elastic plates of the Earth's crust. Similarly, the extraction of fluid during geothermal exploitation creates a pressure reduction within the reservoir, thereby resulting in compression of the rock matrix. Subsidence in the Reykjanes Peninsula has been extensively monitored since the onset of production, initially by levelling and gravity measurements (Eysteinssom, 1993; 2000), and later on additionally by GPS (Magnússon, 2009; 2013; 2015) and Interferometric Synthetic-Aperture Radar (InSAR) analysis (Vadon and Sigmundsson, 1997; Keiding et al., 2008; Receveur, 2018). Extensive geodetic levelling conducted between 1975 to 1992 (Eysteinsson, 1993) revealed a vast, elongated subsidence bowl spanning an area of over 100 km^2, with maximum subsidence centred on the Svartsengi well-field. The subsidence rates during the time intervals; 1975-1982, 1982-1987, 1985-1992 and 1992-1999 (Eysteinsson, 2000) are presented in Figure 22.

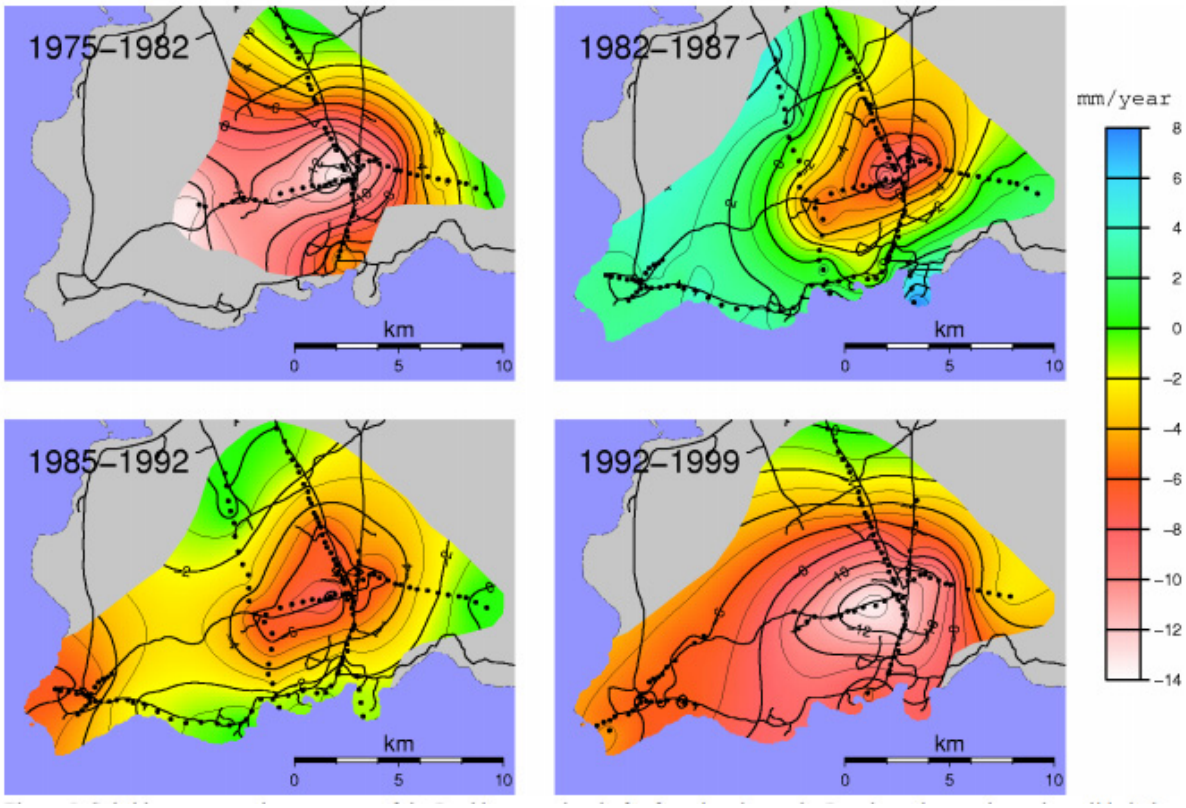

FIGURE 22: Average subsidence rate in the Reykjanes Peninsula from 1975 to 1999 (Eysteinsson, 2000)

The average rate of subsidence in Svartsengi during the first 7 years of production was 14 mm/year, with the maximum located directly at the centre of the wellfield. Between 1982 and 1987, an E-W elongated subsidence ellipse had formed (Eysteinsson, 2000). The mean subsidence rate reduced to 7-8 mm/year from 1982 to 1992, however, during the time interval 1985-1992, the centre of subsidence shifted slightly to the west. The average subsidence increased during 1992-1999 to 14 mm/year, with a further west-ward displacement of the point of maximum subsidence. The mean subsidence rate during 1999-2004 decreased to approximately 6 mm/year (Magnússon, 2009), which correlates to the onset of reinjection in well SV-17 in 2000 (Figure 20). From 2004-2008, there was an increase to 12 mm/year (Magnússon, 2009) that corresponds to an increase in production during this period. From 2008 to 2014, however, there was a slight decrease in the subsidence rate in Svartsengi to approximately 10 mm/year (Magnússon, 2015). This represents an average rate of 10 mm/year during 1999-2014. This decrease in subsidence may be explained by the increase in reinjection during this period (Figure 20). Figures 22–24 present subsidence maps for the period 1999-2014 (Eysteinsson, 2000; Magnússon, 2009; 2013; 2015).

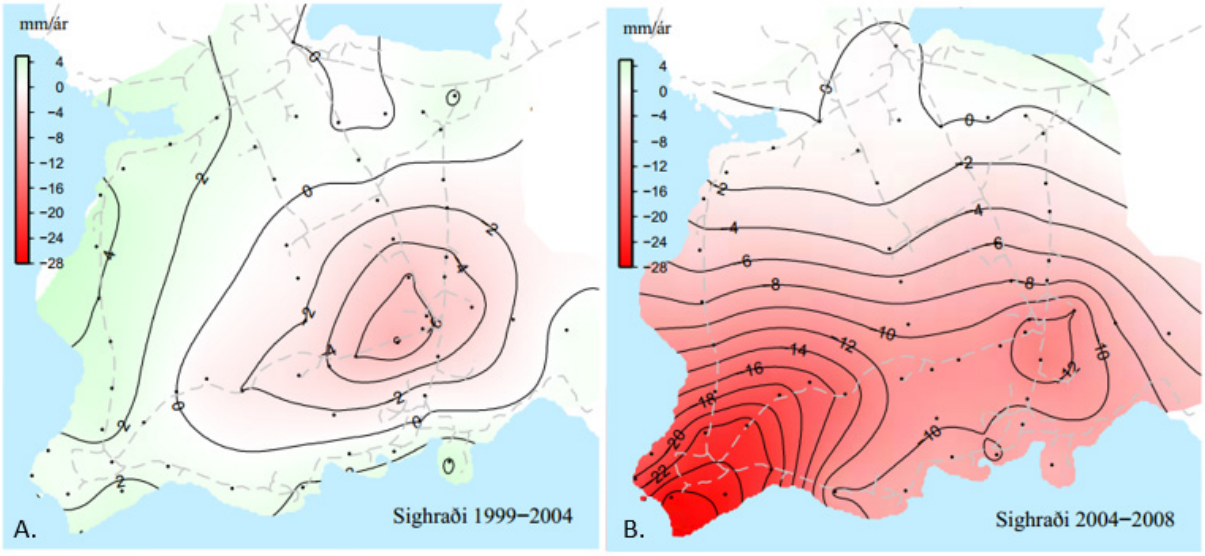

FIGURE 23: Subsidence of the Reykjanes Peninsula inferred from GPS surveys for the period (A) 1999-2004 and (B) 2004-2008 (Magnússon, 2009)

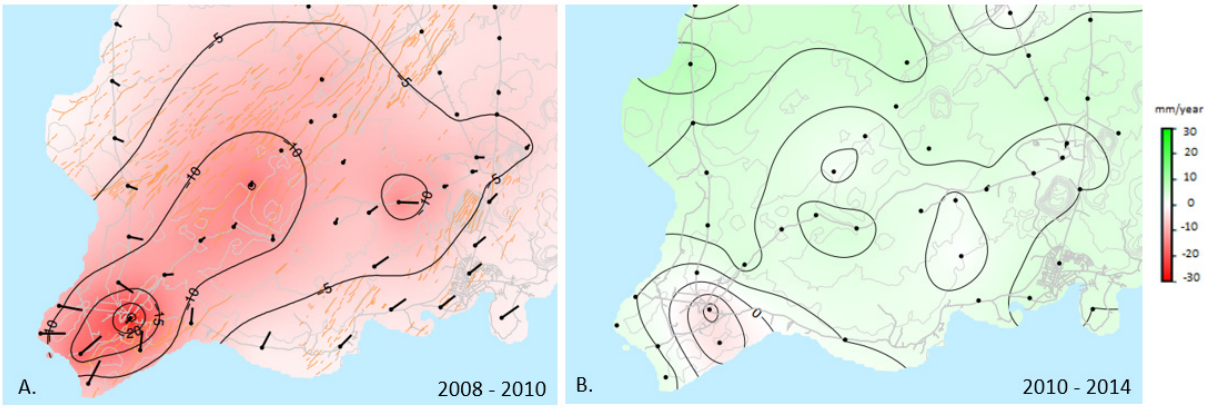

FIGURE 24: Subsidence of the Reykjanes Peninsula inferred from GPS surveys for the period (A) 2008-2010 and (B) 2010-2014 (Magnússon, 2013; 2015)

3.2.2 Interferometric Synthetic-Aperture Radar (InSAR)

InSAR conducted over the Reykjanes Peninsula during the period 1992-1995 (Vadon and Sigmundsson, 1997) revealed the presence of concentric fringes at Svartsengi, with the centre of subsidence located between Svartsengi and Eldvörp (Figure 25) which is comparable to the results of levelling done from 1975 to 1992 (Eysteinsson, 1993). Vadon and Sigmundsson (1997) then used a Mogi source to model the compaction of the reservoir. Modelled interferograms replicated the concentric fringes of Figure 25. The average rate of subsidence reported varied from 25 mm/year in 1992 to 9 mm/year in 1993, whose average is analogous to the geodetic studies conducted between 1992 to 1999 (Eysteinsson, 2000).

Keiding and others (2008) similarly detected strong signals of areal contraction and disturbed shear strain rates around the Svartsengi power plant during 1993-2006 (Figure 26). A notable decrease in the magnitude of the observed strain rates from 1993-1998 to 2000-2006 is related to the decrease in subsidence rate during these periods. Subsidence at Svartsengi was observed to vary almost linearly with pressure decline in boreholes at 900 m depths (Eysteinsson, 2000), so the decrease in the subsidence rate could be attributed to the increase in fluid reinjection into the system during these latter years.

A more recent interferometric analysis of InSAR data from 2015-2017 (Receveur, 2018) reveals subsidence rates at Svartsengi of approximately 8-10 mm/year during this period (Figure 27), analogous to results during the period 2010-2014.

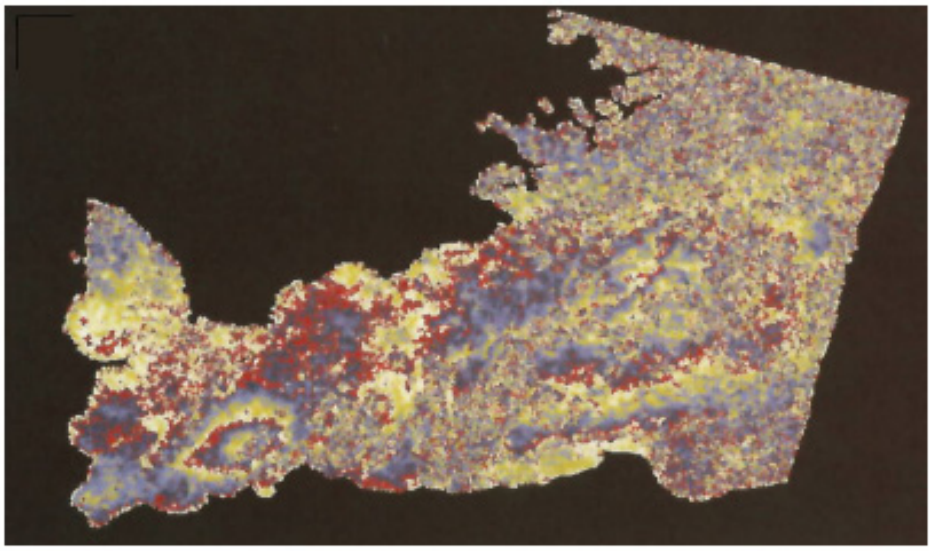

FIGURE 25: Interferogram covering the period 1992-1995, showing the concentric fringes over the Reykjanes central volcanic system, with the parallel fringes over the eastern part of the Peninsula showing regional subsidence along the plate boundary (Vadon and Sigmundsson, 1997)

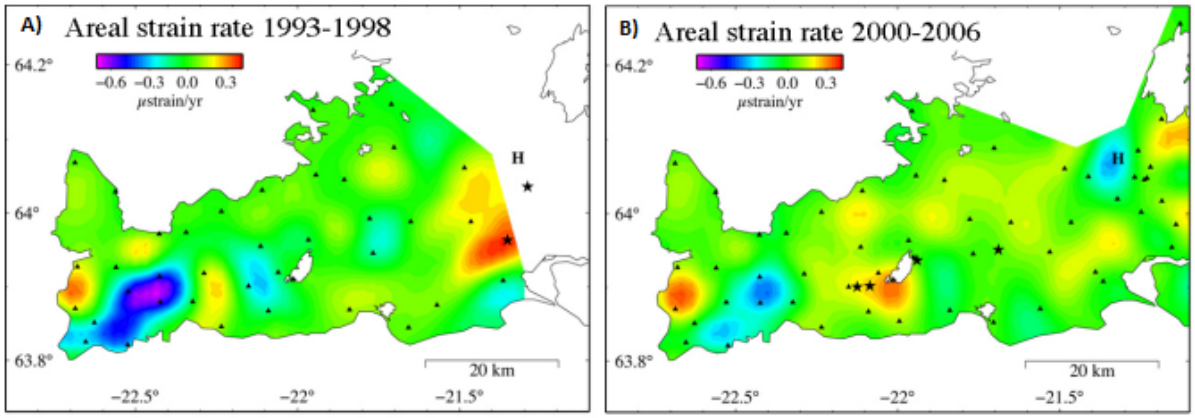

FIGURE 26: Observed strain rates for the period (A) 1993-1998 and (B) 2000-2006 from Keiding et al. (2008)

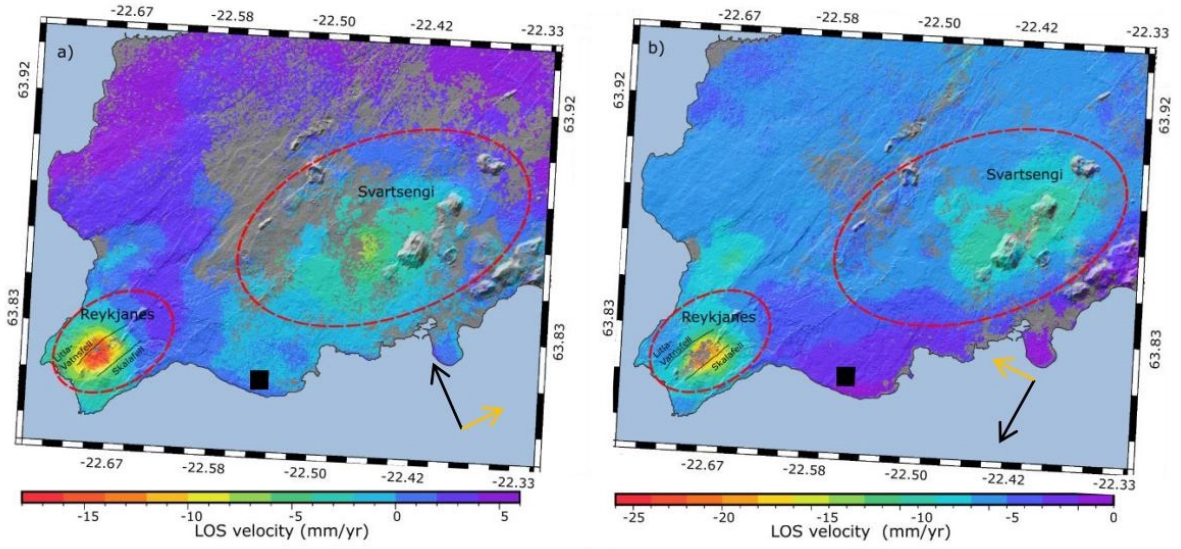

FIGURE 27: InSAR LOS velocities (mm/year) during 2015-2017 with (A) Ascending track T16 and (B) Descending track T155 over Reykjanes and Svartsengi (Receveur, 2018)

Deformation at the Reykjanes Peninsula is not only confined to geothermal exploration, but is due to a combination of different factors such as natural background tectonism, changes in seismicity, load variation and volcanism. Many recent attempts have been made to isolate the different signals that contribute to deformation at the Reykjanes Peninsula (Vadon and Sigmundsson, 1997; Hreinsdóttir et al., 2001; Árnadóttir et al., 2004; Keiding et al., 2008; 2010; Receveur 2018) Overall, Vadon and Sigmundsson (1997) estimated a long term natural subsidence of approximately 6.5 mm/year within the central part of the rift zone.

Lithologic logs of the wells at Reykjanes obtained during the Iceland Deep Drilling Project (IDDP), reveal the presence of shallow marine deposits interbedded with a relatively thin hyaloclatite formation below 500 m depths. Based approximations of the surrounding lithology, marine deposits found in boreholes at 500 and 630 m b.s.l. indicate approximate subsidence velocities during the past 500,000 years at 10.4 and 6.0 mm/year, respectively (Fridleifsson and Richter, 2010). The latter figure is in agreement with Vadon and Sigmundsson (1997).

The analysis of GPS results however, led Hreinsdóttir et al. (2001) to deduce that subsidence at the rate of 8 mm/year, accompanied by a horizontal displacement of 2 mm/year is associated with deformation along the seismic zone.

The Reykjanes Geothermal Field, which is located a few kilometres WSW of Svartsengi is associated with the same deformation signals as Svartsengi. A joint analysis of subsidence around the Reykjanes geothermal power plant is summarised by Axelsson and others (2015) in Figure 28. With reference to GARD/GASK, the average subsidence rate at the Reykjanes Geothermal Field before the onset of production in 2006 was 9 mm/year. However, considering that the site GARD/GASK is subsiding at a rate of 3 mm/year, the corrected 'background' subsidence rate at Reykjanes is estimated at 6 mm/year, which without the influence of geothermal production may be similar in Svartsengi. This corresponds to the range proposed by both Vadon and Sigmundsson (1997) and Fridleifsson and Richter (2010).

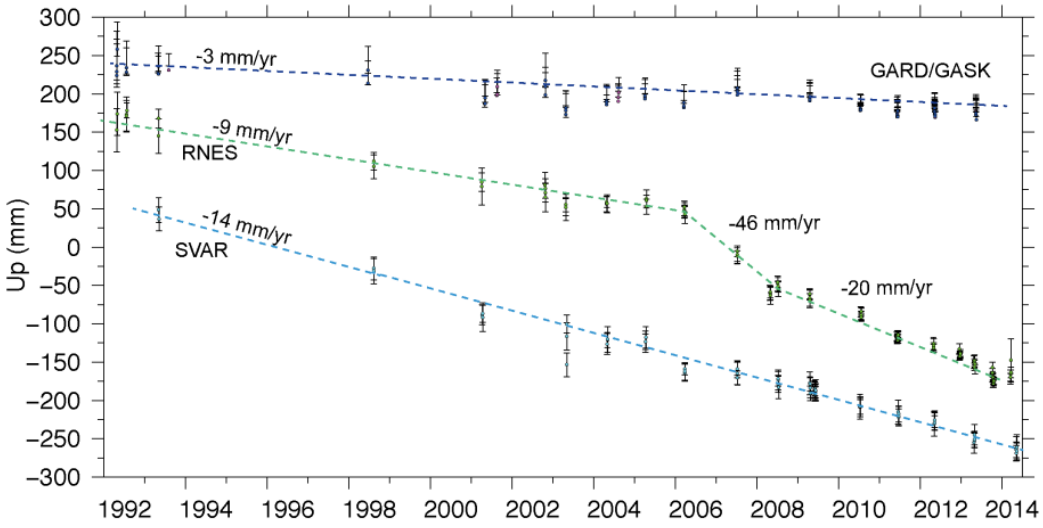

FIGURE 28: Average subsidence at Reykjanes (RNES) and Svartsengi (SVAR) estimated by GPS measurements from 1992 to 2014 with reference to Gardskagi (GARD/GASK) shown outside the affected area (Axelsson et al., 2015)

3.2.3 Gravity and mass changes

Gravity changes have been extensively documented in Svartsengi since 1975 (Eysteinsson, 1993; 2000; Magnússon, 2009; 2013; 2015). Figures 29-31 all reveal the gravity changes that have occurred in the outer Reykjanes region from 1975-2014. Eysteinsson (2000) observed an average gravity reduction of 5 µgal/year during 1975 to 1999 over Svartsengi (Figure 29). The observed gravity reduction was 4 and 7 µgal/year, respectively, for the periods 1999-2004 and 2004-2008. Magnússon (2015) however

observed that this has become somewhat insignificant after 2012 (Figures 30-31). The observed gravity reduction in Figures 29-31 reveals a direct correlation with the subsidence and pressure observed in Figures 22-24.

Eysteinsson (2000) applied Gauss' Law to estimate the total mass change in the geothermal reservoir at Svartsengi causing the changes in gravity (Hammer 1945):

$$\Delta m = \left(\frac{1}{2}\pi G\right) \iint \Delta g \, dS \qquad (1)$$

where G is the universal gravitational constant, and Δg is the change in gravity in a surface area (dS).

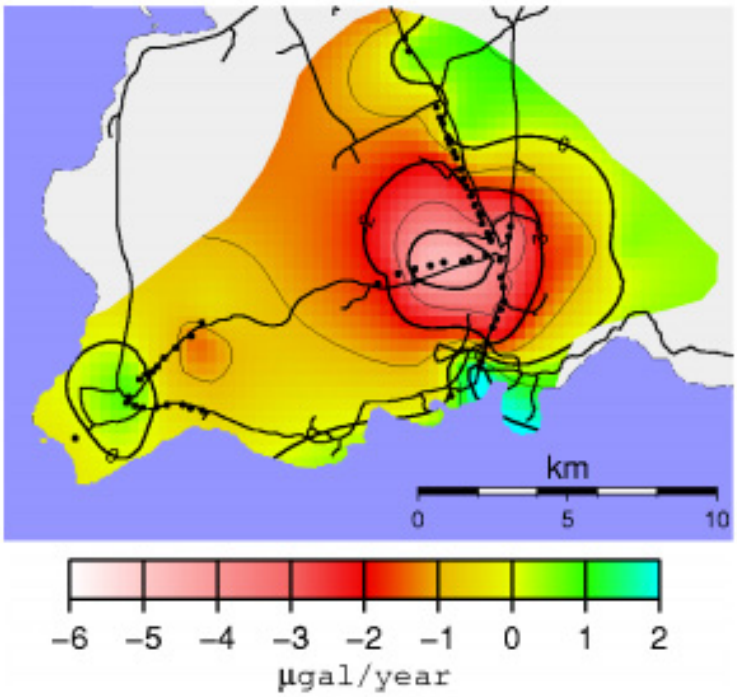

FIGURE 29: Average gravity variation from 1975 to 1999 on Reykjanes (Eysteinsson, 2000)

He applied equation (1) to the average change in gravity for the period 1975-1999, using an area within a 5 km radius around the production well field, giving a total mass change of 2.6 Mt/year. The comparison with the average annual production of 8 Mt/year for that period led Eysteinsson (2000) to conclude that there was approximately 70% annual recharge to the Svartsengi geothermal system. This was later repeated for the period 1999-2004 by Gudnason (2010) who determined a comparable value of 60% natural recharge in Svartsengi. A similar analysis of gravity changes was conducted at Reykjanes for the period 2004-2008 and 2008-2010 (Gudnason et al., 2015), concluding that there was a 30-50% renewal of fluid in Reykjanes. This indicates that Svartsengi is a more open system, allowing more recharge to the geothermal system there than in Reykjanes.

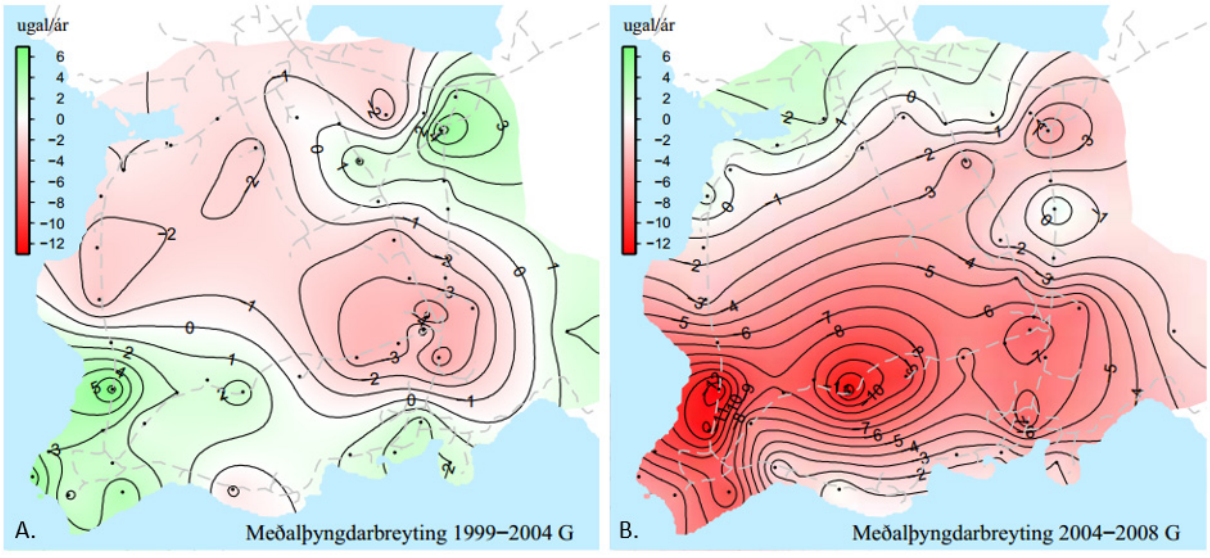

FIGURE 30: Average gravity variation in (A) 1999-2008, and (B) 2004-2008 (Magnússon, 2009)

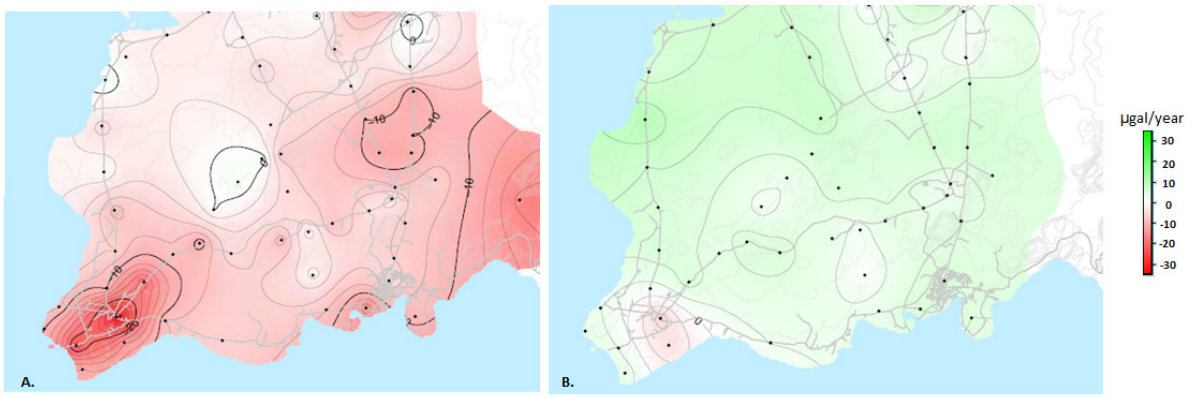

FIGURE 31: Average gravity variation in (A) 2008-2010 (Magnússon, 2013), and (B) 2010-2014 (Magnússon, 2015)

Figures 29-31 all show the gravity low that has developed and enclosed the Svartsengi and Eldvörp fields, which may indicate that they are part of the same reservoir (Eysteinsson, 2000).

4. METHODOLOGY

The ability to assess a given resource during the different stages of its development, as accurately as possible, is vital for its successful geothermal development (Axelsson, 2013). A variety of geothermal modelling methods have been employed during the last several decades to assess geothermal resources during both the exploration and exploitation phases of development. These methods, which all play an essential role in geothermal resource development and management include; geothermometry, volumetric estimates of stored heat, simple analytical modelling, lumped parameter assessment and detailed numerical modelling.

A conceptual model is the first guide to a numerical model (Grant and Bixley, 2011). Numerical models use mathematical models to simulate the physical conditions described by existing conceptual models. Numerical simulations are among the most powerful tools in managing subsurface resources in reservoir engineering. These models have been increasingly utilised in geothermal resource management by approximating the production potential of the system. They are also used to estimate the outcome of different management actions, such as changes in exploitation and reinjection, by predicting the response of reservoir to future production.

4.1 Numerical theory

4.1.1 TOUGH2

TOUGH2 was developed at the Lawrence Berkeley National Laboratory. It is a numerical simulator for multi-dimensional, non-isothermal heat flows of fluid in porous and fractured media. Through the application of Darcy's Law, using the integral finite difference method (IFDM), TOUGH2 solves mass and energy balance equations that describe fluid and heat flow in such systems (Pruess et al., 2012). The TOUGH2 model consists of a number of interconnected elements. For each element, equations defining the accumulated heat and mass as well as the heat and mass flux and points of generation (i.e. heat sources and sinks) are set up. The general form of the mass and energy balance equation governing TOUGH2 is given by:

$$\frac{d}{dt}\int_{V_n} M^k \, dV_n = \int_{\Gamma_n} F^k \cdot n \, d\Gamma_n + \int_{V_n} q^k \, dV_n \qquad (2)$$

Equation 2 expresses the equivalence of the rate of change of fluid mass in sub-volume V_n to the sum of the net inflow across the surface and the net gain from fluid sources and sinks. The first term $\frac{d}{dt}\int_{V_n} M^k \, dV_n$, represents the total mass and heat accumulation integrated over the sub-volume V_n. The $\int_{\Gamma_n} F^k.n \, d\Gamma_n$ term represents the mass and heat fluxes through the surface of sub-volume Γ_n while the $\int_{V_n} q^k \, dV_n$ term represents the sources and sinks of mass and heat.

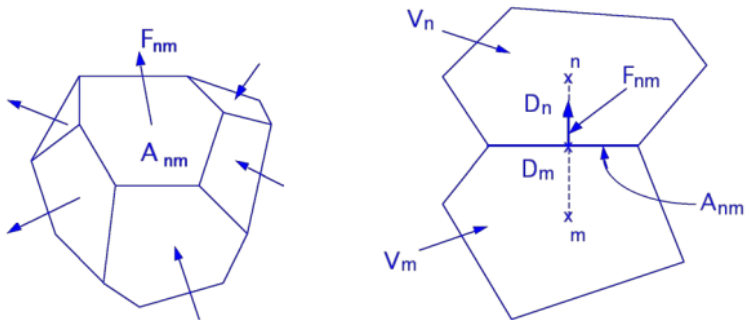

FIGURE 32: Space discretisation and geometrical connection of two domains in the IFDM (Pruess et al., 2012)

For numerical simulation, the continuous space and time is discretised by introducing volume and area averages (Pruess et al., 2012). The governing TOUGH2 equations are discretised as first order finite difference equations, and solved between consecutive time-steps by the Newton-Raphson iteration scheme. The discretisation and geometrical set-up in the IFDM is shown in Figure 32.

The heat accumulation term in Equation 2 becomes:

$$\frac{\mathrm{d}}{\mathrm{dt}}\int_{\mathrm{V_n}} \mathrm{M^k}\ \mathrm{dV_n} = \frac{\mathrm{d}}{\mathrm{dt}}\,\mathrm{V_n M_n} \tag{3}$$

The mass/heat flow term becomes:

$$\int_{\Gamma_\mathrm{n}} \mathrm{F^k}\cdot\mathrm{n}\,\mathrm{d}\Gamma_\mathrm{n} = \sum_m A_{nm}F_{nm} \tag{4}$$

The source and sink term becomes:

$$\int_{\mathrm{V_n}} \mathrm{q^k}\ \mathrm{dV_n} = V_n q_n \tag{5}$$

where M_n is the average value of M in V_n
A_{nm} is the area between V_n and V_m
F_{nm} is the average value of normal flow over A_{nm}

Substituting Equations 3, 4, 5 into 2 gives:

$$\frac{dM_n}{dt} = \frac{1}{V_n}\sum_m A_{nm}F_{nm} + q_n \tag{6}$$

4.1.2 iTOUGH2

iTOUGH2 (Finsterle 2007) is based on the TOUGH2 simulator for nonisothermal multiphase flow in porous and fractured media (Pruess et al., 2012). It is a programme used primarily for parameter estimation through the introduction of inverse modelling concepts for applications in multiphase flow, sensitivity analysis and uncertainty propagation analysis.

iTOUGH2 solves an inverse problem to determine TOUGH2 input parameters. Inverse modelling involves the automatic estimation of model parameters based on the measurements of the system response made during the TOUGH2 iteration process. Parameter estimation by inverse modelling overcomes the time-intensive process of manual model calibration. The error and sensitivity analysis provide further insight in the uncertainty of the estimated parameters, revealing parameter correlations, thereby improving the accuracy of the predicted model-related parameters.

During this project, the subsidence module in iTOUGH2 (Finsterle, 2018a) was utilised in forward mode. Neither inverse modelling, sensitivity analysis nor uncertainty analysis however was utilised.

4.2 Numerical simulation

4.2.1 Natural state

The first step in model calibration is to match the natural state. The natural state of a system is defined as the undisturbed state of the reservoir before the onset of production, usually for a period exceeding 10,000 years. A reservoir model is constructed with a heat and mass input at its base and is run until steady state is achieved. The temperature distribution output obtained is compared with measured data, and input parameters are adjusted until the modelled output is close to that of the observation.

A simple numerical model for the entire Svartsengi geothermal field was developed for this project. A Voronoi grid was created using the Steinar software package developed in Iceland by Vatnaskil. It utilises the Amesh code (Haukwa, 1999) that generates discrete grids for the numerical modelling of flow and transport problems, formulated on the integral finite difference method (Pruess et al., 1999). This grid covers a horizontal area of 468 km^2, and extends from sea level to 2550 m b.s.l. It is divided

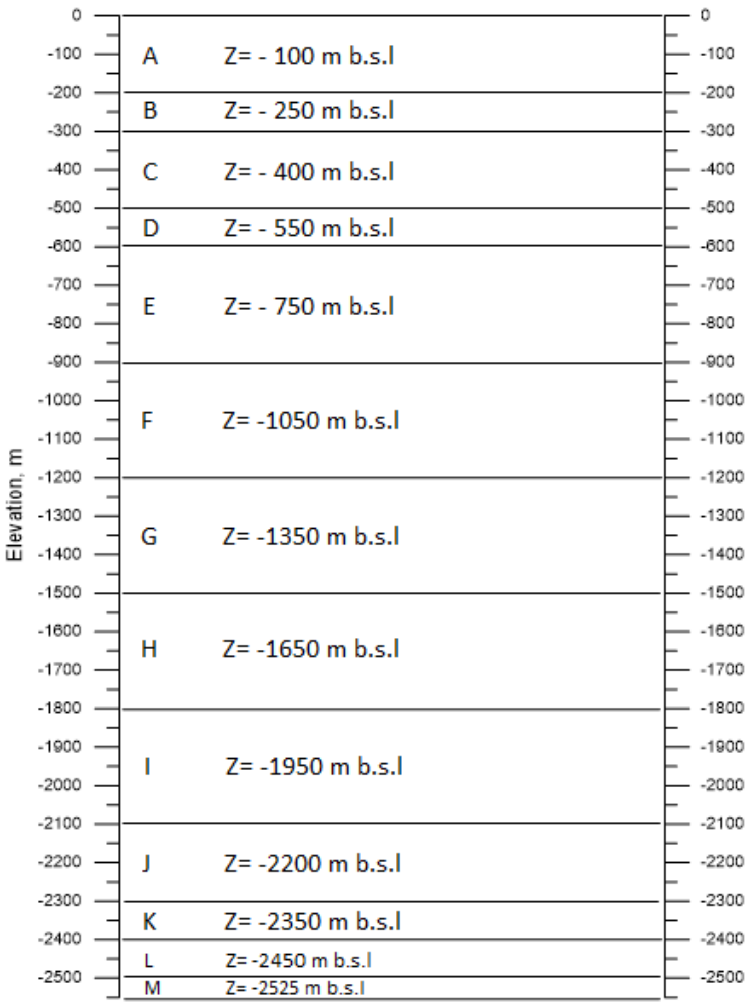

FIGURE 33: Vertical profile of the Svartsengi model, showing layers A-M

vertically into 13 layers of varying thickness- depicted in Figure 33. Each layer consists of 566 elements, yielding a total of 7358 elements throughout the 3D grid. Thinner layers are defined closer to the surface and base, while thicker layers are modelled deeper into the liquid-dominated reservoir (Layers E-J).

The grid is discretised horizontally with rather course elements outside of the wellfield, and finer elements within the well field where more accuracy is required. Dirichlet boundary conditions were applied to the top and bottom layers to control the initial conditions of the reservoir as well as around the lateral edges of the model. A constant geothermal gradient of 100°C/km was fixed over the entire grid, with a surface temperature of 3°C and a corresponding hydrostatic pressure gradient. At the midpoint of the inactive and impermeable surface layer (i.e. at 100 m b.s.l.), the temperature is fixed at 13°C, while in the boundary, the temperature increases with depth according to the geothermal gradient, remaining constant with time. The lateral sides therefore allow the inflow of cooler fluids according to pressure decline within the modelled boundaries.

A low permeability caprock was modelled in Layers B and C, with the reservoir extending from Layer D to the base. In addition to having an 'inactive' high-temperature bedrock of 255°C in Layer M incorporating the background heat flux, mass flow sources were added to Layer L of the model. This was done to simulate the deep upflow from the geothermal plume (O'Sullivan and O'Sullivan, 2016).

Three upflow zones were modelled, with their locations illustrated in Figure 34. Source A represents the upflow along the Eldvörp fissure (Franzson, 1987), while C represents the upflow to the main production area theorised by Björnsson and Steingrímsson (1991). The third source (B), between Eldvörp and Svartsengi was included due to the observations from the MT profile in Figure 8 (Karlsdóttir and Vilhjálmsson, 2015).

Since Eldvörp is a part of the Svartsengi field, it is assumed that all upflow zones are fed by the same source. An initial enthalpy of 1037 kJ/kg, corresponding to a fluid temperature and pressure of 240°C and 33.5 bar, respectively, with initial flow rates of 1 kg/s was applied at each source.

These upflow areas, A, B and C are modelled as vertical fractures with assigned rocks FRAC1, FRAC2 and FRAC3 respectively. These rocks are surrounded by reservoir rocks of lower permeabilities. A schematic of the initial rock distribution throughout the model is presented in Figure 35 and the anisotropic permeabilities modelled by Ketilsson (2007) were assumed.

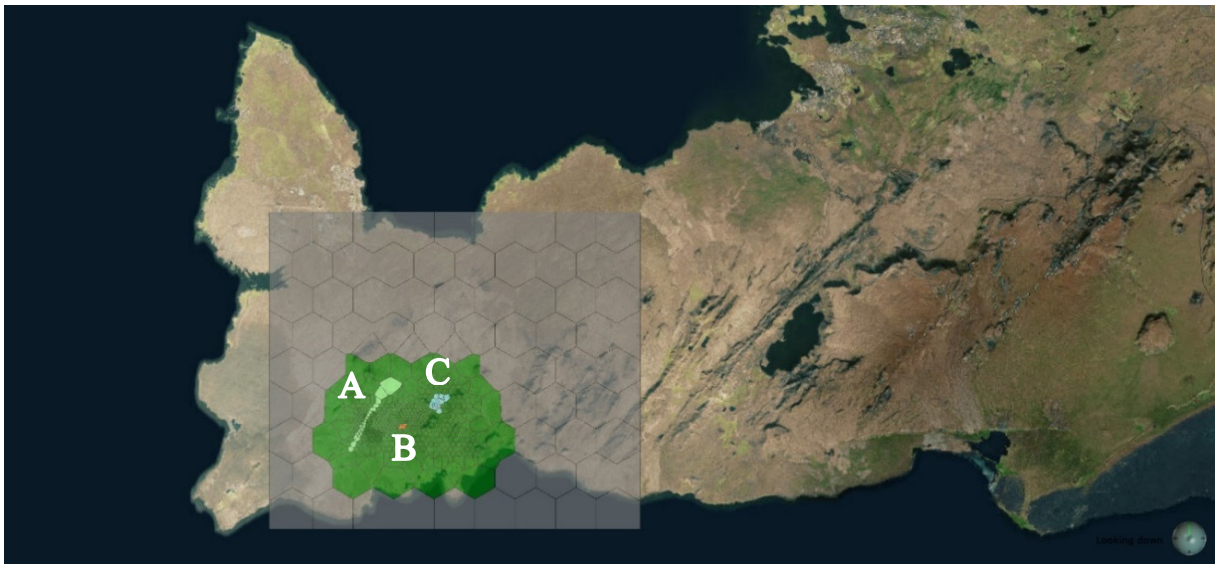

FIGURE 34: Location of upflow zones, A, B and C, modelled in Layer L at -2450 m b.s.l.; the upflow zone lies within the reservoir which is surrounded by an 'inactive' constant temperature and pressure boundary

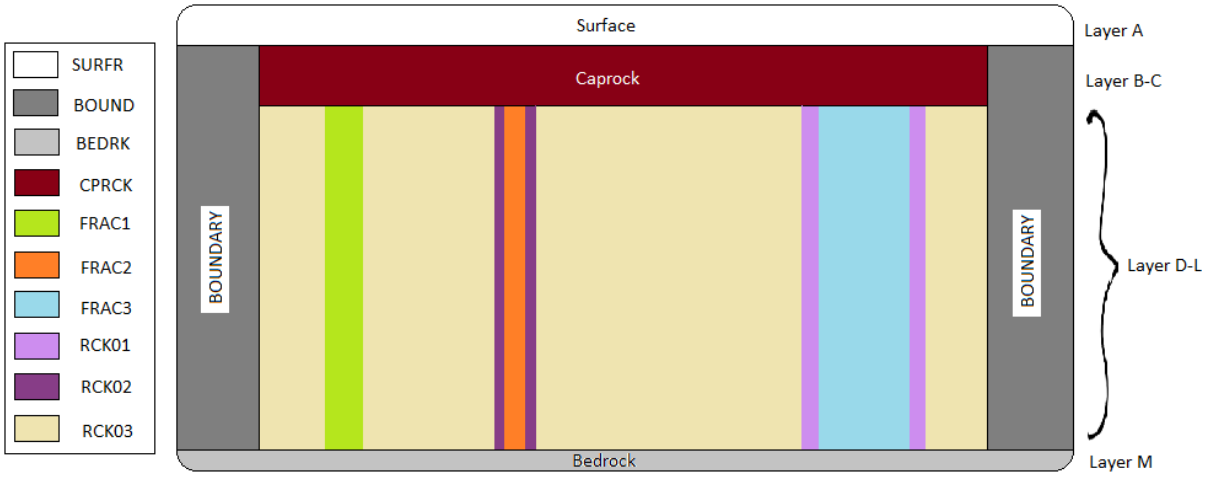

FIGURE 35: A schematic of the initial vertical rock distribution through the Svartsengi system

The constant physical reservoir properties, similar to those of the Svartsengi production model by Bödvarsson (1988) and Ketilson (2007) are listed below in Table 1.

TABLE 1: Physical properties of rocks in the Svartsengi model

Physical properties	Value
Rock density (kg/m^3)	2650
Heat capacity (J/kg°C)	900
Thermal conductivity (W/m°C)	2.1
Relative water permeability	40%
Relative steam permeability	5%

The parameters in Table 1, as well as the rock properties of Ketilsson (2007) were imported into TOUGH2, and using Equation of State 1 (EOS1), the conditions were simulated forward in time for 100,000 years. A PyTOUGH (Croucher, 2017) code was written and used to extract output variables from the TOUGH2 output file. The modelled temperature profiles were compared the formation temperature profile. Rock permeability distribution, fluid enthalpy and mass flow rates were then

manually adjusted in an attempt to achieve equilibrium and model the formation temperature profiles of the wells within the reservoir.

4.2.2 Production model: history matching

Once the natural state has been calibrated, the model was then used to simulate changes under exploitation. The simulated changes are compared to the observed data, and another cycle of parameter adjustments are made to the natural state model.

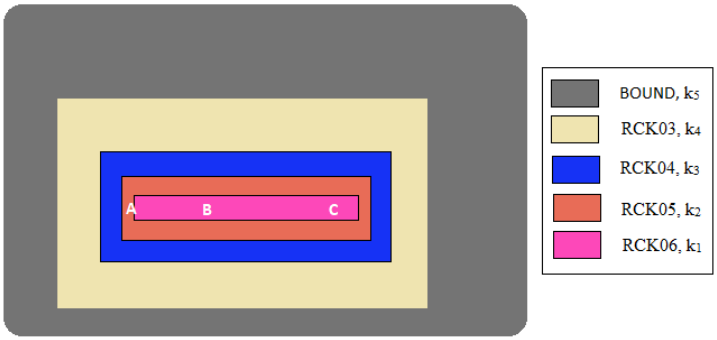

FIGURE 36: A schematic showing the initial horizontal permeability distribution through the production area of the Svartsengi model. The locations of the upflow areas A, B, and C are highlighted

The pressure drawdown observed in Figure 21 between Svartsengi and Eldvörp suggests a strong pressure connection and a zone of high permeability extending from Svartsengi to Eldvörp. A schematic of the initial horizontal permeability distribution can be seen in Figure 36. The model was set up with a horizontal permeability increasing from the inactive boundary towards the centre of the grid, where $k_1>k_2>k_3>k_4>k_5$. A highly permeable rock material connects Svartsengi to Eldvörp, which should establish a connection between the two points.

The model assumes three feed zones; the first being in Layer C (300-400 m b.s.l.) which is used to represent the steam zone. The second feed-zone is in Layer F (900-1200 m b.s.l.) and accounts for production and reinjection in all other wells within the main well field. The third feed-zone accounts for reinjection in SV-17 and SV-24. Production was simulated by distributing the average annual production among production wells in the main wellfield. Reinjected fluid of temperature 98°C, which corresponds to an enthalpy of 3.98 x 10^5 J/kg, was injected in wells SV-05, SV-06, SV-12, SV-17 and SV-24 according to the reinjection history described in Chapter 3.1.1.

These parameters were then input into TOUGH2 and the model ran for 41 years (i.e. from 1975 to 2016). PyTOUGH was used to extract and visualise the modelled pressure drawdown in Layer F for wells EV-02, SV-08, SV-09, SV-11, SV-12 and SV-19. These were compared to the values observed during 1980-2017 in Figure 21. Input parameters were adjusted until there was a good fit between the modelled and observed pressure drawdown throughout the field.

4.2.3 Subsidence matching

Subsidence within geothermal reservoirs are typically attributed to a combination of both poro-elastic and thermo-elastic processes associated with changes in pressure and temperature. At reservoir depths, porous rocks are subjected to both internal and external stresses. External stresses are created from the weight of the overburden, as well as from any accompanying tectonic stresses. Internal stresses however, result from fluid pore pressure. Whereas external stresses tend to cause a reduction in pore volume, and compress the rock matrix, internal stresses have the opposite effect, i.e. it resists pore volume reduction. Volumetric change (dv) within the rock matrix is related to changes in pressure (dP), and temperature (dT) by:

$$dv = \left(\frac{dv}{dT}\right) dT + \left(\frac{dv}{dP}\right) dP \qquad (7)$$

This reduces to:

$$\frac{dv}{v} = \alpha dT + \beta dP \quad (8)$$

where α is the volumetric coefficient of thermal expansion and β is the pore compressibility of the rock matrix.

A newly developed subsidence module in the TOUGH2 simulator in iTOUGH2 was used to model the subsidence based on the calibrated production response at Svartsengi. This module approximates one-dimensional deformation based on porosity changes induced by changes in the model's fluid pressure and/or temperature. The relative porosity changes are calculated between the nodal distances of elements along the z-axis, belonging to the same column. These changes are integrated along the column so that the new z-coordinate is calculated. Since there are no stress or strain computations made, the entire volumetric strain is assumed to lead to deformation in the z-direction only. This is further described in Finsterle (2018a and 2018b). Both the expansion and compression constants are positive whose increase leads to an increase in porosity. The subsidence module thus evaluates porosity rather than bulk volume and since the solid matrix is assumed to be incompressible, $\frac{d\phi}{\phi} = \frac{dv}{v}$. Since all volumetric change is assumed to be vertical in the z-direction, equation (8) becomes:

$$\frac{d\phi}{\phi} = \frac{dz}{z} = \frac{dv}{v} = \alpha dT + \beta dP \quad (9)$$

where ϕ represents the porosity of the rock matrix.

In order to utilise this module, typical values for the pore compressibility and pore expansivity of basaltic rocks, 2.0 x 10^{-11} Pa^{-1} and 1.0 x 10^{-5}°C^{-1} respectively, were initially given. These parameters are defined in the ROCKS block of TOUGH2. iTOUGH2 was then run in Forward mode, and the calculated subsidence was compared to the observed subsidence during the period 1975-2015.

5. RESULTS AND DISCUSSION

A three-dimensional numerical model has been developed for the Svartsengi-Eldvörp high-temperature reservoir as described in Chapter 4. In this chapter, the results of this model development are presented and discussed.

5.1 Numerical modelling results

There are 26 wells currently drilled into the Svartsengi-Eldvörp system. Usually, a well-by-well approach is taken where each well is assigned one specific element, and the element is calibrated according to the observed conditions in that well. In this study, however, wells located close together were grouped and modelled as a single well. This was done to maintain a certain simplicity in the model and justified by the fact that temperature conditions in the main well field are quite uniform. In addition the main purpose of the study was not an accurate and detailed replication of well-by-well variability, but rather the overall effect of mass extraction on reservoir pressure and subsidence. These well-groupings can be seen in Figure 37.

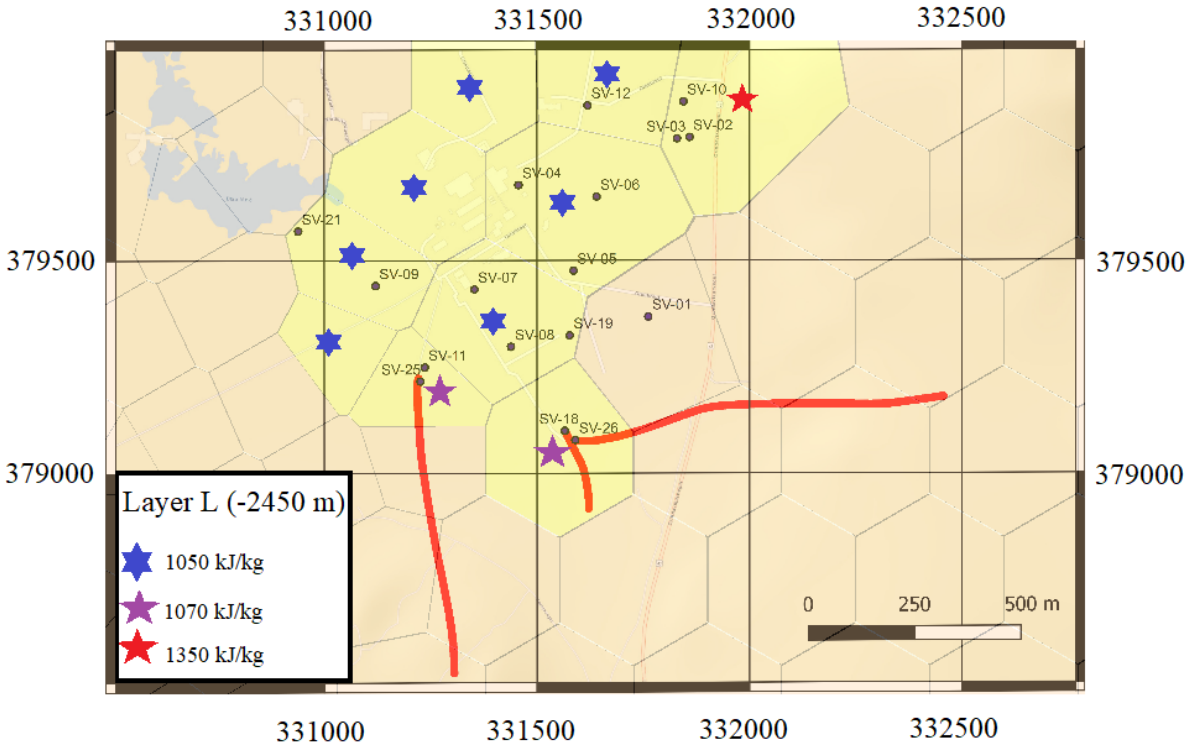

FIGURE 37: Enthalpy of elements making up Source C – the upflow zone to the Svartsengi well field

The numerical model contains 17 different rock types. The final distribution and parameters of the different rock materials, such as permeability and porosity are based on previous studies as well as the result model calibration. The rock distribution of each layer of the model is given in Appendix A.

5.1.1 The natural state calibration

The natural state of the model was successfully calibrated after a simulation period of 100,000 years. Steady state was achieved by manually adjusting the anisotropic permeability distribution of rock materials, as well as the enthalpy and mass flow rates of the up-flow sources A, B and C presented in Figure 34.

The model is heated up from below by a constant temperature boundary. Initially, a temperature of 255°C was uniformly applied to Layer M (base) of the model, however, during the calibration process, a temperature of 280°C was applied in Layer M along the Eldvörp fissure to reflect the more elevated temperatures observed in well EV-02.

The up-flow from the deep geothermal plumes (Figure 8) were simulated by implementing mass flow sources A, B and C in Layer L of the model. In order to achieve steady state, a total of 55 kg/s of fluid, with an enthalpy of 1236 kJ/kg was injected into the highly permeable elements that made up Source A along the Eldvörp fissure system. A total of 40 kg/s of fluid, with enthalpy 1117 kJ/kg was injected up through the vertical 'fracture' at Source B. The lower enthalpy of fluid here reflects a slightly lower temperature that was observed in well SV-17.

Source C, under the main well field in Svartsengi was modelled with a total mass flow rate of 115 kg/s, however the enthalpy of fluid was not uniform in all elements as in sources A and B. The distribution of fluid enthalpy for source C in Layer L is presented in Figure 37.

The total mass flow rate for the elements highlighted by the blue stars in Figure 37 is 55 kg/s. Fluid of slightly higher enthalpy, 1070 kJ/kg, with a total combined flow rate of 50 kg/s was used to simulate the isothermal temperature conditions in the directional wells SV-25 and SV-26. Wells SV-02, SV-03 and SV-10 have been observed to lie in the two phase zone. In order to simulate the temperature in this zone, 10 kg/s of fluid, with an enthalpy of 1350 kJ/kg was applied. In the first active layer of the model (Layer B), a 'safety valve' in the form of a productivity index (PI) of 3 x 10^{-13} m^3 and bottom well pressure of 35 bar was applied to this connection to simulate the release of steam and to maintain the boiling point curve with depth. A comparable approach was taken by both Björnsson (1999) and Ketilsson (2007).

A vertical WSW-ENE trending cross-section (**X-X'**) from Eldvörp through to Svartsengi (location shown in Figure 38) of the extrapolated downhole formation temperatures and modelled well temperatures was generated by Leapfrog Geothermal and is presented in Figure 39. The correlation graphs between the simulated temperature output and downhole formation temperature plots are illustrated in Appendix B.

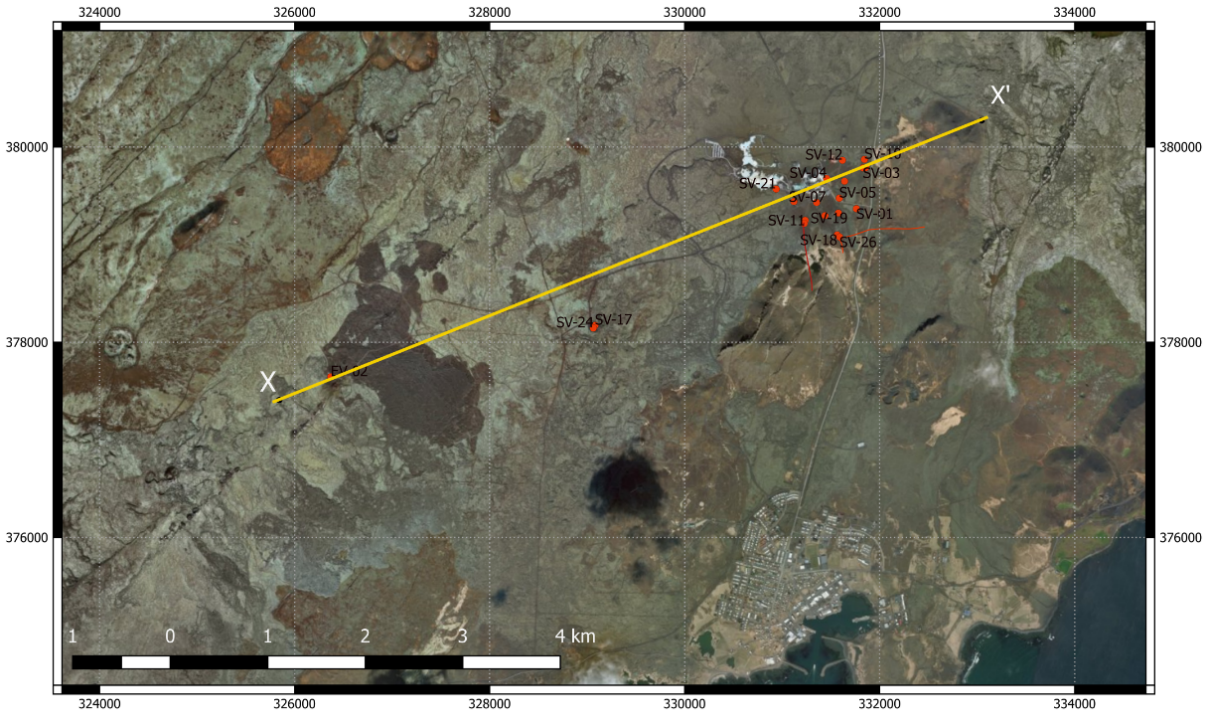

FIGURE 38: Location of the WSW-ENE trending vertical temperature cross-section (X-X')

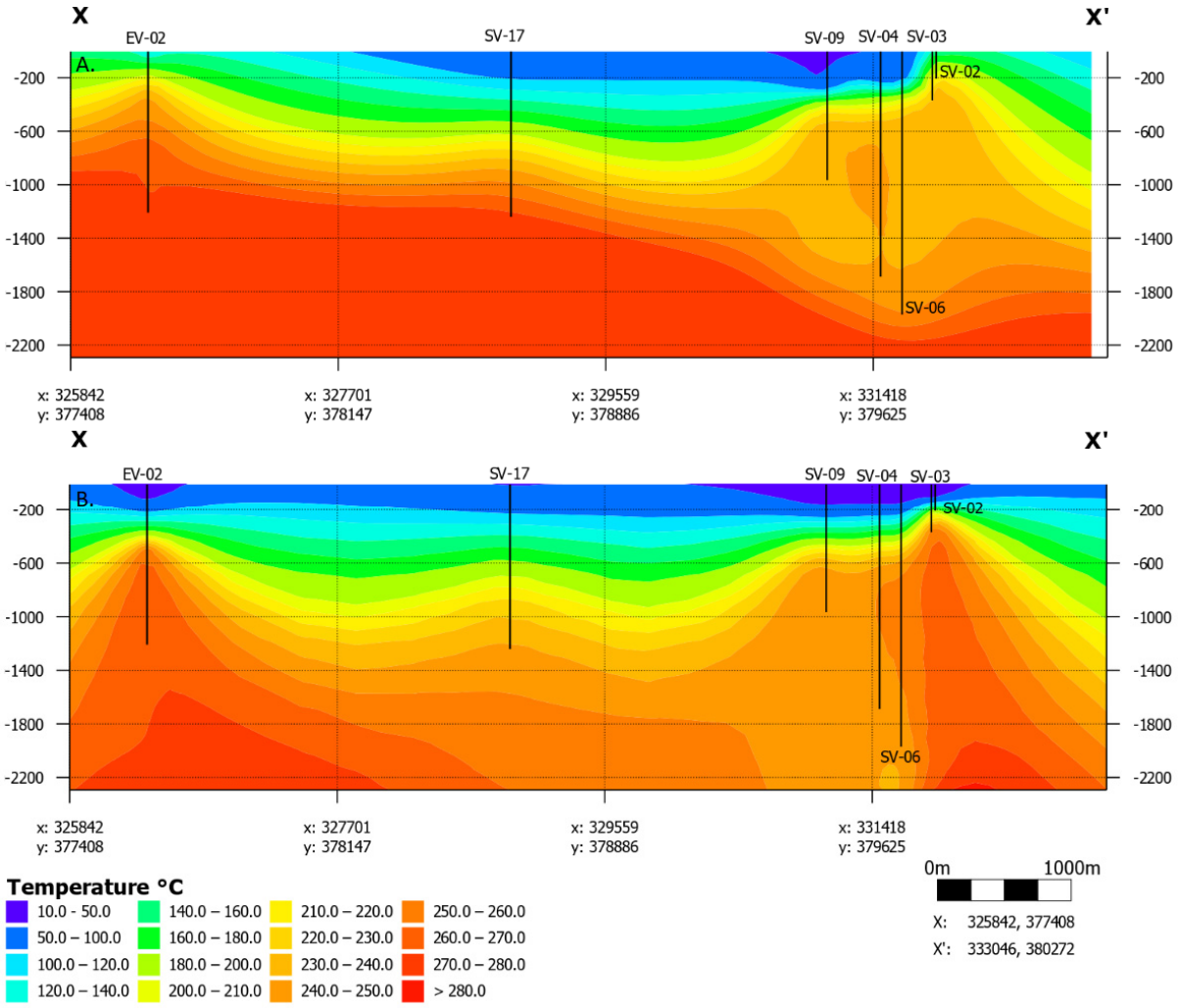

FIGURE 39: A WSW-ENE trending cross-section (X-X') showing a comparison between (A) the downhole formation and (B) modelled temperature profiles, depicted in Figure 38

Overall, Figure 39 shows a good correlation between the modelled and measured temperature. The modelled data, however, shows lower temperatures at the surface down to approximately 200 m b.s.l., which is due to the inactive constant temperature boundary condition applied to Layer A (0 - 200 m b.s.l.). In the model, higher temperatures peaks are observed close to the higher temperature wells EV-02 and SV-17. They however vary slightly when compared to the downhole formation temperature profiles. In the model, the maximum temperatures in Layer F (-1050 m) recorded in wells EV-02 and SV-17 are 267°C and 249.48°C, respectively, as compared to 270°C and 245°C in the measured downhole temperature.

There is an excellent match between the modelled and measured temperature profile in the main well field. Since wells SV-02, SV-03 are shallow wells, producing from the steam zone in the north east part of the field, temperature values below this depth are not known. The modelled temperature profile however simulates temperatures from sea-level to 2550 m b.s.l. The effects of higher enthalpy fluid that flows up the connection to this zone is one of the main discrepancies between the two profiles in Figure 39.

The complete temperature model that incorporates each element generated by TOUGH2 is presented in Figure 40. Here we see that the modelled results replicate the isothermal temperatures of the main well field, which is indicative of good convective mixing within the reservoir.

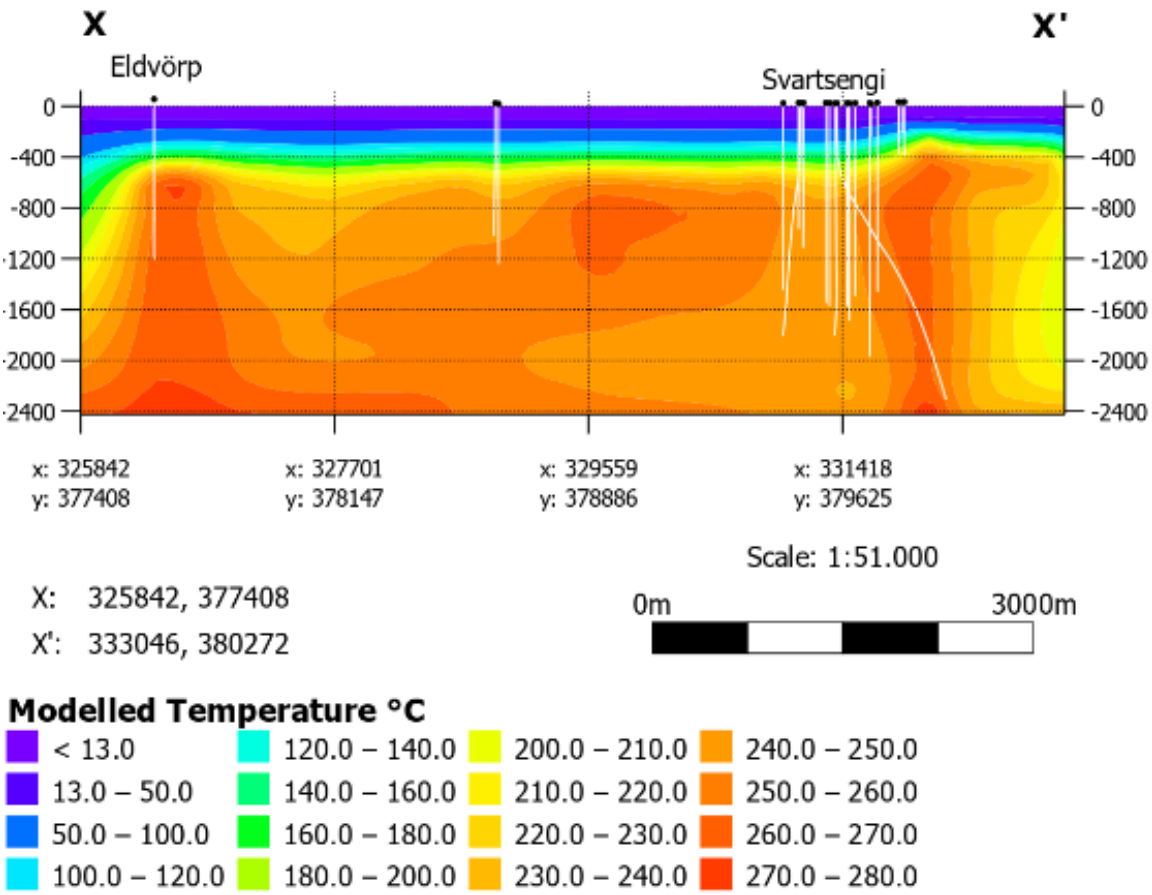

FIGURE 40: Vertical cross-section (X-X') showing the natural state TOUGH2 temperature model of the Svartsengi reservoir

The 13 rock types listed in Table 2 were the primary ones used throughout the model. The calibrated permeabilities and porosities of these materials have also been illustrated in Figure 35 and Figure 36. Four other rock types were modelled based on these original materials in order to have more control over specific areas in different layers (lower permeability RCK07 was for e.g. used in place of RCK06 in Layer K as to allow for a greater up-flow of fluid though the sources A, B and C by restricting fluid flow in the x and y directions).

TABLE 2: Porosity and permeability values for the main rock materials used in the natural state calibration

Material	Permeability, mDarcy			Porosity
	x	y	z	
FRAC1	180	300	350	0.3
FRAC2	50	100	200	0.3
FRAC3	2	100	250	0.3
RCK01	50	100	200	0.2
RCK02	100	100	150	0.1
RCK03	200	350	1	0.1
RCK04	0.1	0.01	1	0.1
RCK05	2	10	1	0.1
RCK06	200	350	1	0.3
SURFR	1	1	1	0.09
CPRCK	0.01	0.01	0.01	0.1
BDRCK	0.01	0.01	0.01	0.1
BOUND	0.0001	0.0001	0.0001	0.05

5.1.2 The production response

The average annual production and reinjection data from 1975-2015 was used for further calibration of the numerical model. The output from the natural state model was used as the initial conditions for the production response model. The average annual production was distributed equally among the production wells in the main well-field, and was simulated for 40 years. The modelled pressure was taken at 1050 m b.s.l. while the measured drawdown is observed at 900 m b.s.l. This accounts for a hydrostatic pressure difference of approximately 40 bars. The correlation graphs between the measured and modelled pressure response are presented in Figure 41-43. There is a fairly good correlation between measured and modelled drawdown, however the modelled drawdown is slightly underestimated by approximately 5-10 bars for the observation period 1985 to 2010. This disparity may be largely due to the high mass flow from the upflow sources, in particular, the upflow under the main well field, which has a total flow rate of 155 kg/s which may have provided additional pressure support to the model. The overall average modelled drawdown from 1975 to 2015 is comparable to that of the observed values, although from the year 2000, after the onset of large scale reinjection, when the pressure drawdown in the monitoring wells appear to be stabilising, the modelled response show less recovery than observed for this period in all monitoring wells. The modelled plots all show a steady, pressure decrease, although the rate of drawdown appears to have decreased slightly after 2000.

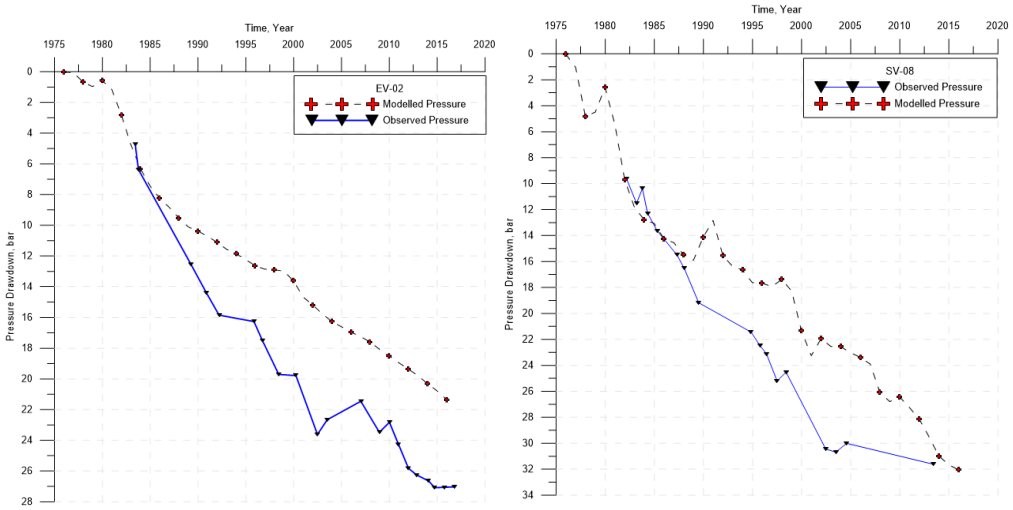

FIGURE 41: Comparison between observed and modelled pressure drawdown in wells EV-02 and SV-08

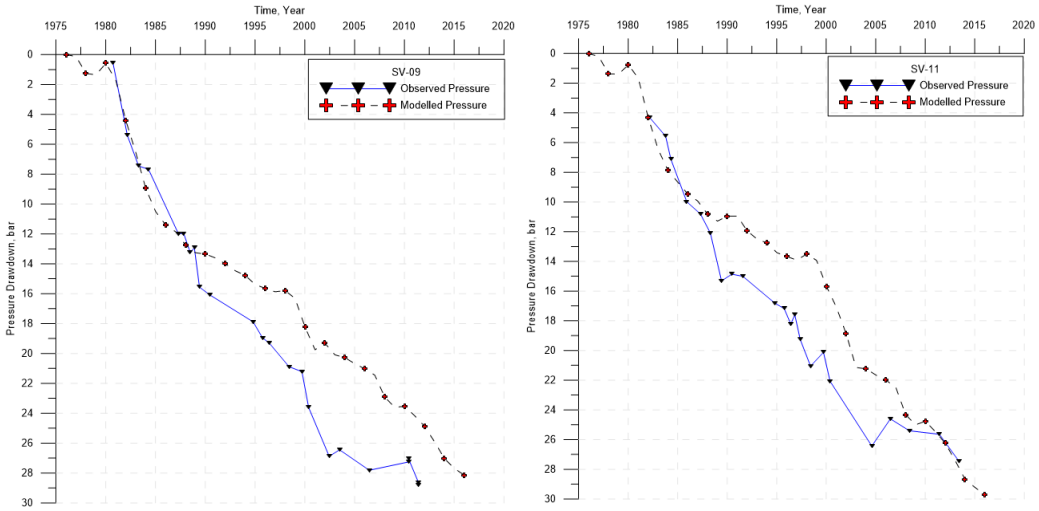

FIGURE 42: Comparison between observed and modelled pressure drawdown in wells SV-09 and SV-11

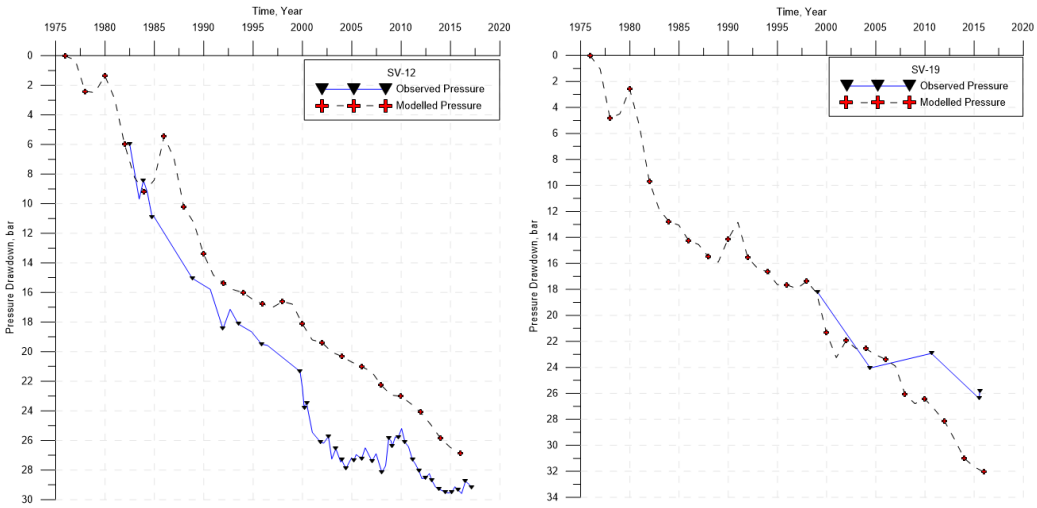

FIGURE 43: Comparison between observed and modelled pressure drawdown in wells SV-12 and SV-19

The total average modelled pressure drawdown in the Svartsengi reservoir during 1975-2015 is 30 bars. From around 1987 to 2005 however, the modelled drawdown is approximately 5-10 bars lower than the measured drawdown. Figure 44 shows a horizontal contour plot of the pressure drawdown at 900 m b.s.l. in a Leapfrog generated model from the TOUGH2 output. A pressure drawdown of between 25-30 bars is modelled around the main well-field at Svartsengi, with a maximum drawdown of approximately 32 bars observed around wells SV-07 and SV-08. Pressure recovery is observed around the reinjection site SV-17.

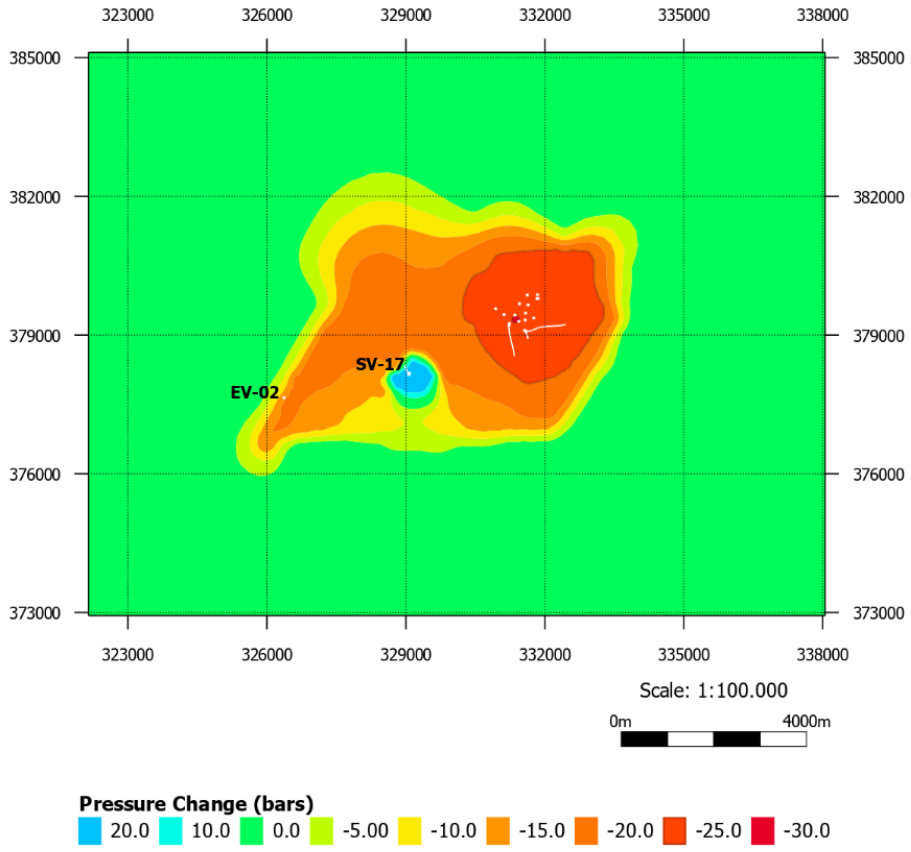

FIGURE 44: Horizontal map of the Svartsengi reservoir, showing the modelled pressure drawdown from 1975 to 2015. Wells are illustrated in white, with EV-02 and SV-17 labelled for reference

Although Icelandic rocks typically have a porosity between 10-15%, rock materials that were modelled as fractures (i.e. FRAC1, FRAC2, FRAC3, RCK06) were given higher porosities of 30% (Table 5.1). During the calibration, because of the rapid pressure drop that occurred in the north-east portion of the field due to the expanding steam zone, another rock type (RCK10) was introduced for the steam zone from Layer C to Layer E with permeabilities of an average of 290 mDarcy and 80 mDarcy in the horizontal and vertical directions, respectively. In order to sustain a high enthalpy in these layers, a porosity of 60% was applied in order to simulate the higher steam enthalpy. This should be viewed as an artificial parameter selection, used to achieve the desired effect, without complicating the modelling process. This is justified by the fact that the focus of this study is not the steam zone, but rather the subsidence.

Model calibration was achieved overall by:

1. Modelling up-flow zones A, B and C as vertical fractures (FRAC1, FRAC2, and FRAC3) with high vertical permeabilities (Figure 35).

2. Inserting a narrow, high permeability zone extending from Eldvörp to Svartsengi (RCK06) and increasing the permeability of each layer from the boundary (BOUND) towards this high permeability zone (Figure 36) from Layers E-L. This reduced the pressure support from the reservoir boundaries, therefore increasing the pressure connection between Eldvörp and Svartsengi. This was done primarily because of the model's production response, to simulate pressure drawdown in Eldvörp.

5.1.3 Subsidence

The subsidence module in iTOUGH2 was applied to the production model to calculate the changes in elevation of each element. These changes were integrated along the vertical column of each element. Elevation changes generated by iTOUGH2, with respect to the fixed 'inactive' TOUGH2 boundary for the periods; 1975-1980, 1980-1985, 1985-1990, 1990-1999, 1999-2004, 2004-2008, 2008-2010 and, 2010-2015 are given in Figure 45 - Figure 52.

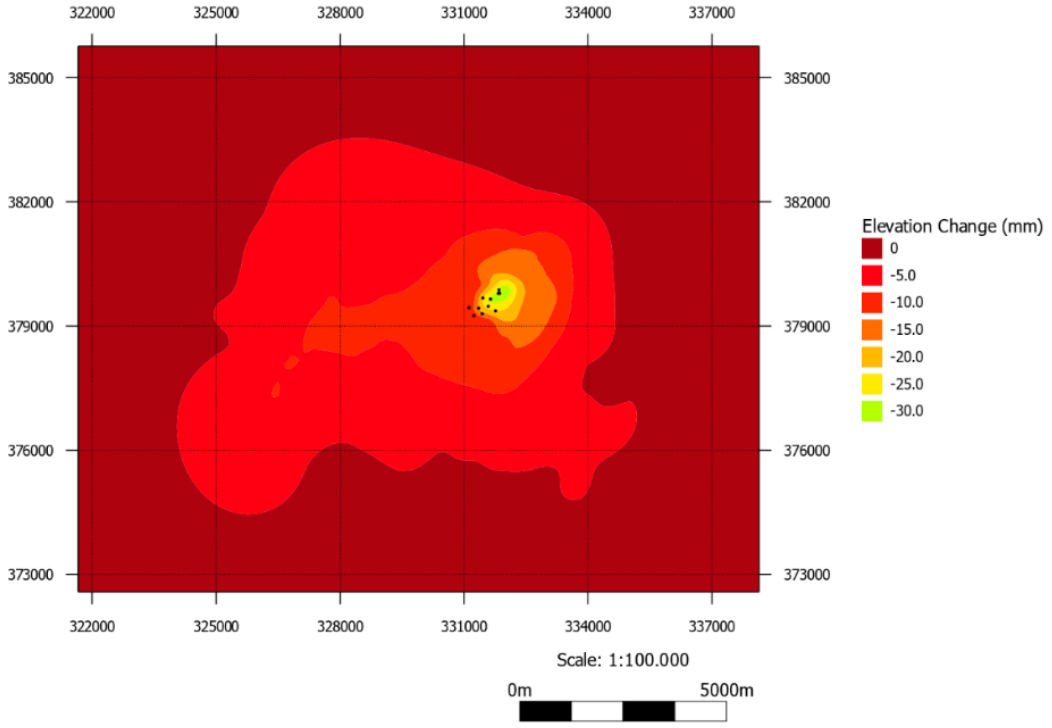

FIGURE 45: Horizontal contour map showing the modelled elevation changes in the Eldvörp-Svartsengi Region during 1975-1980

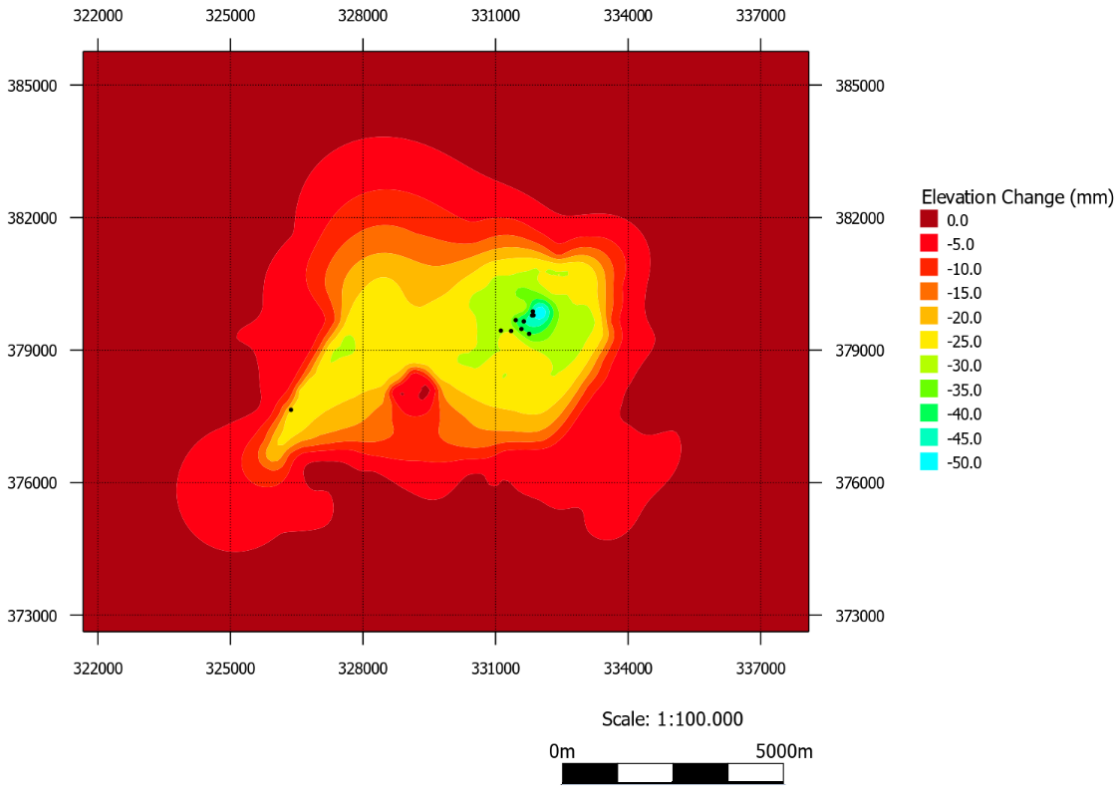

FIGURE 46: Horizontal contour map showing the modelled elevation changes in the Eldvörp-Svartsengi region during 1980-1985

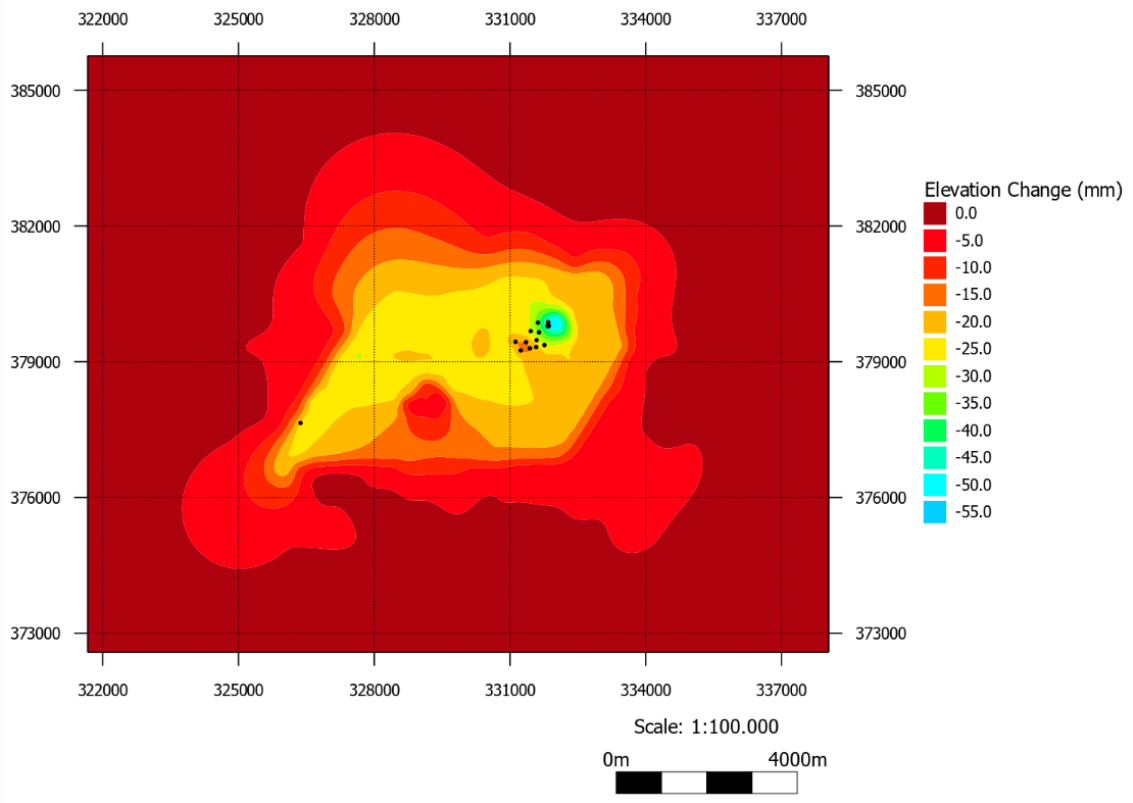

FIGURE 47: Horizontal contour map showing the modelled elevation changes in the Eldvörp-Svartsengi region during 1985-1990

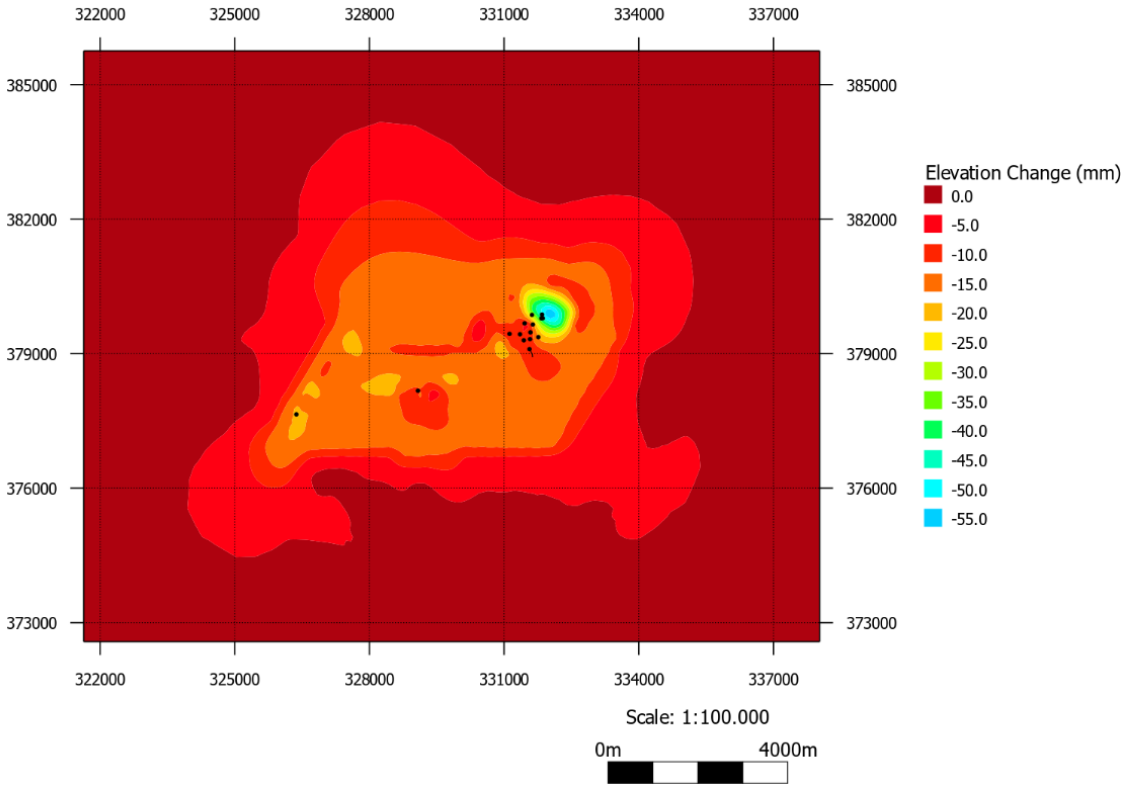

FIGURE 48: Horizontal contour map showing the modelled elevation changes in the Eldvörp-Svartsengi Region during 1990-1999

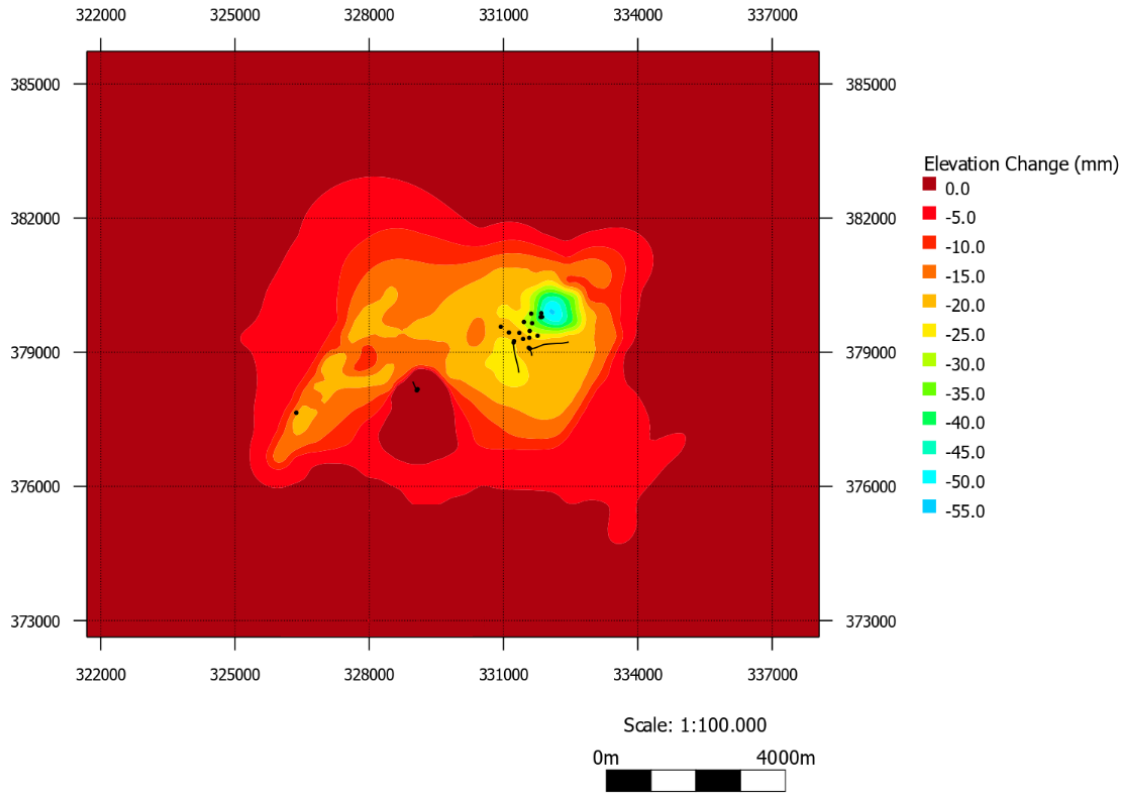

FIGURE 49: Horizontal contour map showing the modelled elevation changes in the Eldvörp-Svartsengi region during 1999-2004

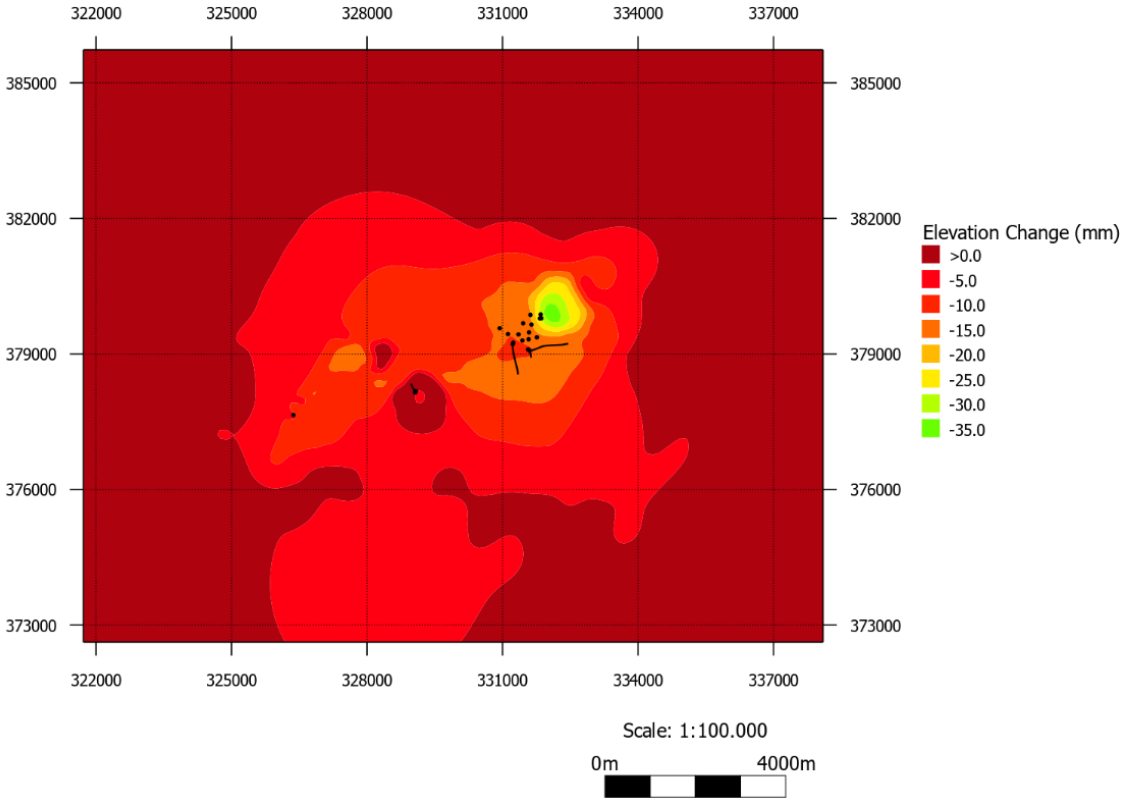

FIGURE 50: Horizontal contour map showing the modelled elevation changes in the Eldvörp-Svartsengi region during 2004-2008

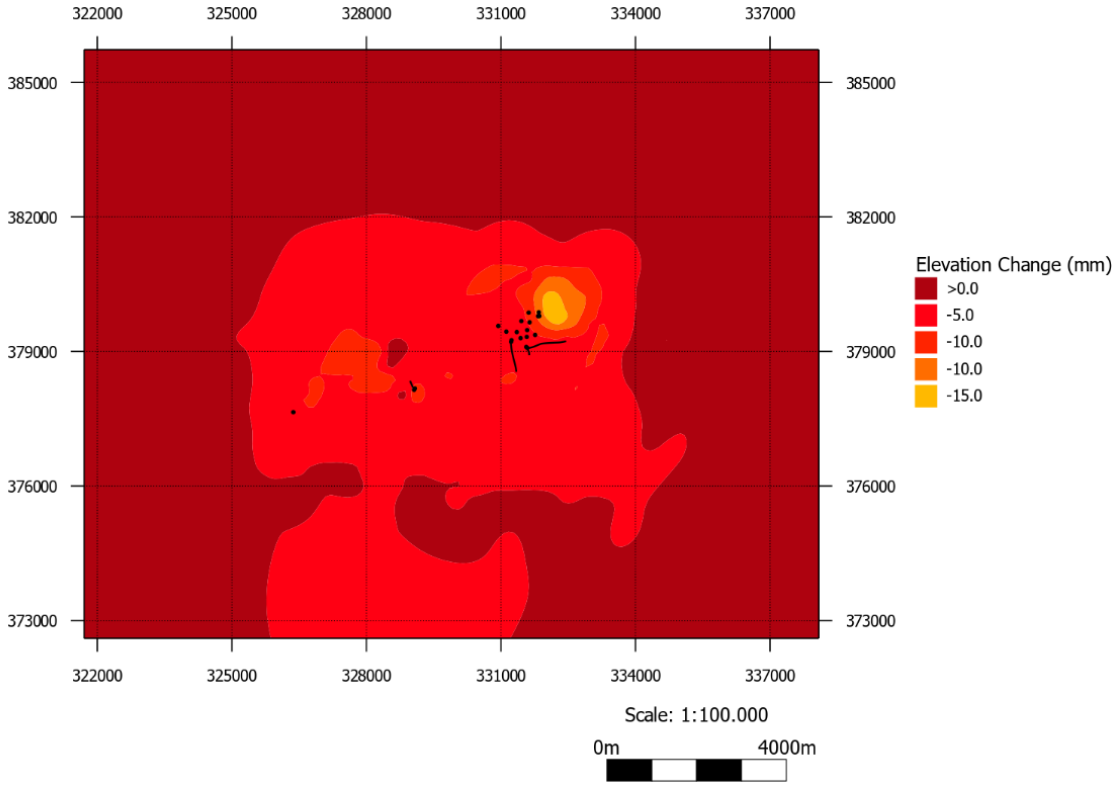

FIGURE 51: Horizontal contour map showing the modelled elevation changes in the Eldvörp-Svartsengi region during 2008-2010

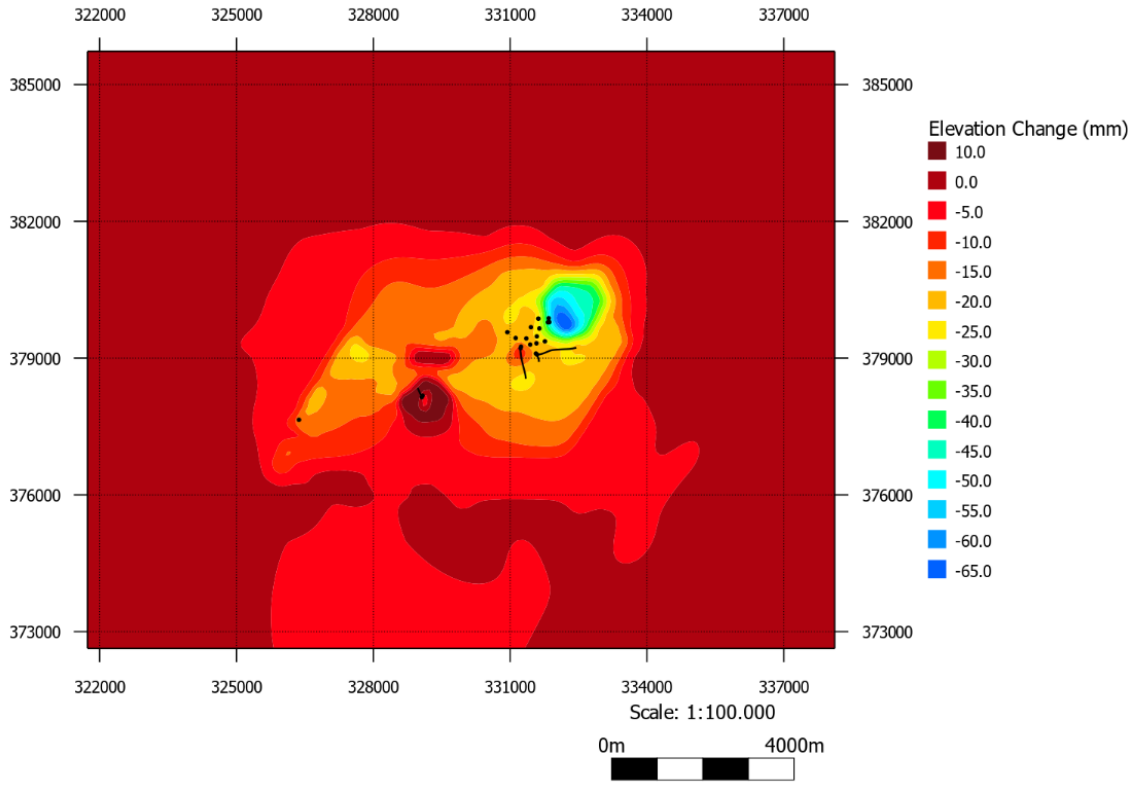

FIGURE 52: Horizontal contour map showing the modelled elevation changes in the Eldvörp-Svartsengi region during 2010-2015

Figure 45 shows the modelled extent of vertical deformation that developed after the first 5 years of production, with the centre of maximum subsidence between 20-30 mm, located in the main well field. Following that, the model calculations show a rapid change in elevation during 1980-1985 (Figure 46) throughout the entire field. A sharp decrease in elevation is observed in the north-east part of the field, which is likely due to the development of the steam zone during this period. Despite the fact that reinjection into well SV-17 didn't commence until 2000, less subsidence is observed in this area in Figure 46 as compared to surrounding regions in Eldvörp and Svartsengi. This may be attributed to the low permeability reservoir rock of the model in this area incorporated to calibrate the pressure drawdown in the field. This general trend continued until 1990, with even sharper changes in elevation around wells SV-02, SV-03, SV-10 (Figure 47).

The period 1990-1999 saw a drastic decrease in the subsidence rate with an average elevation change of 20 mm for this period from Eldvörp to Svartsengi (Figure 48). Reinjection into SV-17 commenced in 2000, which is illustrated by a noticeably reduced change in elevation modelled during 1999-2004 (Figure 49). There was a small change in elevation from 2004-2010 throughout the field. Despite an increase in reinjection from a rate of approximately 180 kg/s in 2010 to an estimated 280 kg/s in 2015, the modelled subsidence rate showed a steady increase during 2010-2015 (Figure 52) with a maximum subsidence of 65 mm near wells SV-02, SV-03 and SV-10. This is contrary to observed subsidence, which has been reported to be insignificant after 2010 (Magnússon, 2015).

Figure 53 shows the overall modelled subsidence over the Eldvörp-Svartsengi region during the 40 years of production from 1975 to 2015. Based on the model, with respect to the reservoir boundaries, the reservoir has subsided by an average of 100-200 mm during this period, with a maximum subsidence of 350 mm (0.35 m) in the steam zone. This is approximately equal to the maximum subsidence of 0.359 m observed in the main well field in 2015 (Magnússon, 2015).

The subsidence map in Figure 53 is closely related to the modelled pressure drawdown in Figure 44 for the same period. A profile was taken along the highly permeable region extending from Eldvörp to

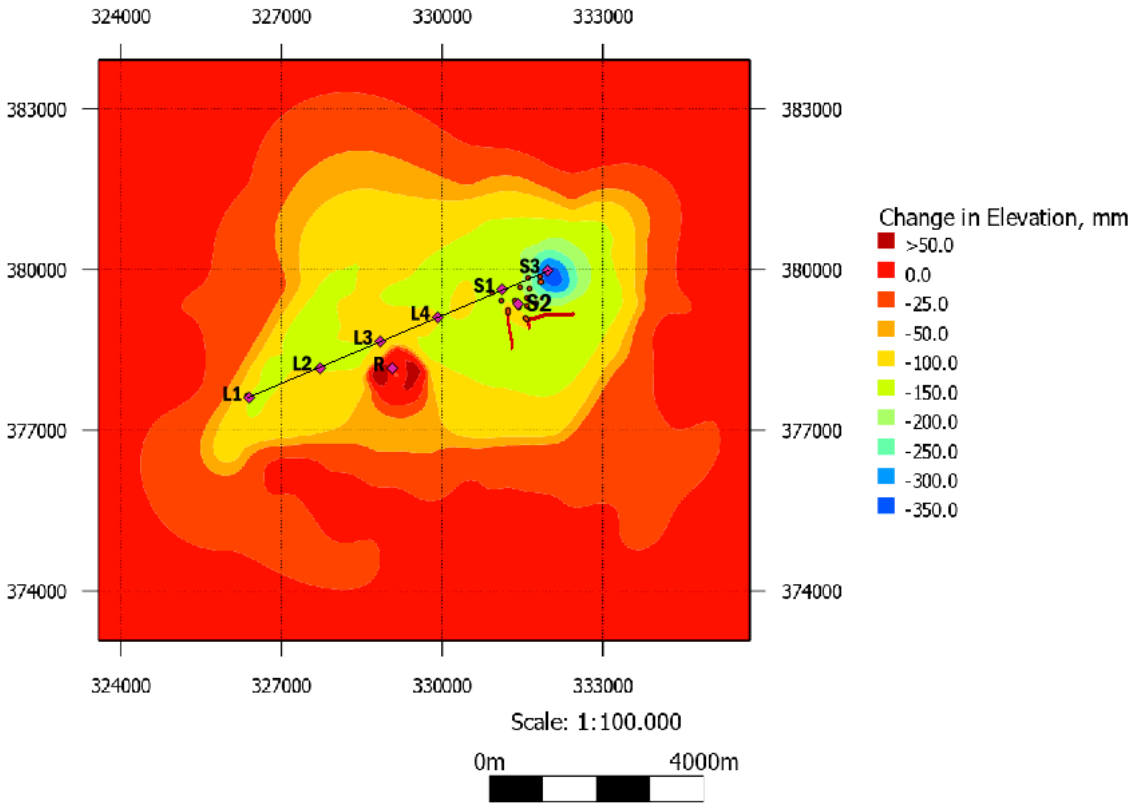

FIGURE 53: Map showing modelled elevation changes in the Eldvörp-Svartsengi region during 40 years of production (1975-2015). The figure shows the location of a cross-section were modelled pressure changes and subsidence are compared (Figures 54-57)

Svartsengi as illustrated in Figure 53. Annual modelled values of subsidence and pressure were selected for each point highlighted in Figure 53 from 1975-2015. These can be seen from Figures 54-57.

Figures 54-57 all show a rather direct correlation between modelled drawdown and modelled subsidence along the field from Eldvörp to Svartsengi, which is not unexpected. As pressure drawdown increases, this leads to a reduction in the pore pressure of surrounding reservoir rocks, thus creating a reduction in the rock matrix, and thereby subsiding. Point S3, which is located in the steam zone, however, shows slight deviation, which may imply that there is another causal factor responsible for subsidence, such as a decrease in temperature, which may be linked with the development of the steam zone. Figures 54-57

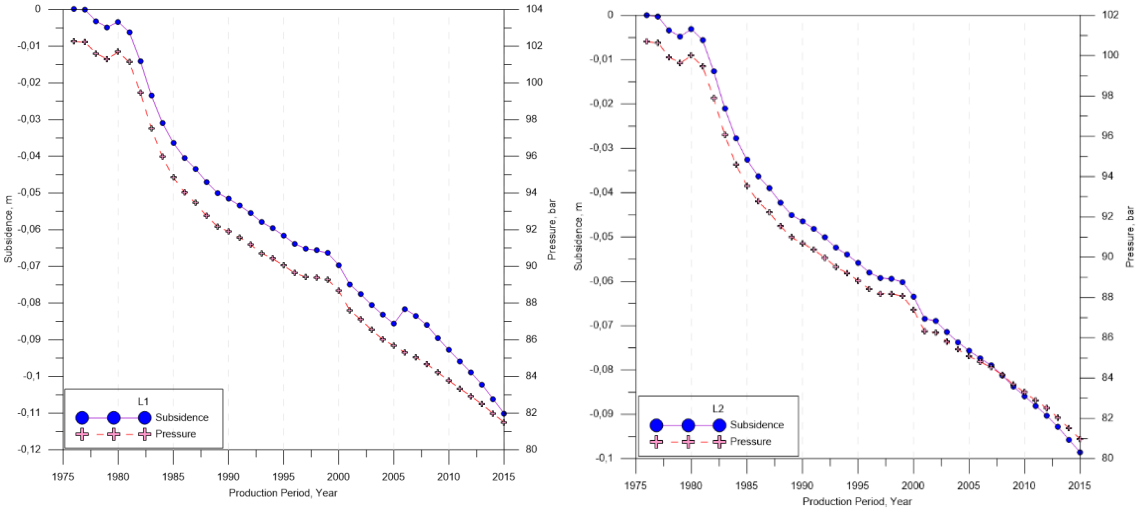

FIGURE 54: Comparison between modelled subsidence and pressure decline at points L1 and L2 from 1975 to 2015

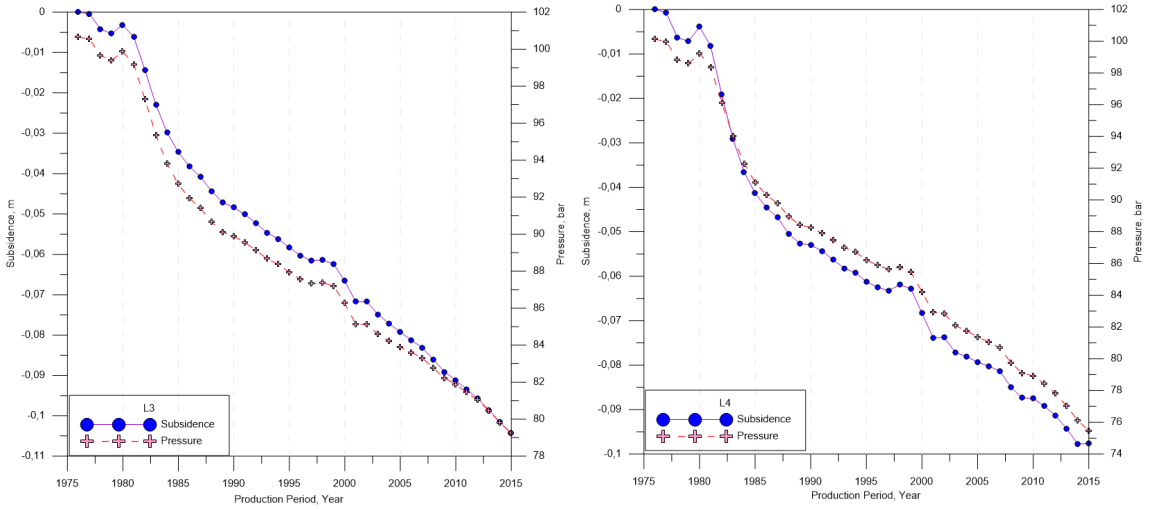

FIGURE 55: Comparison between modelled subsidence and pressure decline at points L3 and L4 from 1975 to 2015

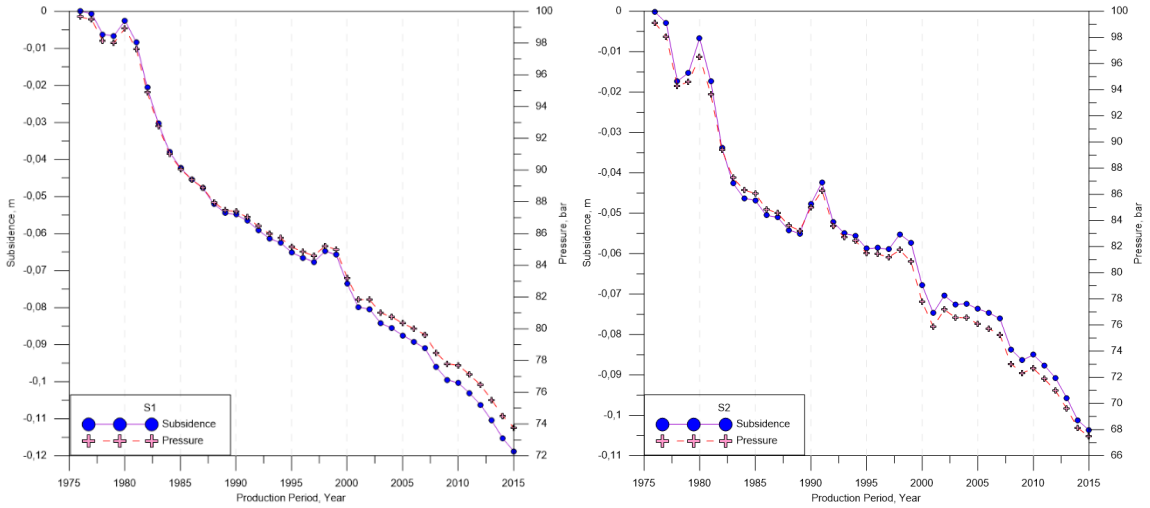

FIGURE 56: Comparison between modelled subsidence and pressure decline at points S1 and S2 from 1975 to 2015

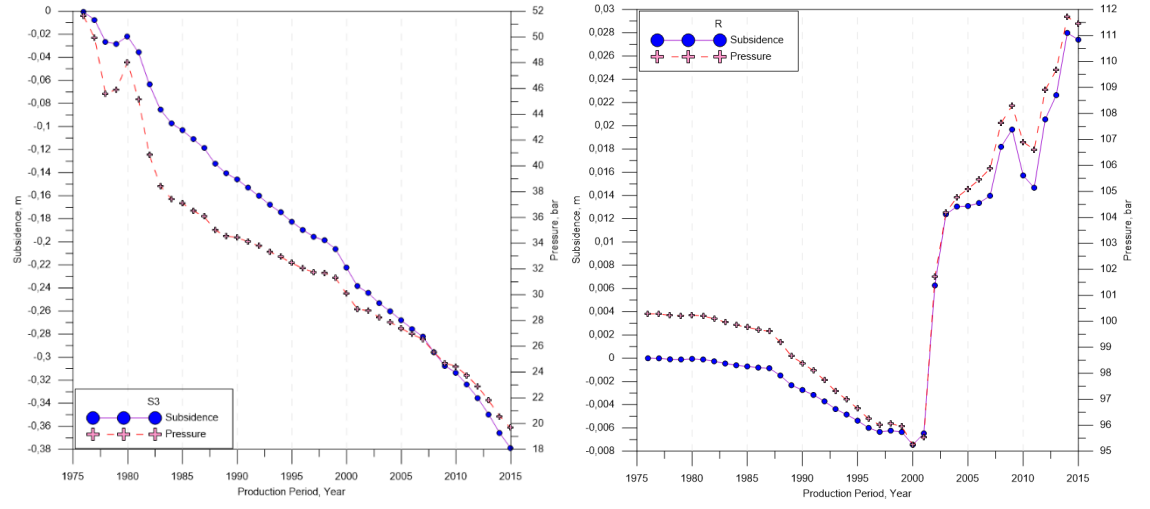

FIGURE 57: Comparison between modelled subsidence and pressure decline at points S3 and R from 1975 to 2015

are in general agreement with observations during 1975 to 2010, although they deviate from the observed rate after 2008. With increased reinjection into SV-17 and SV-24, subsidence has been reported as being somewhat insignificant after 2010 (Magnússon, 2015). However, the modelled results show a slight increase in subsidence towards the main well field during 2010-2015. To study this further, the rate of change of subsidence and pressure with time were calculated for the periods 1975-1980; 1980-1985; 1985-1990; 1990-1995; 1995-2000; 2000-2005; 2005-2010; and 2010-2015. The results of these are presented in Figures 54-57 and Tables 3-4.

TABLE 3: Table showing the average subsidence rates from 1975 to 2015 for points L1, L2, L3, L4, S1, S2, S3 and R

Period	Subsidence rate (mm/year)							
	L1	**L2**	**L3**	**L4**	**S1**	**S2**	**S3**	**R**
1975-1980	-1	-1	-1	-1	-1	-1	-4	0
1980-1985	-7	-6	-6	-7	-8	-8	-16	0
1985-1990	-3	-3	-3	-2	-3	0	-8	0
1990-1995	-2	-2	-2	-2	-2	-2	-7	-1
1995-2000	-2	-2	-2	-1	-2	-2	-8	0
2000-2005	-3	-2	-3	-2	-3	-1	-9	4
2005-2010	-1	-2	-2	-2	-3	-2	-9	1
2010-2015	-3	-3	-3	-2	-4	-4	-13	2
Average	**-3**	**-2**	**-3**	**-2**	**-3**	**-3**	**-9**	**1**

TABLE 4: Average modelled pressure drawdown rates from 1975-2015 for points L1, L2, L3, L4, S1, S2, S3 and R

Period	Drawdown rate (bars/year)							
	L1	**L2**	**L3**	**L4**	**S1**	**S2**	**S3**	**R**
1975-1980	-0.14	-0.17	-0.19	-0.22	-0.18	-0.64	-0.89	-0.01
1980-1985	-1.37	-1.29	-1.43	-1.63	-1.77	-2.09	-2.19	-0.09
1985-1990	-0.59	-0.57	-0.57	-0.57	-0.54	-0.21	-0.53	-0.28
1990-1995	-0.37	-0.37	-0.39	-0.41	-0.45	-0.70	-0.40	-0.35
1995-2000	-0.28	-0.29	-0.33	-0.40	-0.39	-0.74	-0.47	-0.28
2000-2005	-0.60	-0.46	-0.48	-0.57	-0.57	-0.34	-0.54	1.97
2005-2010	-0.38	-0.36	-0.40	-0.49	-0.53	-0.68	-0.59	0.36
2010-2015	-0.45	-0.46	-0.53	-0.69	-0.78	-1.04	-0.95	0.91
Average	**-0.52**	**-0.50**	**-0.54**	**-0.62**	**-0.65**	**-0.81**	**-0.82**	**0.28**

The greatest subsidence at an average rate of 6-7 mm/year is observed during 1980-1985 throughout the field, with the steam zone subsiding at a rate of 16 mm/year. The subsidence rate decreased to an average rate of 2 mm/year during following years, after which it maintained a steady rate of approximately 3 mm/year until 2010.

Pressure recovery and uplift (or reduction in the subsidence rate) is modelled on approaching the well field at the point S2 (Figure 56) during the periods 1989-1991, 1997-1998, 2000-2002, 2008-2010, which may be an effect of increased reinjection in SV-17 and SV-24 during this period. This relationship between subsidence and reinjection will be further discussed in Chapter 5.2

The numerical model developed here only considers vertical deformation due to the mass production at Svartsengi, and ignores all other signals of deformation. Based on the results calculated by this model, the surface of the Eldvörp-Svartsengi geothermal field with reference to the reservoir boundary, is subsiding at an average rate of 3 mm/year. This value increases on approaching the steam zone where the modelled subsidence is greatest, at an average rate of 9 mm/year.

5.2 General discussion

Iceland's location has made it a geological 'hot-spot' for many crustal deformation processes. Subsidence in the Reykjanes Peninsula has been extensively monitored, with numerous studies done to isolate the various signals that contribute to ground deformation. Active tectonism, volcanism and seismicity have long been major contributors to ground deformation in Svartsengi with observed subsidence rates fluctuating in the range of 7 mm/year to 14 mm/year during 1975 to 2015 (Eysteinsson, 2000; Magnússon, 2009; 2013; 2015). The onset of geothermal production at Svartsengi in 1976 saw the formation of a large subsidence bowl extending from Svartsengi, down to and around Eldvörp, which initially led to the theory that Svartsengi and Eldvörp were part of the same reservoir. Further comparison between the pressure drawdown and subsidence showed a direct correlation, which led Eysteinsson (2000) to infer that geothermal production at Svartsengi was one of the major contributors to the vertical deformation observed from 1975-2015.

This study has sought to isolate the geothermal contribution of the total subsidence observed in Svartsengi through the creation of a TOUGH2 numerical model, which has been calibrated against pre-production physical conditions and the production response due to 40 years of geothermal exploitation. It assumes one-dimensional vertical deformation due to geothermal production while ignoring the effects of all other signals that affect the subsidence in Svartsengi.

The model reveals that pressure drawdown and changes in production and reinjection have played major roles in the vertical deformation at Svartsengi. For a more accurate comparison, subsidence at point S2 (Figure 53) which is located in the same element as wells SV-07, SV-08 and SV-19, has been plotted alongside the pressure drawdown observed in well SV-08 (Figure 21) from 1975-2015. These were compared with the average annual production and reinjection at Svartsengi from 1975-2015 and the results are presented in Figure 58.

Figure 58 reveals a close correlation between observed drawdown in well SV-08 and modelled subsidence at point S2 from 1982 to 2005. Observed drawdown in SV-08 did exhibit a rapid decline of an estimated 10 bars during 1982-1989 correlating to high rates of both observed subsidence (Eysteinsson, 2000) and modelled subsidence during this period. A slight decrease in the modelled subsidence from 1991 to 1999 correlates with a reduction in the pressure drawdown from 1990 to 1994. Modelled subsidence also appears to be affected by the reduced production, and the introduction of reinjection in the main well field around this period.

A considerable reduction in pressure drawdown has, however, been observed from since around 2002 as a response to the onset of reinjection of fluid into well SV-17 in 2000, despite an increase in the average production to 11.39 million tonnes/year, equivalent to 370 kg/s. The period (2000-2005) similarly experienced a reduction in both the observed subsidence (Figure 23) and modelled subsidence. The modelled subsidence however appears to deviate from observed after 2008 despite a large decrease in the net production, due to a large increase in the volume of fluid being injected into SV-17 and SV-24. The model, although it reacts well to early reinjection within the wellfield, deviates from expected, with a somewhat greater than expected modelled drawdown and subsidence (Figures 41-43 and Figures 54-57).

A few years after production started, the area of maximum subsidence was observed at a point between Svartsengi and Eldvörp (Eysteinsson, 2000). This, however, was not reproduced in the model, with maximum subsidence occurring in the steam zone. This deviance may, however, be explained by a limited resolution or accuracy in the observed data due to the larger distances between elevation stations, whereas in the model, the subsidence was calculated for each element, which is a much denser network than what was measured in reality.

Another factor that may contribute to these divergences between measured and modelled results, is a low permeability barrier modelled around the reinjection site to simulate the great pressure drawdown in well EV-02. The model's permeability distribution can be seen in Appendix A. This low permeability barrier appears to have created too much pressure support in that zone from around 1980, made evident

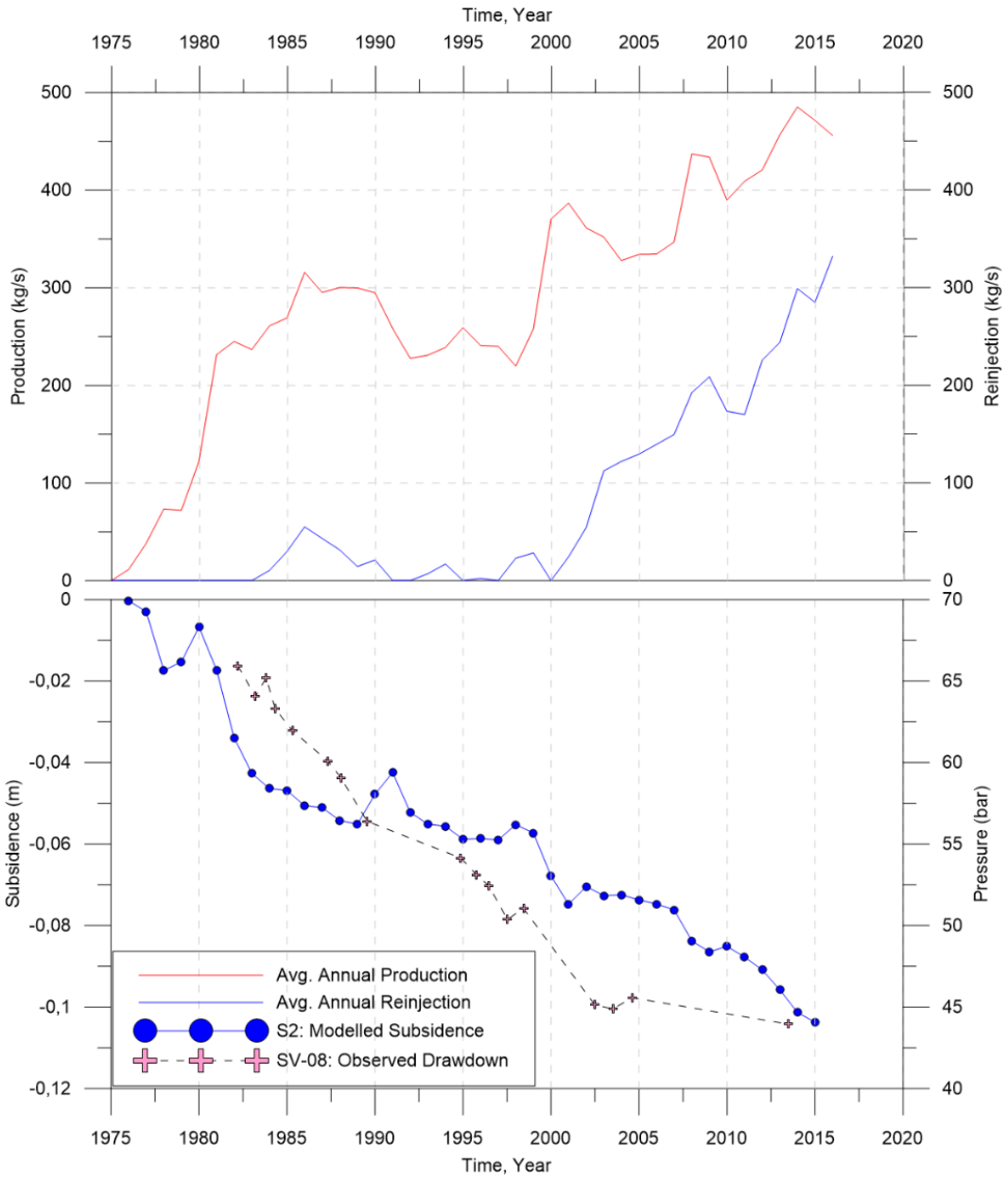

FIGURE 58: A graph showing the correlation of the annual average production and reinjection, on one hand, with observed pressure drawdown in well SV-08 and modelled subsidence at point S2, on the other hand

by the low rate of subsidence modelled there, seen in Figure 46 -Figure 52, which would have reduced the pressure support in the reservoir. This would have resulted in an increased drawdown, and thus increasing the rate of subsidence from 3 mm/year before 2010 to 4 mm/year after 2010. This shows the dependency of subsidence, not only on pressure drawdown due to geothermal production, but on permeability of reservoir rocks.

An additional factor contributing to divergence from observed/expected values is an overestimation of volumetric strain in the z-direction. Since the subsidence module in iTOUGH2 only models one-dimensional deformation, all deformation is assumed to be vertical, whereas in reality, some horizontal deformation will also occur.

Even though these factors are very likely to explain the modelled deviation, at least partly, another possible explanation of this disparity could be changes due to seismicity as a result of recorded seismic events around this period. Approximately 82 earthquakes of magnitudes ranging between -0.9 to 1.9 M_L were recorded around the reinjection wells, around 3 km WSW of the production field during December

2008 – May 2009, with epicentres located between 2 and 5 km depth (Gudnason, 2014). A significant earthquake swarm with a total of 29 earthquakes occurred within a five hour period on March 6, 2009. It was centred approximately 500 m north-west of the injection boreholes at Svartsengi with magnitudes ranging from 0.17 M_L to 1.26 M_L (Gudnason, 2014). In such cases, unexplained pressure recovery may occur despite stable production from the reservoir as observed in Thykkvabær in 2000 (Björnsson et al., 2001). This may explain the decrease in pressure drawdown observed in the Svartsengi well field in 2008. This seismic signal is not included in this model, therefore modelled recovery after 2008 would not have been possible.

This modelling study shows that the average subsidence rate throughout the Eldvörp-Svartsengi geothermal field is 3-4 mm/year, with up to 8-9 mm/year in the north-east part of the field during 1975-2015. This increase in the north-east is due to the expansion of the steam zone, where subsidence would be greater due to the higher compressibility of steam, as compared to that of liquid water and basaltic reservoir rocks.

Overall, there was a direct correlation between pressure drawdown, subsidence, and changes in production and reinjection. This when added to the natural rate of subsidence along the central volcanic rift of the Reykjanes Peninsula, represents the contribution of geothermal production to vertical crustal deformation at Svartsengi.

6. CONCLUSIONS AND RECOMMENDATIONS

This project sought to contribute to previous deformation studies conducted at Svartsengi through the development of a TOUGH2 numerical model of the Svartsengi geothermal system. It was calibrated against initial thermodynamic conditions, the average annual mass extraction and reinjection rates during 40 years of production from 1975 to 2015, and the resulting reservoir response (mainly pressure decline).

Spanning an area of 468 km^2 and extending from sea-level to a depth of 2550 m, this model is heated from below by a constant temperature boundary, corresponding to an enthalpy of 2799 kJ/kg. It is fed by three pre-determined mass flow sources, A, B and C, producing a thermal output of 68 MW_t, 45 MW_t and 124.8 MW_t respectively. Formation temperature profiles revealed isothermal temperatures of 240°C at depths exceeding 900 m indicating the convective nature of the Svartsengi geothermal system. The numerical model was successfully calibrated through the application of:

1. High vertical permeabilities along the upflow zones A, B and C; and
2. High horizontal permeabilities traversing from Eldvörp to Svartsengi.

The output from the natural state model was used as initial conditions for the production model. The modelled drawdown from 1975 to 2015 at 1050 m b.s.l. is comparable to the observed drawdown in wells EV-02, SV-08, SV-09, SV-11, SV-12, SV-19 (Figures 41-43) at 900 m b.s.l., although the modelled response showed less recovery than observed after 2000. One-dimensional subsidence modelling was performed with the model, using a newly developed subsidence module in iTOUGH2. Using typical values for pore compressibility and thermal expansivity of basaltic rocks, the vertical deformation was calculated due to the average annual rates of production and reinjection from 1975 to 2015.

The current conceptual model of the Svartsengi high-temperature system assumes a direct, high permeability connection traversing through Eldvörp and Svartsengi. The initial set-up of the model followed this assumption, however, as reinjection in SV-17 commenced, there was little pressure decline modelled at Eldvörp, which indicates that there was too much pressure support from reinjection in the model. In order to simulate increased drawdown at Eldvörp, the permeability structure was slightly modified as seen in Appendix A. A low-permeability barrier was placed around Source B, so as to reduce the pressure support to Eldvörp. This indicates that the existing conceptual model should be modified to reflect this change.

The modelled results reveal a close correlation between pressure drawdown and subsidence within the field. Changes in production, reinjection, permeability and pressure drawdown were found to be major causal factors for the modelled subsidence. The numerical model calculated an average subsidence velocity of 3-4 mm/year as a result of geothermal exploitation at Svartsengi, with a maximum subsidence of 0.35 m above the steam zone of the reservoir in 2015. This should be added to the natural background subsidence rate of 6 mm/year along the central volcanic rift zone on the Reykjanes Peninsula previously proposed by a combined analysis of a variety of geodetic studies. Compared with the total observed subsidence at Svartsengi, this is within the observed range of 7 mm/year to 14 mm/year from 1975 to 2015.

The simulations performed in this thesis correlate well with the observed conditions in the Svartsengi geothermal system, however there were observed deviations between both datasets. The following recommendations are proposed as further improvements:

1. Modelled parameters were manually adjusted throughout the development of the numerical model. In an effort to better estimate these parameters, inverse modelling with iTOUGH2 is recommended. Parameter estimation, along with a sensitivity and error analysis should be performed. This would: (a) estimate parameters with a greater accuracy; (b) determine the most sensitive parameters affecting the modelled response, and: (c) determine a statistical fit between modelled and observed data, thereby increasing accuracy and confidence in the modelled

response. With a better calibrated fit, the subsidence module can then be tested on a more complex model, such as Vatnaskil's existing reservoir model of the Svartsengi system.

2. Accuracy could be further improved by calibrating the model against mass changes observed as gravity changes due to mass extraction and reinjection. Gravity calibration is extremely useful in detecting the areal extent of boiling within the reservoir. Coupled with changes in elevation, this will serve as a further calibration tool for numerical modelling.

3. As a recommendation for future work in ground deformation studies at Svartsengi, a two or three-dimensional subsidence model can be set up to model the extent of the subsidence bowl that was created after the commencement of production in 1976. This can be done through the combined analysis of InSAR, geodetic modelling methods such as Mogi Modelling and reservoir modelling employing the Integral Finite Difference Method, thereby giving a more holistic view of the elevation changes along the Svartsengi Geothermal System.

Despite only considering one-dimensional subsidence, the model accurately simulates the subsidence observed at Svartsengi. The newly developed subsidence module is therefore a valuable tool that can be used for predictions due to future geothermal production at Svartsengi and Eldvörp. The addition of subsidence data to reservoir models not only has the potential to increase its accuracy, but the direct correlation of subsidence and pressure makes it possible to calibrate the model in parts of the reservoir where there are no drawdown measurements, or no wells drilled.

REFERENCES

Árnadóttir, Th., Geirsson, H., and Einarsson, P., 2004: Coseismic stress changes and crustal deformation on the Reykjanes Peninsula due to triggered earthquakes on 17 June 2000. *J. Geophysical Research, 109,* 1-12.

Árnadóttir, Th., Jiang, W., Feigl, K., Geirsson, H., and Sturkell, E., 2006: Kinematic models of plate boundary deformation in southwest Iceland derived from GPS observations. *J. Geophysical Research 111 (B7),* 1-16.

Árnason, K., Karlsdóttir, R., Eysteinsson, H., Flóvenz, Ó.G., and Gudlaugsson, S.Th., 2000: The resistivity structure of high-temperature geothermal systems in Iceland. *Proceedings of the World Geothermal Congress WGC2000, Kyushu-Tohoku, Japan,* 923-928.

Axelsson, G., 2013: Dynamic modelling of geothermal systems. *Proceedings of Short Course V on Conceptual Modelling of Geothermal Systems, Santa Tecla, El Salvador, UNU-GTP and LaGeo,* 21 pp.

Axelsson, G., Arnaldsson, A., Berthet, J-C.C., Bromley, C.J., Gudnason, E.A., Hreinsdóttir, S., Karlsdóttir, R., et al., 2015: Renewability assessment of the Reykjanes geothermal system, SW-Iceland. *Proceedings of the World Geothermal Congress WGC2015, Melbourne, Australia*, 10 pp.

Björnsson, G., 1999: Predicting future performance of a shallow steam-zone in the Svartsengi geothermal field, Iceland. *Proceedings of the 24th Workshop on Geothermal Reservoir Engineering, Stanford University, Stanford, CA,* 7 pp.

Björnsson, G., and Steingrímsson, 1991: *Temperature and pressure in the Svartsengi geothermal system – Initital status and changes due production.* Orkustofnun, Reykjavík, report prepared for Hitaveitu Sudurnesja, OS-91016/JHD-04 (in Icelandic with English summary), 69 pp.

Björnsson, G., Flóvenz, Ó.G., Saemundsson, K., and Einarsson, E., 2001: Pressure changes in Icelandic geothermal reservoirs associated with two large earthquakes in June 2000. *Proceedings of the 26th Workshop on Geothermal Reservoir Engineering, Stanford University, Stanford, CA*, 8 pp.

Bödvarsson, G.S., 1988: Model predictions of the Svartsengi reservoir, Iceland. *Water Resources Research, 24-10,* 1740-1746.

Clifton, A.E., and Kattenhorn, S.A., 2006: Structural architecture of a highly oblique divergent plate boundary segment. *Tectonophysics, 419,* 27-40.

Croucher, A., 2017: *PyTOUGH user's guide*. University of Auckland, Auckland, New Zealand.

DeMets, C., Gordon, R.G., Argus, D.F., and Stein, S., 1994: Effect of recent revisions to the geomagnetic reversal time scale on estimates of current plate motions. *Geophys. Res. Lett., 21*, 2191-2194.

Einarsson, P., 2008: Plate boundaries, rifts and transforms in Iceland. *Jökull, 58,* 35-58.

Einarsson, P., and Saemundsson, K., 1987: Earthquake epicentres 1982-1985 and volcanic systems in Iceland (map). In: Sigfússon, Th. (ed.), *As a matter of fact. Festschrift for Thorbjörn Sigurgeirsson.* Menningarsjódur, Reykjavík.

Einarsson, P., Sigmundsson, F., Sturkell, E., Árnadóttir, Th., Pedersen, R., Pagli, C., and Geirsson, H., 2006: Geodynamic signals detected by geodetic methods in Iceland. *Wissenschaftliche Arbeiten der Fachrichtung Geodäsie und Geoinformatik der Universität Hannover, 258* (in German), 39-57.

Einarsson, P., Björnsson, S., Foulger, G., Stefánsson, R., and Skaftadóttir, Th., 1981: Seismicity pattern in the South Iceland Seismic Zone. In: Simpson, D. and Richards, P. (eds.), *Earthquake prediction – an international review. American Geophys. Union, Maurice Ewing Series, 4*, 141-151.

Eysteinsson, H., 1993: *Elevation- and gravity measurements on the outer Reykjanes Peninsula 1992.* Orkustofnun, Reykjavik, report OS-93029/JHD-08 (in Icelandic), 53 pp.

Eysteinsson, H., 2000: Elevation and gravitational changes at geothermal fields on the Reykjanes Peninsula, SW-Iceland. *Proceedings of the World Geothermal Congress WGC2000, Kyushu-Tohoku, Japan,* 559-564.

Finsterle, S., 2007: *iTOUGH2 User's Guide*. Lawrence Berkeley National Laboratory, report LBNL-40040, Berkeley, CA.

Finsterle, S., 2018a: *Enhancements to TOUGH2 simulator integrated in iTOUGH2*. iTOUGH2, user manual. Finsterle GeoConsulting, Ca.

Finsterle, S., 2018b: *iTOUGH2 v7.1.1 command reference*. iTOUGH2 V7.1.1 manual. Lawrence Berkeley National Laboratory, Berkeley, CA.

Franzson, H., 1983: The Svartsengi high-temperature field subsurface geology and alteration. *Geothermal Resources Council, Trans. 7,* 141-145.

Franzson, H., 1987: The Eldvörp high-temperature area, SW-Iceland. Geothermal geology of the first exploration well. *Proceedings of the 9th New Zealand Workshop, Auckland, NZ,* 179-185.

Franzson, H., 1990: *Svartsengi: Geothermal model of a high-temperature system and its surroundings.* Orkustofnun, Reykjavík, report OS-90050/JHD-08 (in Icelandic), 42 pp.

Franzson, H., 2017: Svarts*engi-Eldvörp, a conceptual geological model of the geothermal reservoir.* ÍSOR – Iceland GeoSurvey, Reykjavík, report ÍSOR-2017/017 (closed), 69 pp.

Fridleifsson, G.Ó., and Richter, B., 2010: The geological significance of two IDDP-ICDP spot cores from the Reykjanes geothermal field, Iceland. *Proceedings of the World Geothermal Congress WGC2010, Bali, Indonesia,* 7 pp.

Geirsson, H., Árnadóttir, T., Hreinsdóttir, S., Decriem, J., LaFemina, P.C., Jónsson, S., Bennett, R.A., et al., 2011: Overview of results from continuous GPS observations in Iceland from 1995-2010. *Jökull 60,* 3-22.

Georgsson, L.S., 1981: A resistivity survey on the plate boundaries in the Western Reykjanes Peninsula, Iceland. *Geothermal Resources Council, Transactions 5,* 75-78.

Grant, M., and Bixley, P., 2011: *Geothermal reservoir engineering* (2nd ed.). Acad. Press, NY, 378 pp.

Gudmundsdóttir, V., 2016: *Svartsengi-Reykjanes reservoir temperature and pressure monitoring report 2015*. ÍSOR – Iceland GeoSurvey, Reykjavík, report ÍSOR-2016/032 (closed), 85 pp.

Gudmundsson, J.S., 1983: Injection testing in 1982 at the Svartsengi high-temperature field in Iceland. *Geothermal Resources Council, Transactions 7,* 423-428.

Gudmundsson, J.S., and Thórhallsson, S., 1986: The Svartsengi reservoir in Iceland. *Geothermics, 15-1,* 3-15.

Gudnason, E.Á., Arnaldsson, A., Axelsson, G., Berthet, J-C.C., Halldórsdóttir, S., and Magnússon, I.Th., 2015: Analysis and modelling of gravity changes in the Reykjanes geothermal system in Iceland, during 2004-2010. *Proceedings of the World Geothermal Congress WGC2015, Melbourne, Australia*.

Gudnason, E.Á., 2010: *Use of repeated gravity and elevation measurements to estimate the effect of production in a geothermal system.* University of Iceland, Reykjavík, BSc final project.

Gudnason, E.Á., 2014: *Analysis of seismic activity on the western part of the Reykjanes Peninsula, SW Iceland, December 2008 - May 2009*. University of Iceland, Reykjavík, MSc thesis, 81 pp.

Hammer, S., 1945: Estimating ore masses in gravity prospecting. *Geophysics, 10,* 50-62.

Haukwa, C.B., 1999: *AMESH, A mesh creating program for the integral finite difference method, user's guide version 1.0*. Lawrence Berkeley National Laboratory, report, 54 pp.

Hreinsdóttir, S., Einarsson, P., and Sigmundsson, F., 2001: Crustal deformation at the oblique spreading Reykjanes Peninsula, SW Iceland: GPS measurements from 1993-1998. *J. Geophysical Research,* 106-B7, 13,803-13,816.

Jónsson, J.E., 2012: *Simulation of output curves and wellhead pressure from high enthalpy wells in the Svartsengi geothermal field, SW-Iceland*. University of Iceland, Reykjavík, MSc thesis, 92 pp.

Karlsdóttir, R., 1998: *TEM-resistivity measurements in Svartsengi, 1997.* Orkustofnun, Reykjavík, report OS-98025 (closed – in Icelandic), 46 pp.

Karlsdóttir, R., and Vilhjálmsson, A.M., 2015: *Svartsengi-Eldvörp-Sandvík 3D inversion of MT data*. ÍSOR - Iceland GeoSurvey, Reykjavík, report ÍSOR-2015/001 (closed), 166 pp.

Keiding, M., Árnadóttir, Th., Sturkell, E., Geirsson, H., and Lund, E., 2008: Strain accumulation along an oblique plate boundary: the Reykjanes Peninsula, Southwest Iceland." *Geophysical J. International, 172,* 861-872.

Keiding, M., Árnadóttir, Th., Jónsson, S., Hooper, A., and Decriem, J., 2010: Plate boundary deformation and man-made subsidence around geothermal fields on the Reykjanes Peninsula, Iceland. *J. Volcanology and Geothermal Research, 194,* 139-149.

Ketilsson, J., 2007: *Production capacity assessment of geothermal resources by numerical modelling*. University of Iceland, Reykjavík, MSc thesis.

Kjaran, S.P., Halldórsson, G.K., Thórhallsson, S., and Elíasson, J., 1979: Reservoir engineering aspects of Svartsengi geothermal area. *Geothermal Resources Council, Transactions, 3*, 337-339.

Kjaran, S.P., Elíasson, J., and Halldórsson, G.K., 1980: *Svartsengi – Examination of geothermal production.* Orkustofnun, Reykjavík, report prepared for Hitaveitu Sudurnesja, OS080021/ROD10-JHD17 (in Icelandic), 98 pp.

Koros, W., O'Sullivan, J., Pogacnik, J., and O'Sullivan, M., 2016: Modelling of subsidence at the Wairakei geothermal field, New Zealand. *Proceedings of the 38th New Zealand Geothermal Workshop, Auckland, NZ*, 8 pp.

Kristjánsson, L. and Jónsson, G., 2018: A total-field magnetic anomaly map of the Reykjanes Peninsula, Southwest Iceland. *Jökull, 67,* 43-49.

Magnússon, I.Th., 2009: *GNSS- and gravity measurements on the outer Reykjanes Peninsula 2008.* ÍSOR - Iceland GeoSurvey, Reykjavík, report prepared for HS Orka Ltd., ÍSOR-2009/029, 60 pp.

Magnússon, I.Th., 2013: *GNSS- and gravity measurements on the outer Reykjanes Peninsula 2010.* ÍSOR - Iceland GeoSurvey, Reykjavík, report prepared for HS Orka Ltd., ÍSOR 2013/066.

Magnússon, I.Th., 2015: *GNSS- and gravity measurements on the outer Reykjanes Peninsula 2014.* ÍSOR - Iceland GeoSurvey, Reykjavík, report prepared for HS Orka Ltd., ÍSOR 2015/053, 82 pp.

O'Sullivan, J., and O'Sullivan, M., 2016: The effect of bottom boundary conditions on predictions of steam production from geothermal reservoir models. *Proceedings of the 41st Workshop on Geothermal Reservoir Engineering, Stanford University, Stanford, CA*, 12 pp.

Pruess, K., Oldenburg, C., and Moridis, G., 2012: *TOUGH2 User's Guide, Version 2.* Lawrence Berkeley National Laboratory, Berkeley, CA.

Receveur, M., 2018: *Ground deformation induced by geothermal utilization at Reykjanes, SW-Iceland, inferred from interferometric analysis of Sentinel-1 Synthetic Aperture Radar Images (InSAR)*. University of Iceland, Reykjavík, MSc thesis, 143 pp.

Sturkell, E., Sigmundsson, F., Einarsson, P., and Bilham, R., 1994: Strain accumulation 1986-1992 across the Reykjanes Peninsula plate boundary, Iceland, determined from GPS measurements. *Geophysical Research Letters, 21-2,* 125-128.

Thórhallsson, S., Hauksson, T., Kjaran, S.P. Ólafsson, M., and Albertsson, A., 2004: *Reinjection in Svartsengi – from experiments to steady operation.* Geothermal Association of Iceland, Workshop, Reykjavík.

Vadon, H., and Sigmundsson, F., 1997: Crustal deformation from 1992 to 1995 at the Mid-Atlantic Ridge, Southwest Iceland, mapped by Satellite Radar Interferometry. *Science, 275,* 193-197.

Verkís, 2016: *Svartsengi power plant*. Verkís Consulting Engineering, website (Oct. 5, 2016): *www.verkis.com/projects/energy-production/geothermal-energy/nr/936.*

Wolfe, C.J., Bjarnason, I.Th., Van Decar, J.C., and Solomon, S.C., 1997: Seismic structure of the Iceland mantle plume. *Nature, 385*, 245-247.

APPENDIX A: Rock distribution

The rock material layout used to set up this numerical model is given for each layer in Figures A1-A13. This model consists of 17 different rock types, according to the methodology employed in Chapter 4.

The model is divided into 13 layers of varying thickness. Layer A (Figure A1) and Layer M (Figure A13) are made up of the 'inactive' surface and basement materials, respectively. Based on the conceptual model discussed in Chapter 2, the clay cap layer, which observed between 300-600 m b.s.l., is modelled in layers B and C, seen in Figures A2 and A3, respectively.

Three upflow zones, A, B and C with high vertical permeabilities are modelled throughout layers D to L as described in Chapter 4.2.1. In order to reduce pressure support from the model's boundaries, the permeabilities in layers D to I were set up according to the methodology outlined in Chapter 4.2.2. The current conceptual model of the Svartsengi high-temperature system assumes a direct, high permeability connection traversing through Eldvörp and Svartsengi. The initial set-up of the model in Chapter 4.2.2 followed this assumption, however, as reinjection in SV-17 commenced, there was little pressure decline modelled at Eldvörp, signalling that there was too much pressure support from reinjection. In order to simulate increased drawdown at Eldvörp, the permeability structure was slightly modified as seen in Figures A4-A9. A low permeability barrier was placed around Source B, so as to reduce the pressure support to Eldvörp.

In an effort to simulate the high temperatures in the two-phase zone, rock material RCK08 was applied around the steam zone and were given high horizontal permeabilities to support the pressure drop associated with the creation of the steam zone.

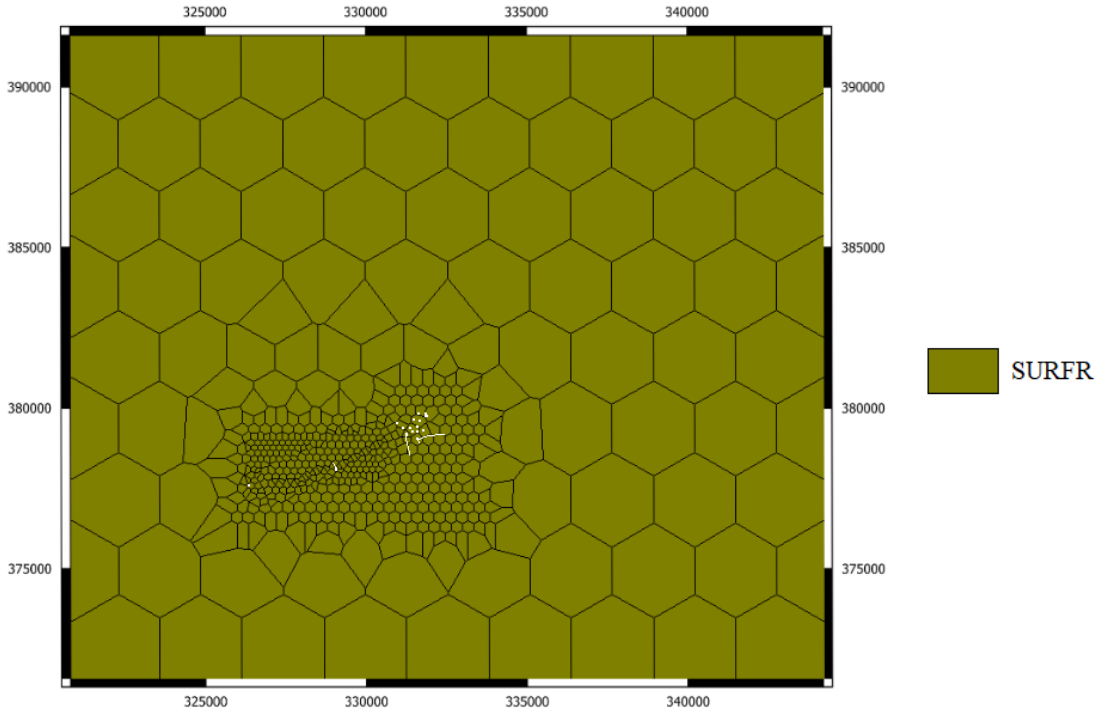

FIGURE A1: Rock distribution in Layer A, with well traces shown as a reference

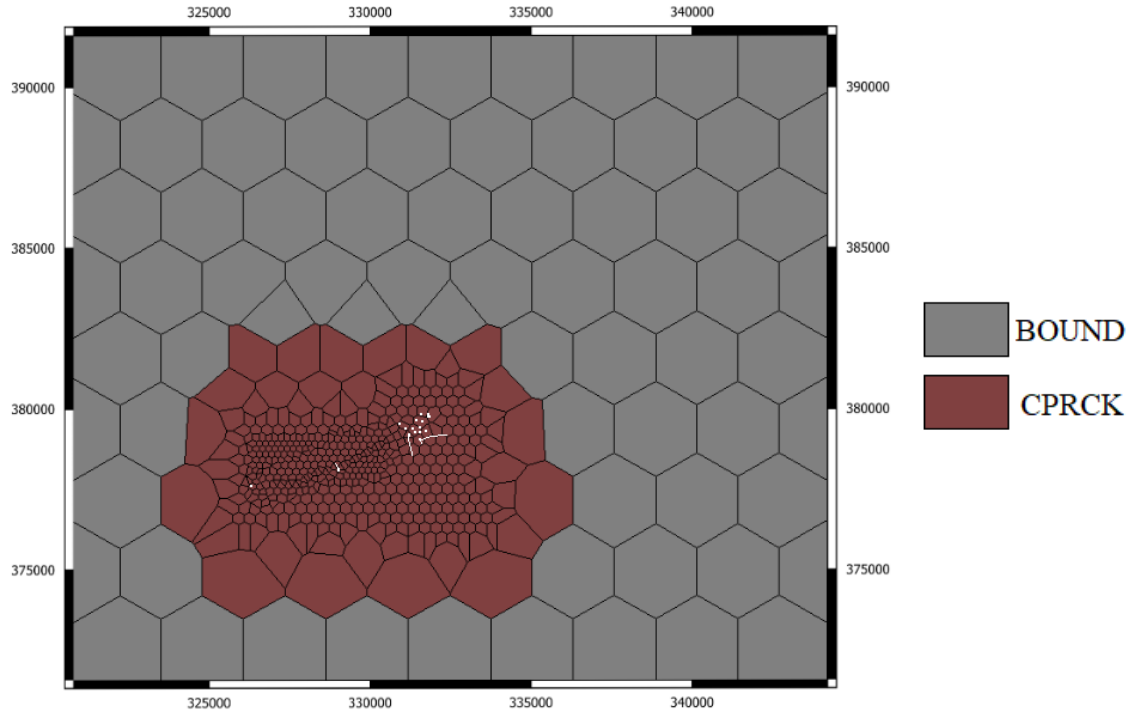

FIGURE A2: Rock distribution in Layer B, with well traces shown as a reference

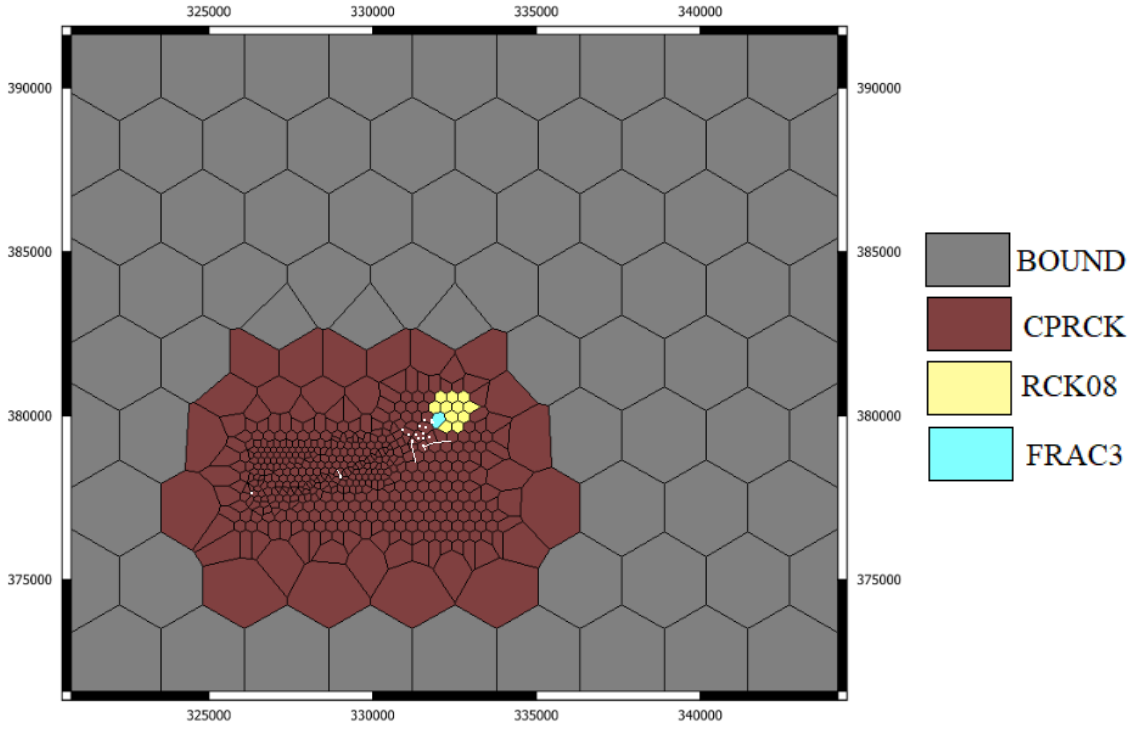

FIGURE A3: Rock distribution in Layer C, with well traces shown as a reference

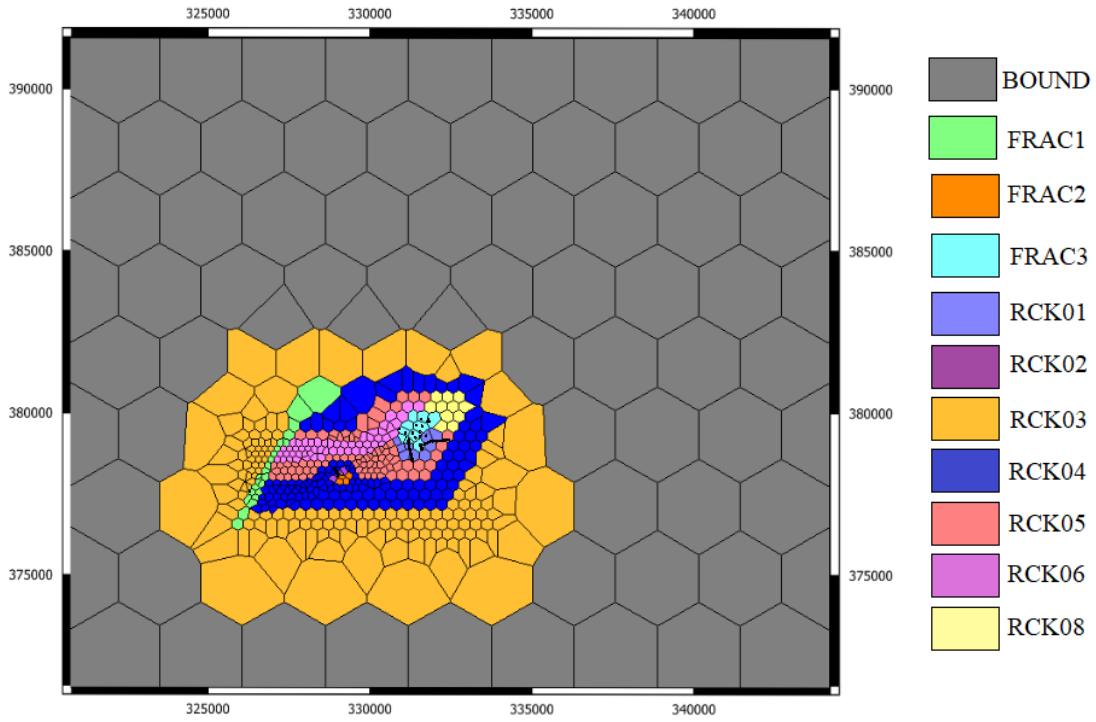

FIGURE A4: Rock distribution in Layer D, with well traces shown as a reference

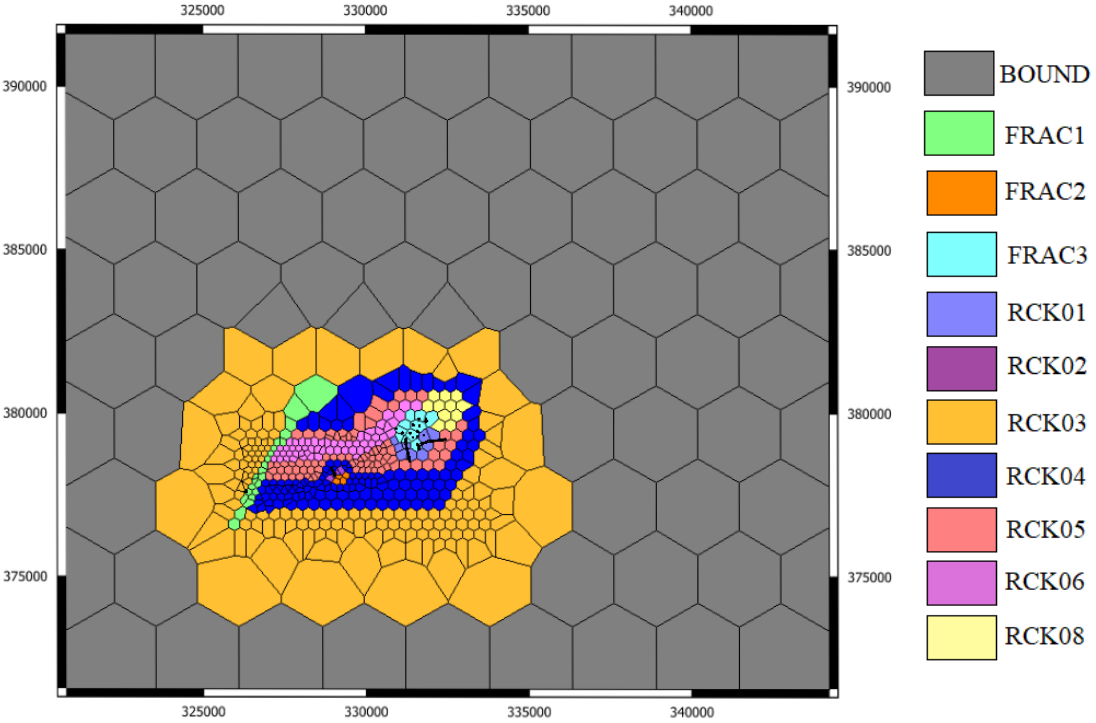

FIGURE A5: Rock distribution in Layer E, with well traces shown as a reference

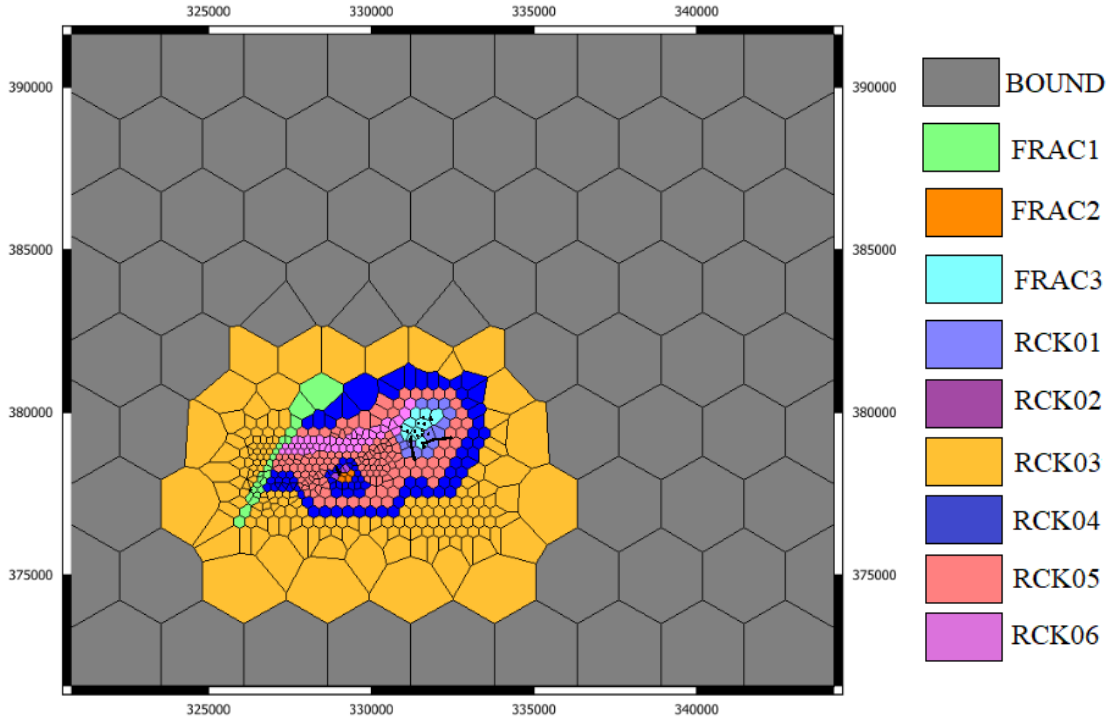

FIGURE A6: Rock distribution in Layer F, with well traces shown as a reference

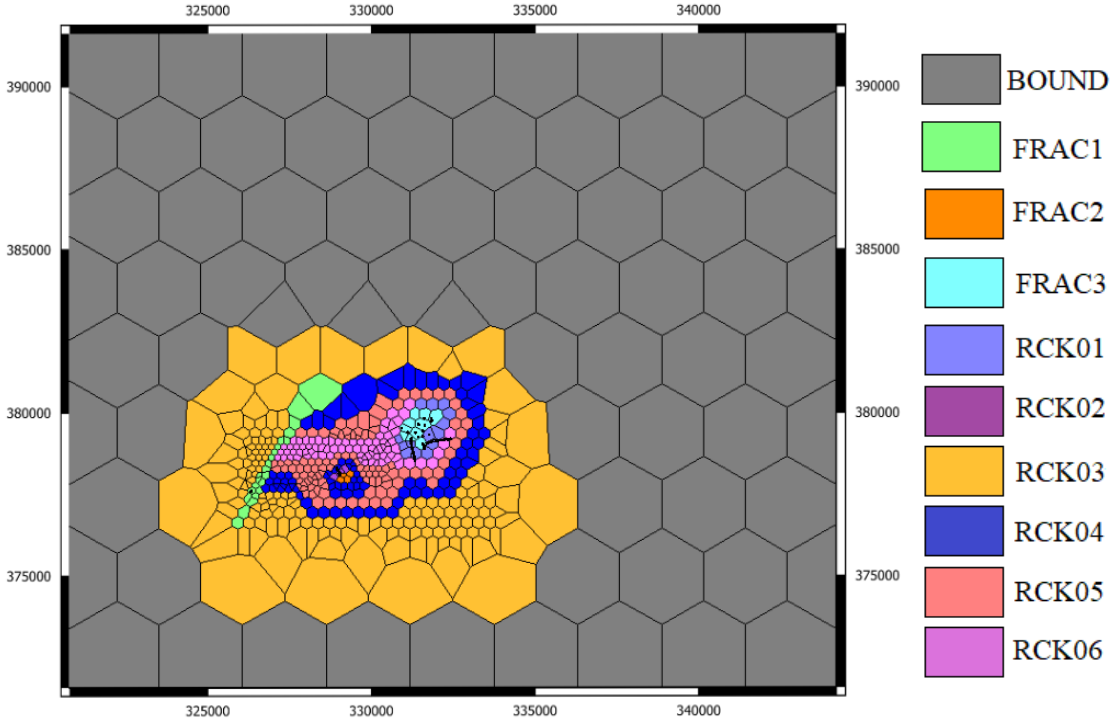

FIGURE A7: Rock distribution in Layer G, with well traces shown as a reference

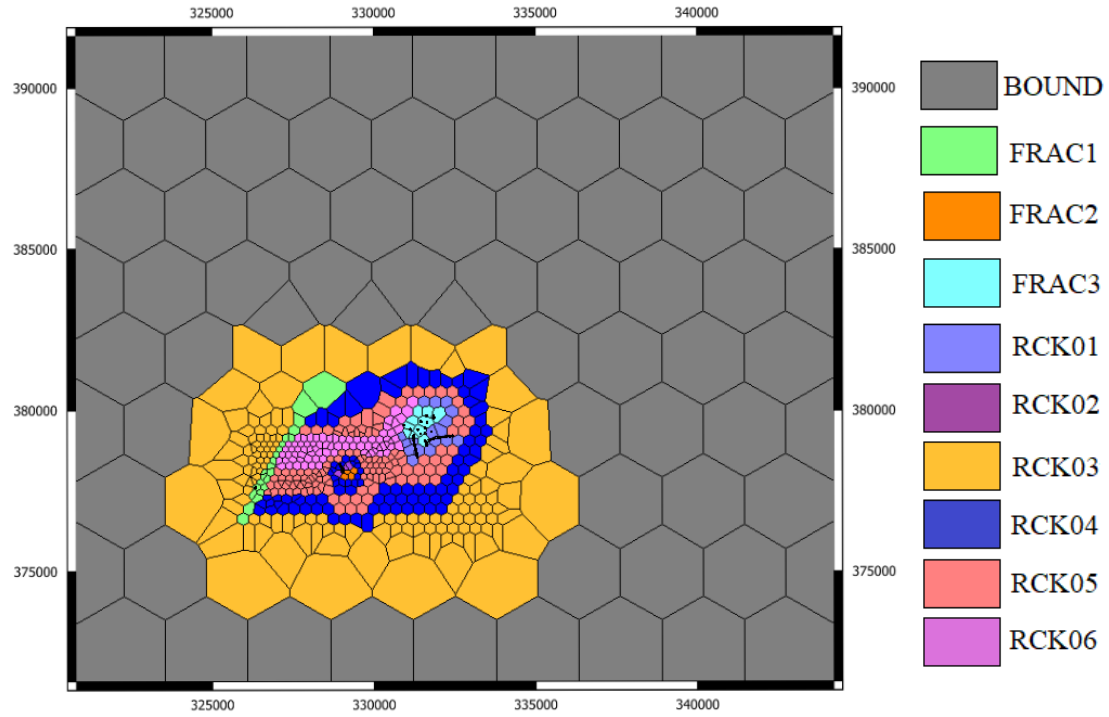

FIGURE A8: Rock distribution in Layer H, with well traces shown as a reference

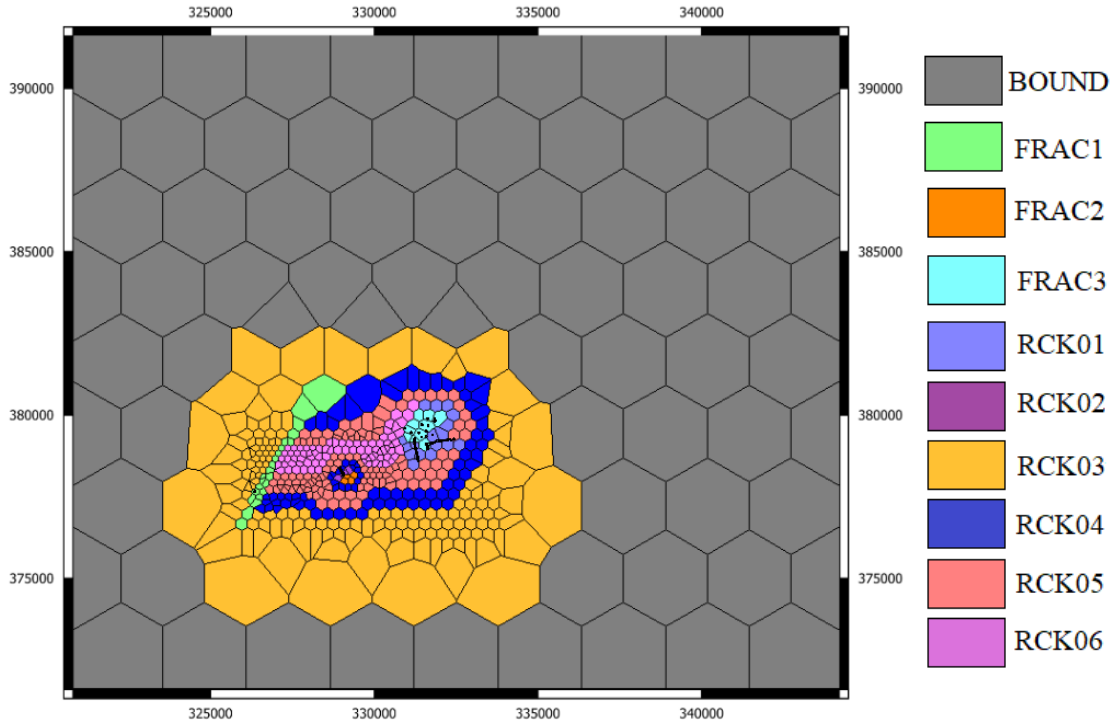

FIGURE A9: Rock distribution in Layer I, with well traces shown as a reference

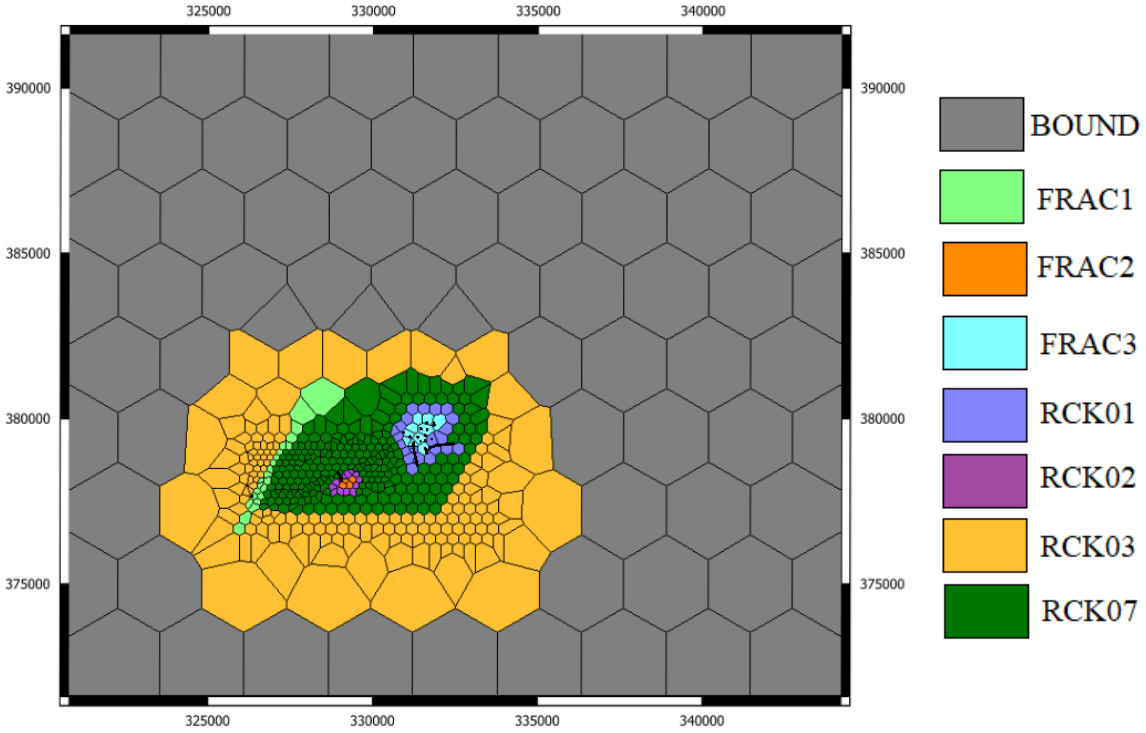

FIGURE A10: Rock distribution in Layer J, with well traces shown as a reference

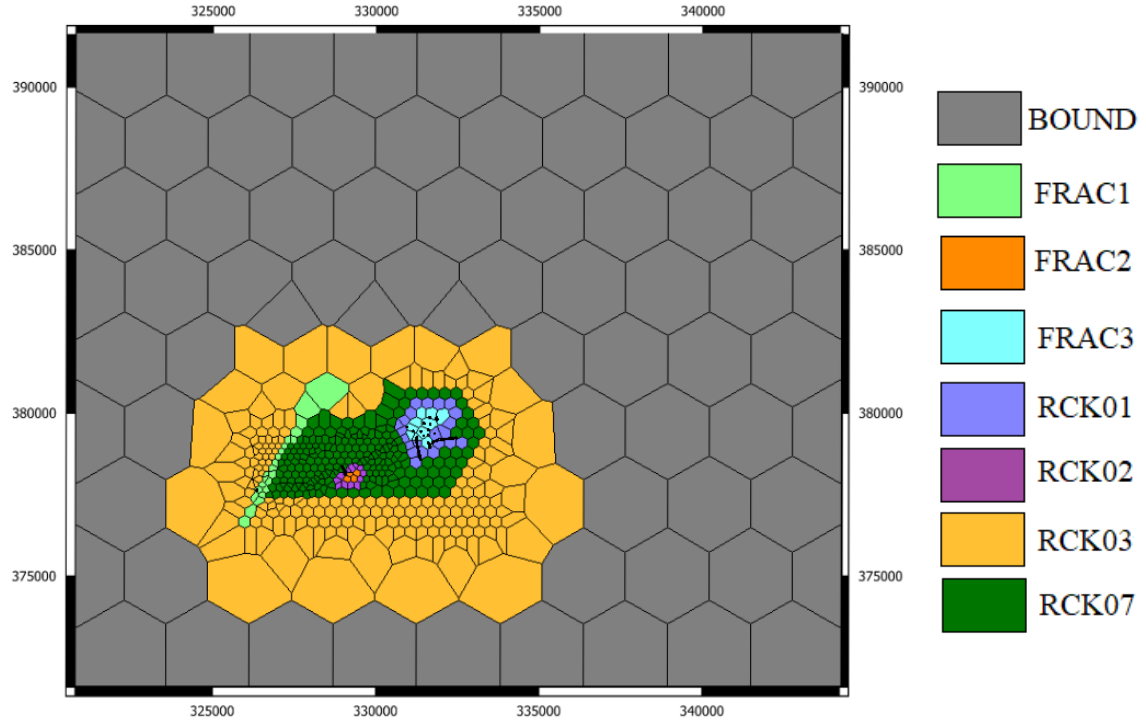

FIGURE A11: Rock distribution in Layer K, with well traces shown as a reference

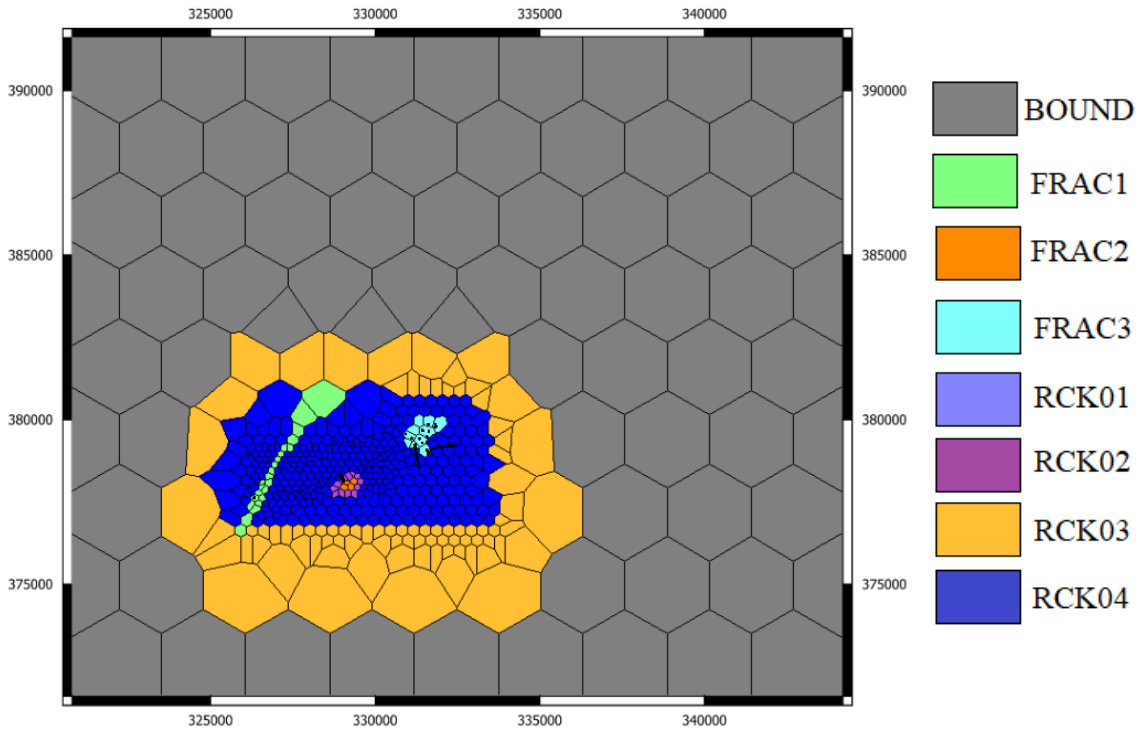

FIGURE A12: Rock distribution in Layer L, with well traces shown as a reference

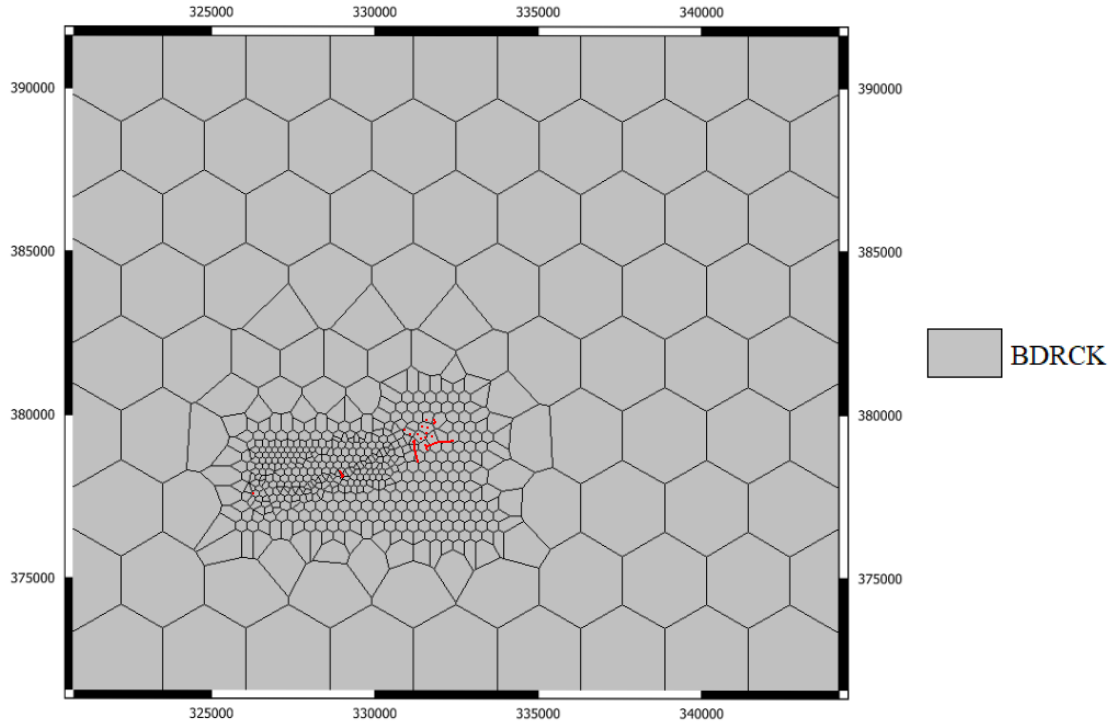

FIGURE A13: Rock distribution in Layer M, with well traces shown as a reference

APPENDIX B: Natural state calibration

The correlation graphs between the simulated natural state temperature and formation temperature profiles are presented in Figures B1- B5.

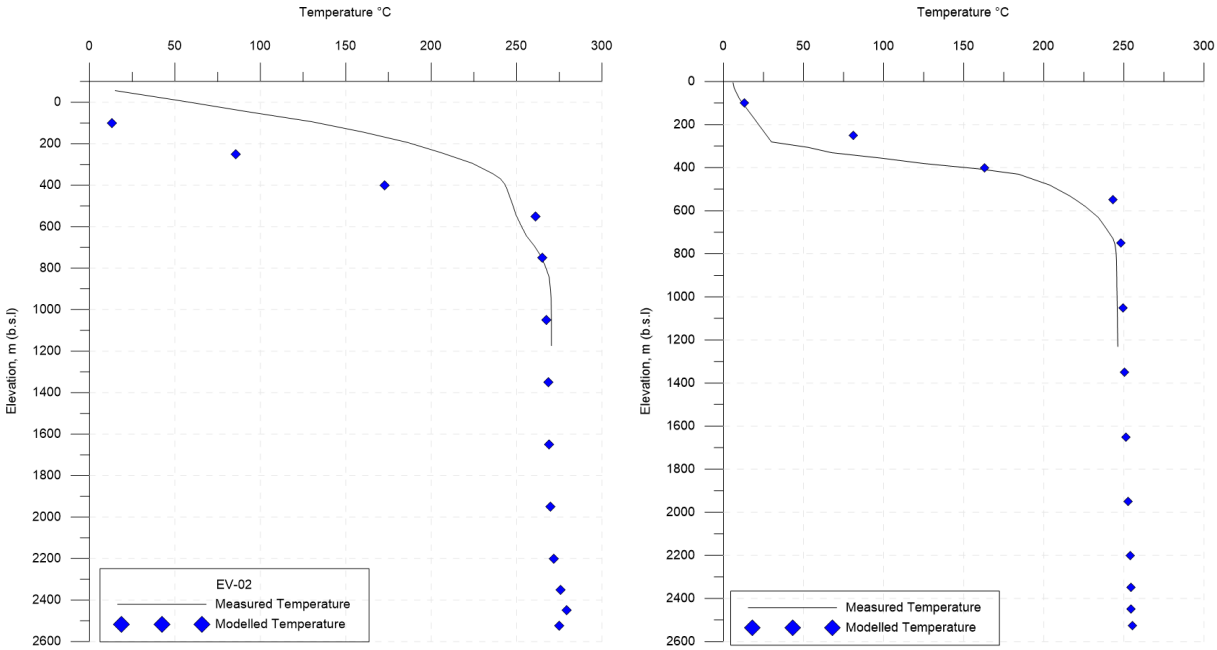

FIGURE B1: Comparison between formation temperature and simulated natural state temperature for wells EV-02 and SV-17

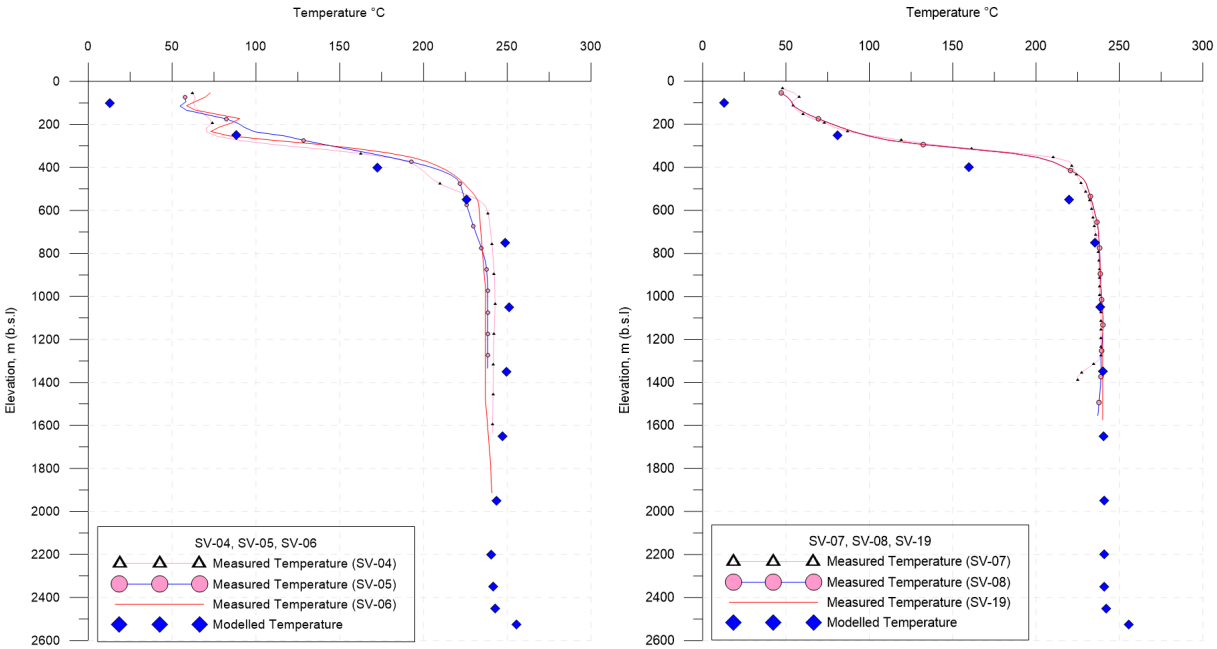

FIGURE B2: Comparison between formation temperature and simulated natural state temperature for wells SV-04, SV-05, SV-06, SV-07, SV-08 and SV-19

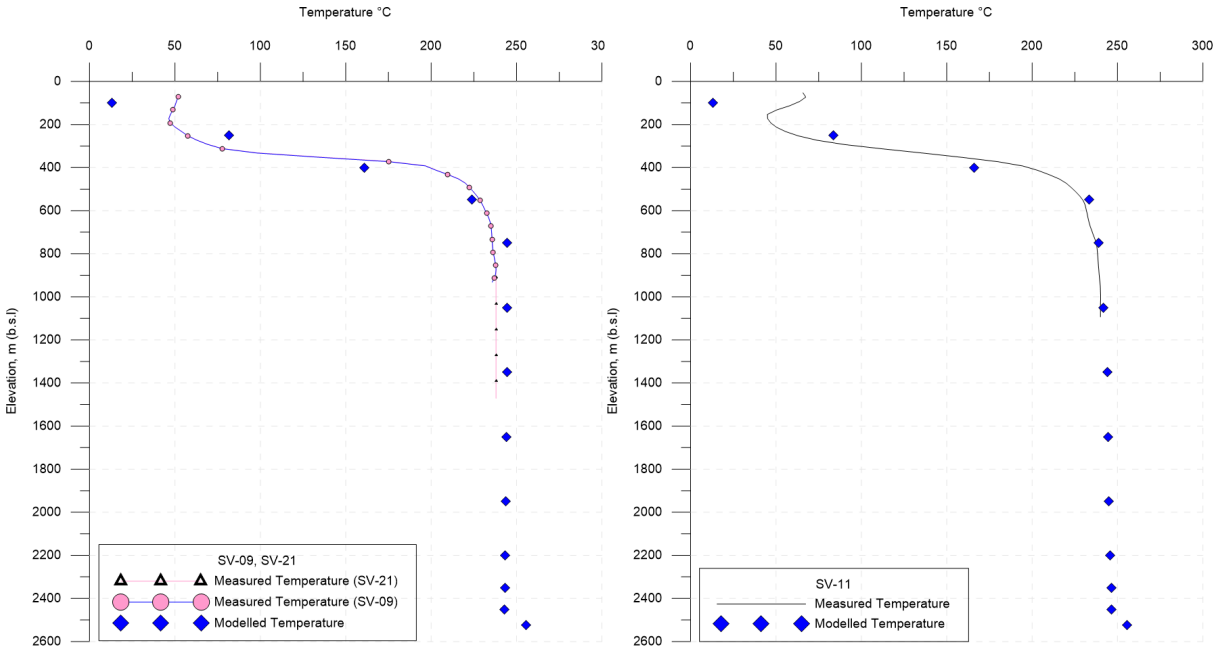

FIGURE B3: Comparison between formation temperature and simulated natural state temperature for wells SV-09, SV-21 and SV-11

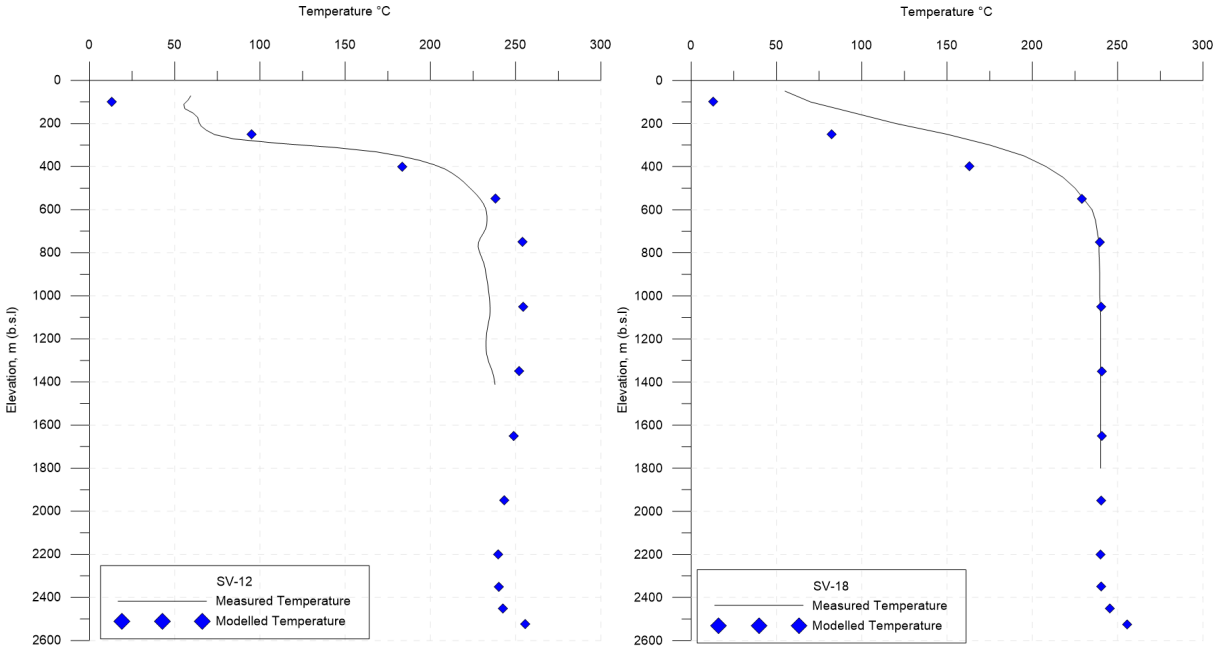

FIGURE B4: Comparison between formation temperature and simulated natural state temperature for wells SV-12 and SV-18

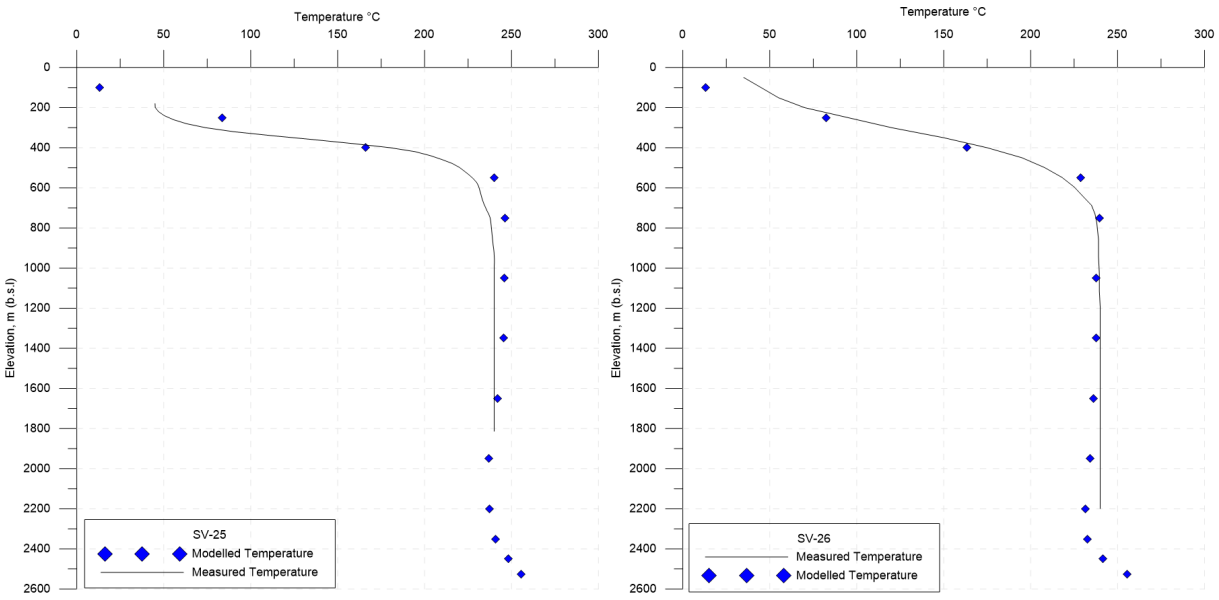

FIGURE B5: Comparison between formation temperature and simulated natural state temperature for wells SV-25 and SV-26

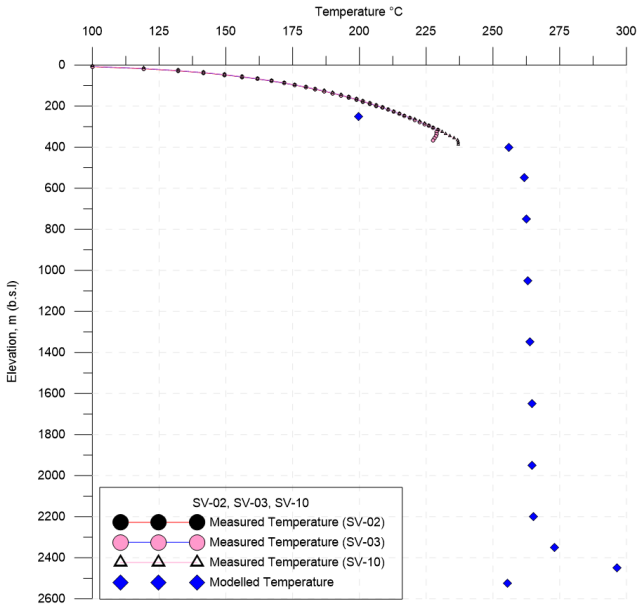

FIGURE B6: Comparison between formation temperature and simulated natural state temperature for wells SV-02, SV-03 and SV-10